AN INVESTIGATION INTO USING REGENERATED CELLULOSE-BASED ELECTRO-CONDUCTIVE COMPOSITES FOR ACTUATION AND DRUG DELIVERY

Nargis Afroj Chowdhury

PhD

2014

Auckland, New Zealand

An Investigation into Using Regenerated Cellulose-based Electro-conductive Composites for Actuation and Drug Delivery

Nargis Afroj Chowdhury

A thesis submitted to Auckland University of Technology

in fulfilment of the requirements for the degree of

Doctor of Philosophy (PhD)

May, 2014

Faculty of Design & Creative Technology

School of Engineering

Auckland University of Technology

Auckland, New Zealand

Primary Supervisor : Professor Ahmed Al-Jumaily

Declarations

I hereby declare that this submission is my own work and that, to the best of my knowledge and belief, it contains no material previously published or written by another person nor material which to a substantial extent has been accepted for the award of any other degree or diploma of a university or other institution of higher learning, except where due acknowledgement is made in the acknowledgements.

Signature Date 15/05/2014

Nargis Afroj Chowdhury

I further authorise the Auckland University of Technology to reproduce this thesis by photocopying or by other means, in total or in part, at the request of other institutions or individuals for the sole purpose of scholarly research.

Signature Date 15/05/2014

Nargis Afroj Chowdhury

Borrowers Page

The Auckland University of Technology requires the signatures of all people using or photocopying this thesis. Accordingly, all borrowers are required to fill out this page.

Date	Name	Address	Signature

Acknowledgements

I would like to thank my primary supervisor Professor Ahmed-Al-Jumaily, Auckland University of Technology (AUT) University, for his support and encouragement throughout the years in this research. Additional thanks go to Dr. John Robertson, Senior Lecturer, School of Applied Sciences, and special thanks go to Dr. Maximiano V. Ramos, Senior Lecturer, School of Engineering, AUT University, who also supported me, and to the Institute of Biomedical Technologies (IBTec), AUT University, for giving me the chance to work there. I must appreciate the help of several technicians at the School of Applied Sciences. Among them Yan Yang and Saeedeh Sadooghy-Saraby, laboratory officer, Applied Science Programmes who offered kind-hearted cooperation during my studies. I would like to thank Senior Research Officer Patrick Conor from faculty of Design & Creative Technologies for helping in taking SEM images. I must mention Saabiq A. Chowdhury (my son) and Research Fellow Dr. Lulu Wang's contribution in formatting this thesis. Finally, I am thankful to my son and my husband for their support and encouragement throughout the years of studies.

Abstract

Under the influence of an electric field, ionic electro-active polymers generally bend or deswell, depending on the shape of the polymer matrices and its position relative to the electrodes. In this study, we investigate the bending behaviour of regenerated cellulose-based ionic electro-active composites for the fabrication of soft actuators with improved actuation force and durability. This research also focuses on the externally induced (electrically and magnetically) matrices deswelling and other responses, which affect the release of drug from the matrices. For actuation studies, we prepared matrices by combining carbon nanofibers, conducting polymers, and ionic liquids (through blending, doping, or coating) into the regenerated cellulose. We observed that actuators coated by polypyrrole doped with anthraquinone-2-sulfonic acid sodium salt monohydrate showed improved electrical conductivity and durability compared to that of using perchlorate ion as the dopant. This is due to the preparation process and the effect of dopants that play an important role to improve the performance of the regenerated cellulose-based ionic electro-active actuators. In addition, we investigated the influence of electrode design (layer-by-layer structure) on the properties of the actuators.

Further, in this study, we developed three types of matrices consisting of regenerated cellulose/functionalized carbon nanofibers, regenerated cellulose/functionalized carbon nanofibers/polypyrrole, and regenerated cellulose/γ-ferric oxide/polypyrrole. We investigated the effects of electric field strength and electrode polarity on the release rate of sulfosalicylic acid (drug) in an acetate buffer solution with pH 5.5 and temperature 37 °C during a period of 5 h. Drug release rate from the matrices containing carbon nanofibers (additives) increased effectively with increasing applied electric field.

The mechanism of drug release from drug-doped polypyrrole coated matrices includes expansion of conductive polymer chain and the electrostatic force between electron and drug. The novelty of the work is- the matrices can also work under magnetic field and consequently, one can be beneficial from a contactless actuation. In this study, we also investigated electrical conductivity, morphology, swelling behaviour of the composite matrices, electro-active composite-drug interaction, and in vitro drug release behaviour of the matrices. Further, a comparative study was performed on the rate of drug release from the matrices induced by electric and magnetic field.

Table of Contents

List of Figures

List of Tables

Abbreviations

AC	Alternating current
ACMF	Alternating current magnetic field
APS	Ammonium peroxydisulfate
AQSA	Anthraquinone- 2-sulfonic acid
AQSA-Na	Anthraquinone- 2-sulfonic acid sodium salt monohydrate
ATR	Attenuated total reflectance accessory
ATR-FTIR	Attenuated total reflection Fourier transform infrared spectrometer
$BMIMBF_4$	1-butyl-3-methylimidazolium-tetrafluoroborate
BMIMCL	1-butyl-3-methylimidazolium chloride
CEP	Conductive electro-active polymer
CNFs	Carbon nanofibers
CNT	Carbon nanotube
CP	Conducting Polymer
DC	Direct current
DI water	Deionized water
DMSO	Dimethylsulfoxide
DPW	Degree of polymerization weight
RC	Regenerated cellulose
EAP	Electro-active polymer
EAPap	Electro-active paper
FCNFs	Functionalized carbon nanofibers
$FeCl_3$	Ferric chloride
$Fe\ (NO_3)_3$•9H2O	Ferric nitrate Nona hydrate

f-MWCNT	Functionalized multiwalled carbon nanotube
FTIR	Fourier transform infrared spectroscopy
HPLC	High performance liquid chromatography
H_2SO_4/HNO_3	Sulphuric acid/ Nitric acid
ILs	Ionic liquids
IPA/DI	Isopropyl alcohol/Deionized
IPMCs	Ionic Polymer-Metal Composites
IR	Infrared spectroscopy
KCl	Potassium chloride
LiCl	Lithium chloride
LiCl/DMAc	Lithium chloride/N, N-dimethylacetamide
Li^+ (DMAc)x	Lithium-Dimethyl acetamide macro cation
MWCNTs	Multi-walled carbon nanotubes
$[NR_4]^+$	Tetraalkylammonium cation
SWNTs	Single-walled nanotubes
PEG	Polyethylene glycol
$[PF_6]^-$	Hexafluorophosphate ion
PMMA	Polymethyl methacrylate
PPy	Polypyrrole
PPySSA	Sulfosalicylic acid doped polypyrrole
$R_1R_2IM]^+$	Alkylimidazolium cation
SEM	Scanning electron microscope
SPE	Solid polymer electrolyte
SPION	Super paramagnetic iron oxide nanoparticles
SSA	5-sulfo-salicylic acid dihydrate
TDD	Transdermal drug delivery

Tg	Glass transition temperature
$[Tf_2N]^-$	Bis-(trifluoromethanesulfonyl)amide ion
TS	Tensile strength
UV/Vis	UV/Visible spectrophotometer
XPS	X-ray photoelectron spectroscopy
γ-Fe_2O_3	Gamma ferric oxide

Symbols

A	Surface area of the layer exposed to the medium
C	Concentration
C_S	Solubility of the drug in the material
Cl^-	Chloride ion
D	Diffusion coefficient
M_0	Initial concentration
M_t	Cumulative absolute amount of drug released at time t
M_∞	Cumulative absolute amount of drug released at infinite time
Na^+	Sodium ion
n	Exponent
Li^+	Lithium ion
K	Kinetic constant
^0C	Degree celsius
V	Volts
V_{pp}	Volts (peak-to-peak)
μg	Microgram
ε	Strain
R^2	Correlation coefficient
σ_s	Conductivity

Chapter 1 **Introduction**

1.1 Background and Motivation

This research focuses on the actuation and drug delivery behaviour of regenerated cellulose-based electro-conductive composites prepared by combining carbon nanofibers, polypyrrole, ionic liquids, and gamma ferric oxide (through blending, doping, or coating) into the regenerated cellulose. Drug delivery is normally processed through material actuation specifically, deswelling and change of shape due to ion movement. This makes it worthwhile to combine actuation and drug delivery in this investigation.

Among conducting polymers, polypyrrole has achieved much attention from researchers in recent years for the development of actuators since they possess both ionic and electrical conductivity. Recently, Baughman [1] has reported the potential applications of conducting polymers as artificial muscles, micro-valves, robotics, and soft actuators. However, these applications have not yet been fully developed due to the following reasons: [2]

- They can be operated at low voltages but their wetness should be maintained
- The devices are capable of delivering low forces
- Instable performance of the conducting polymer actuators

Many researchers have experienced problems to combine conducting polymers with conventional polymers because of the insolubility of conducting polymers in common solvents. Regenerated cellulose/conducting polymer composites provide some possibilities in this regard. Among conducting polymers, polypyrrole has strong affinity to regenerated

cellulose. However, a combination of the two materials is expected to improve different application aspects of the electro-active paper composites driven by electric potential. In addition, if the composites possess appreciable electrical conductivity, that could be operated at low voltages with improved response time [3].

In 2006, Jaehwan et al. reported a few conjugated conducting polymer/electro-active paper (regenerated cellulose) actuators that can work in air but that have some drawbacks [4], which are:

- Their complicated configurations require expensive multistage processing including sputter deposition of metallic layer electrodes on the substrate and electrochemical deposition of conducting polymer layers [5]
- They show nearly 50 % performance degradation within 4000 s because of the damage of the gold electrode coating on the actuators caused by the trapped dimethylacetamide, reactive Li^+ ions, and initial aging of the material for electrical actuation [6]
- There are chemical interactions between counterions and PPy and that lead to decreased electrical conductivity [7]
- They show little displacement output even at 70 % relative humidity [4]
- Force output and frequency are also small [8]

Drug delivery is the process of introducing drugs into our body. Oral, injection, and transdermal are three different routes by which drugs can be administered into our body. Table 1-1 shows the advantages and disadvantages of different types of drug delivery routes.

Table 1-1: Advantages and disadvantages of different types of drug delivery routes

Routes	Advantages	Disadvantages
Oral	May provide sufficient dose of drug initially	The dose decreases over a short time period [9]
Injection	May provide suitable dose of drug initially	The dose decreases over a short time period [9]
Transdermal Patch	i) Avoids the first-pass metabolism [10] ii) Provides on-demand release of drug to the targeted area of the body	Extremely low drug release rate from the matrix and the low permeability of drug through the skin [11]

Drug delivery carriers fabricated from hydrophilic matrices have several distinguishing features such as a good in vitro–in vivo correlation, inexpensive and easy to fabricate. In addition, it is also possible to formulate hydrophilic matrices with high molecular weight drugs [8]. The main problems in the formulation of these carriers are:

- The lack of a suitable large scale production method
- To achieve a suitable rate of drug release over the time desired [12]
- To reduce burst effect [13]
- Loading of drugs into the matrices
- The cytotoxicity of the drug carriers [14]

Cellulose is known as the earth's major biopolymer and has economic importance globally. In this study, regenerated cellulose is used for developing soft actuators and drug delivery matrices as regenerated cellulose is biocompatible and is more environmental friendly than synthetic electro-active polymers (EAPs). It has some distinguishing features, which are: [15]

- It is inexpensive
- It is hydrophilic
- It actuates with low voltages
- It consumes low power
- It is lightweight
- It works at ambient and humid conditions
- It has strong affinity to polypyrrole and makes it with improved electrical conductivity

Under the influence of an electric field, electro-active papers made from regenerated cellulose generally bend or deswell, depending on the shape of the papers and their positions relative to the electrodes. Bending occurs when an electric field is applied across the thickness direction (paper lies parallel to the electrodes) whereas deswelling occurs when the paper lies perpendicular to the electrodes [16]. Bending behaviour has mainly been studied for the production of mechanical devices such as valves, soft-actuators, and artificial fingers/muscles. Electrically induced deswelling affects the release of drug from the drug-loaded matrices.

1.2 Research Objectives

This is a two-fold purpose thesis. First, to investigate the possibility of improving the performance of actuators developed from regenerated cellulose-based electro-conductive composites, and second, to investigate the possibility of using these types of composites in drug delivery specifically:

- Develop regenerated cellulose-based actuators with improved electrical conductivity, durability, and actuation force, which can be used as valves, soft-actuators, and artificial fingers/muscles
- Develop drug carriers, which respond well under external stimuli such as electric and magnetic field for drug delivery. Magnetic field induced carriers are much more desirable as they give contactless actuation
- Reduce the burst effect (initial large amount of drug released before reaching a stable release profile) of highly water-soluble drugs
- Investigate the best biomedical applications suitable for these composites

1.3 Thesis Overview

We explained the motivation for this work and the objectives in this chapter. The remaining chapters of this thesis will proceed on in the following orders: Chapter 2 covers review of literature. It focuses on the possibility and challenges of using regenerated cellulose-based electro-conductive composites as actuators. In addition, it describes different types of drug delivery devices based on the mechanism controlling the drug release. Further, it reviews devices used for transdermal drug delivery. Chapter 3 describes preparation process of regenerated cellulose-based electro-conductive actuators. It also investigates into the impact of dopants on the performance of the electro-active actuators. In addition, it describes techniques used for the characterization of the actuators. In chapter 4, a novel systematic design for actuators is developed. It also investigates the performance of the layer-by-layer casting actuators in terms of bending displacement, actuation force, and power consumption. Chapter 5 investigates (in vitro) the release kinetics of a model drug from conductive regenerated cellulose-based matrices under external stimuli (electric and magnetic fields). Chapter 6 also evaluates controlled drug delivery from regenerated cellulose-based electro-conductive matrices containing magnetic particles under external stimuli such as electric and magnetic fields. Finally, Chapter 7 summarizes conclusions and the potential future work.

Chapter 2 Literature Review

Although the focus of this work is to develop regenerated cellulose based electro-active materials, a review of the literature on the development of electro-active polymers is appropriate at this stage. The discussion under Heading 2.1of literature review section focuses on regenerated cellulose-based electro-conductive composite materials as actuators. Heading 2.2 of literature review section focuses on the different types of drug delivery systems. In addition, shortcomings of the drug delivery techniques, and the potential use of hydrophilic materials as drug delivery carriers are presented in this section.

2.1 Material Selection

The development of new electro-active polymer (EAP) materials that exhibit large displacement [17] has received much attention since 1990s. Indeed, based on the activation mechanism, EAP materials are divided into two major categories such as electronic driven by electric field and ionic involving mobility of ions. Electronic EAPs require high voltage for activation. In contrast, devices fabricated from ionic EAP materials, such as conductive polymers, ionic polymer–metal composites [18] and carbon nanotubes [1] can be operated at low voltages. However, their wetness should be maintained. Ionic polymer-metal composites (IPMCs) are capable of producing large bending motion when subjected to a low applied electric field (~10 kV m^{-1}) across the conductive surface. They show fast response time of ≥ 120 Hz and reliable bending motion ≥ 100,000 times with large bending displacement [19]. However, IPMCs as actuators have limited applications because they generate low actuation force. In addition, the operating voltage of water hydrated ionic polymer actuators is limited to 1.23 V. Above this voltage, electrolysis of water occurs,

which leads to performance degradation of the IPMCs actuators [17]. Thus, it is desirable to develop regenerated cellulose-based actuators.

2.1.1 Regenerated cellulose as an electro-active polymer

Electro-active paper (EAPap) developed from Regenerated cellulose can be actuated electrically because of the combined effect of ion migration and piezoelectricity of cellulose [20]. Piezoelectricity in cellulose originates from the dipolar orientation and monoclinic crystal structure of cellulose. The existing EAPap actuators are sensitive to environmental humidity. They show little displacement output at ambient humidity. Force output and frequency are also small. The performance of the actuator tends to degrade with time [21]. To resolve this problem an ionic liquid named 1-butyl-3-methylimidazolium-tetrafluoroborate ($BMIMBF_4$) was dispersed in regenerated cellulose solution [22]. The actuator showed ~62.9 % performance degradation at 50 % relative humidity after activating for 11 h. The performance degradation is because of the highly hygroscopic $BMIMBF_4$,which absorb water and resulted in depletion of ions in the film [22]. Thus, the main objective of this work is to develop durable actuators, which can operate in air at low voltages both at ambient and highly humid conditions. To fabricate actuators working in air, some kind of electrolyte such as either a “solid polymer electrolyte” (SPE) which contains some liquid to allow ion migration, or a liquid electrolyte surrounded by some kind of encapsulation is required.

Regenerated cellulose paper can be synthesized by dissolving cellulose fibers into a suitable solvent and casting it on a glass petri dish. Derivative and direct methods can be used to dissolve cellulose fibers. The viscose method is a derivative method in which cellulose

xanthogenate is formed by the reaction of pulp with carbon disulfide as a metastable intermediate. This method leads to emission and environmental problems [23]. The direct dissolution without derivation is possible with some solvent systems. Among various non-aqueous solvent systems with inorganic salts lithium chloride/N,N-dimethylacetamide (LiCl/DMAc) is advantageous because of several reasons such as (i) a high level of polymer-solvent interactions and (ii) after a long period of storage, a negligible reduction of the viscosity of the polymer [24].

In 1981, McCormick first reported the dissolution of cellulose in lithium chloride (LiCl)/N, N-dimethylacetamide (DMAc) solvent system [25]. By using this solvent system a homogeneous solution containing 16-17 % cellulose was obtained [25]. The time required for dissolution of cellulose was reduced by prior activation of the cellulose with a solvent exchange series: water, methanol, DMAc. Using this procedure, a clear solution with concentrations up to 5 % was obtained in less than an hour and concentrations of 6-15 % in 24-48 h. The time required for dissolution was further reduced by heating the mixture to 155 ^{0}C and allowing it to cool slowly [26]. In the LiCl/DMAc solvent system, hydroxyl protons of the anhydroglucose units are associated with the chloride anions by hydrogen bonding. The chloride ion (Cl^-) is associated with a Li^+(DMAc)x macrocation as shown in Figure 2.1 [27]. The lithium ions ($Li^{+)}$ are tightly linked with the carbonyl group (C=O) of DMAc while the chloride ions are left unencumbered. Thereby, chloride ions are highly active as nucleophilic base and play a major role by breaking up the inter- and intra-hydrogen bonds. Some authors attribute to Cl^- the ability to complex the three hydroxyl groups of the anhydroglucose unit by hydrogen bonding, while the counterpart of the solvent complex, the [Li DMAc]$^+$ macrocation, is believed to be more loosely bound [25]. More recently, it has been proposed that cellulose takes part in the coordination sphere of

Li+, this being one of the driving forces in the dissolution of the polymer [28]. Ionic interactions have been observed between the lithium cation and the carbonyl oxygen of DMAc. The electro-negative oxygen atom tends to bind the lithium cation, while the amide with larger alkyl groups tends to stabilize the cation most effectively (Figure 2.1).

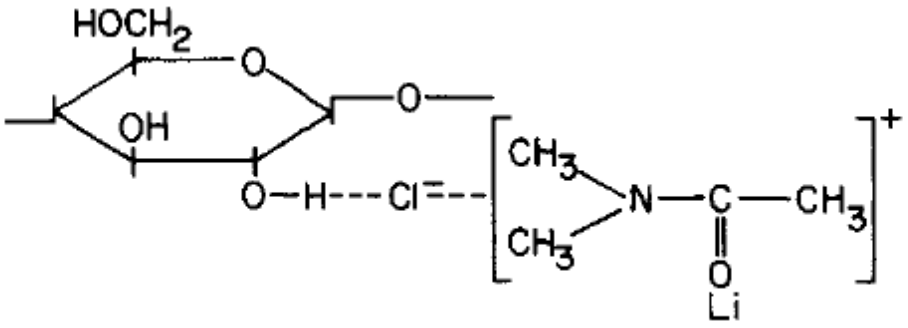

Figure 2.1 Dissolution mechanism of cellulose in the LiCl/DMAc solvent system [6]

The formation of layer-by-layer structure of cellulose is hindered due to the presence of trapped DMAc and Li^+(DMAc)x macrocations between cellulose chains. As a result, cellulose possesses low-mechanical properties [29]. Therefore, trapped DMAc and Li^+ (DMAc)x macrocations should be removed from the polymer solution. DMAc can be completely removed by distillation and later washing the films with an isopropyl alcohol/ deionized (IPA/DI) water mixture. Li^+ cations may reunite with the chloride anions, which thus form a cellulose-LiCl complex. When the films are subjected to running water, running water may pull out the Li^+ ions from the cellulose-LiCl complex, as the solubility of LiCl in DI water is very high (63.7 g) compared to ethanol (42.4 g) per 100 mL of water. In addition, Li^+ ions are highly water-soluble. Furthermore, LiCl behaves as an ionic compound, although an Li^+ ion is very small [30]. IPA/DI water mixture also assists to fabricate wrinkle-free cellulose films. In addition, it helps enhance mechanical properties,

and improve the actuation durability by minimizing electrode damage [29]. Indeed, the 40:60 ratio (IPA/DI water mixture) is enough to decrease Li+ ions concentration to 86 ppm and sufficient enough to elimination of DMAc from the cellulose films [21].

Regenerated cellulose has ordered (crystalline) and disordered regions. In the disordered region, water molecules are found attached to the hydroxyl groups (Figure 2.2) [31].

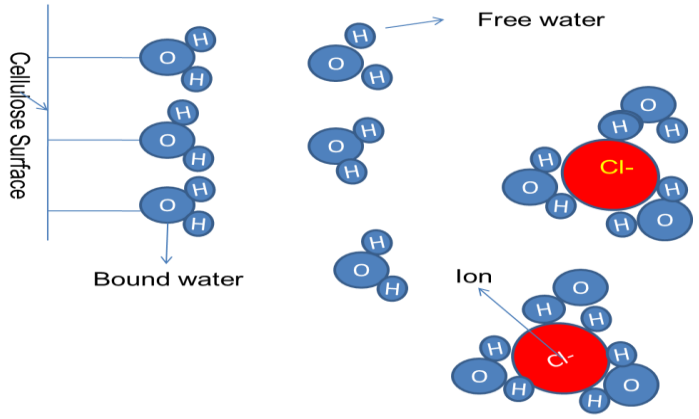

Figure 2.2: The schematic of distribution of water molecules with Cl^- ions in the regenerated cellulose film [32]

The regenerated cellulose paper coated with thin gold electrodes shows bending displacement under the application of an electric field [6]. During the paper making process, chloride ions are injected in the paper fibre [32]. These ions along with the water molecules in the disordered region of cellulose can migrate to the anode under electric field. This ionic and water transport across the polymer under an electric field results in volumetric changes, which in turn leads to bending [31].

Kim et al. reported that when 0.25 V/μm of excitation voltage was applied to 30 mm long EAPap beam, more than 4 mm of tip displacement was observed [31]. This excitation voltage is very low as compared to other electro-strictive polymers. Since the EAPap actuators consume less than 10 mW cm^{-2} power, which is below the safety limit of

microwave driven power, consequently, they can be actuated remotely driven by microwave power [32]. There is an optimum thickness for achieving good performance of EAPap actuator. Because the thickness is associated with the bending stiffness that strongly affects the bending deformation and the force output of the actuator [33]. When the thickness is increased, the electric field required for activating the EAPap actuator is high, as a result, the energy consumption is increased and the efficiency of the EAPap is decreased [33]. According to Sungryul et al., 30-μm thick films shows the highest efficiency of 3.3 %, which is 60 times higher than the films with thickness 40-μm. Therefore, 30 μm is an optimum thickness for the best performance of the EAPap actuators [33]. In order to improve actuation force and actuation frequency functionalized multiwalled nanotube/cellulose EAPap actuator was developed. The actuator showed improved actuation force and frequency at the highly humid condition but the power consumption of the actuator was increased with the increase of the humidity [34]. However, there are major opportunities for the development of regenerated cellulose-based actuators as regenerated cellulose has better biocompatibility and is more environmental friendly than synthetic EAPs. The use of renewable bio-based products is a potential alternative to petroleum-based and synthetic products [35].

2.1.2 Polypyrrole as an electro-active polymer

Among conducting polymers (CP), polypyrrole (PPy) has experienced a great deal of attention from researchers due to its relatively low cost, physicochemical stability, good conductive, optical, and sensor properties [36]. However, there is a major problem of using PPy because of its insolubility in an aqueous solution, and its poor mechanical characteristics. Therefore, researchers are working on alternative approach using PPy in the form of conducting composites or blends with conventional polymers [35].

The performance of EAPap actuators was improved by developing a polypyrrole coating on EAPap actuators by electrochemical polymerization as described in ref .[4]. The coating of conducting polymer on regenerated cellulose can be performed either by chemical or electrochemical polymerization. Chemical oxidative polymerization can occur through three modes: (i) in a homogeneous solution [37]; (ii) at an interphase of two immiscible solutions [38]; (iii) in the vapour phase [39]. The advantages and disadvantages of chemical and electrochemical polymerization methods are summarized in Table 2-1[40].

Table 2-1: Comparison of the advantages and disadvantages of chemical and electrochemical polymerization methods

Polymerization approach	Advantages	Disadvantages
Chemical polymerization	• Large-scale production possible • CP backbone can be modified covalently • Post-covalent modification of bulk CP is possible	• Cannot make thin films • Synthesis is more complicated
Electrochemical polymerization	• Ease of synthesis • Thin film synthesis is possible • Entrapment of molecules in CP	• Post-covalent modification of bulk CP is difficult • Difficult to remove film from the electrode surface

In the process of the chemical oxidative polymerization of pyrrole, a neutral molecule of pyrrole monomer (a) yields cation radical species (b). Cation radicals then recombine, yielding a di-cation of bipyrrole (c). After its deprotonation, a neutral bipyrrole molecule is formed (d). The bipyrrole molecule undergoes further oxidation, deprotonation and recombination steps (e), resulting in PPy as the product of oxidative polymerization (Figure 2.3). In chemical polymerization, strong chemical oxidants like ammonium peroxydisulfate (APS), ferric ions, and permanganate or dichromate anions are used. These oxidants are able to oxidize the monomers in appropriate solution, leading to chemically active cation radicals of the monomers used [41].

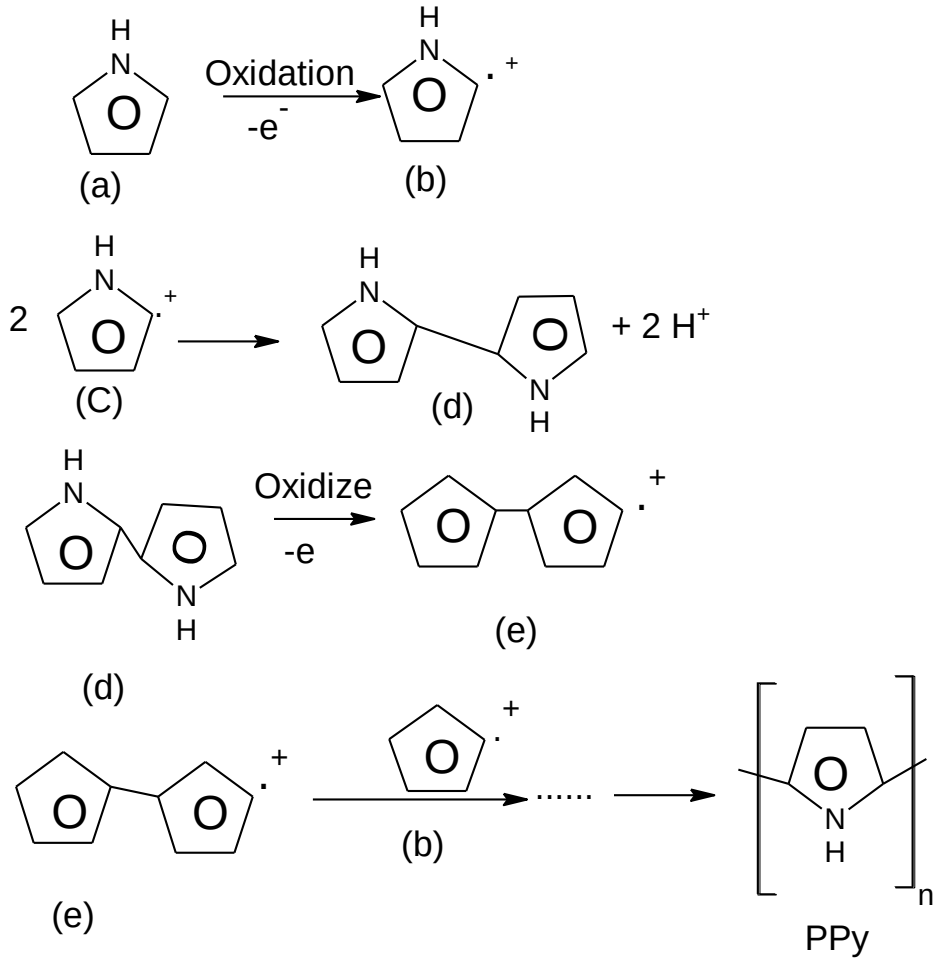

Figure 2.3: Oxidative polymerization of pyrrole to polypyrrole [42]

Generally, the process of chemical polymerization occurs in the bulk of the solution, and the resulting polymers are precipitated as insoluble solids. However, a part of conductive electro-active polymer (CEP), formed by chemical polymerization, can deposit spontaneously on the surface of materials immersed into the polymerization solution. The precipitated and deposited forms of CEP depend on the concentration ratio of oxidant to monomer, and the reaction temperature. A reasonably high yield of surface-deposited CEP can be obtained by adjusting the reaction conditions [41].

In the process of the chemical oxidative polymerization, the change of the colour of the polymerization solution is usually visible. At first, the colourless solution turns, blue and dark blue, indicating the formation of di and oligomers. Later, precipitate of black solid polymer is observed. The rate of the process depends on the nature of the oxidant used, and the concentration of the reactants [42]. Most of the CEP are precipitated as insoluble solids after the reaction is completed. However, a part of the CEP can spontaneously be deposited as a thin layer on the substrates immersed in the reaction medium. This process can obtain a coating of PPy with nanometer thickness. Repeating this process with the fresh solution, the thickness of the PPy coating can be increased [43].

In oxidative chemical polymerisation of pyrrole, Iron (III) chloride is one of the best chemical oxidants and water is the best solvent in terms of desirable conductivity characteristics [44]. The chemical polymerisation of PPy with ferric chloride oxidant is shown in Figure 2.4.

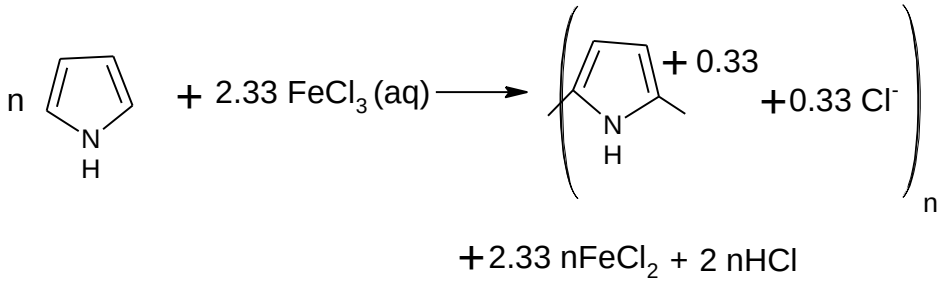

Figure 2.4: The stoichiometry resulting from chemical polymerisation of PPy with ferric chloride oxidant [7]

The $FeCl_3$/Pyrrole mole ratio for polymerisation by aqueous iron (III) chloride solution at 19 °C has been found to be 2.33 (Figure 2.4) [45]. During the process of chemical polymerisation of pyrrole, anions of the chemical oxidant are incorporated as counter ions to maintain the electro-neutrality of the polymer matrix. For example, when $FeCl_3$ is used

as an oxidant, Cl^- ion is incorporated into the polymer matrix. It has been reported that solvent, reaction temperature, time, and the molar ratio of pyrrole/oxidising agent, affect the oxidation potential of the solution which in turn influences the final conductivity of the synthesised polypyrrole [46]. Elemental analysis data has shown [47] that the composition of polypyrrole prepared either chemically or electrochemically is almost identical [47].

Polypyrrole is electro-active in both organic and aqueous solutions environment. The electro-active nature of PPy has been utilized as the basis of most proposed applications such as sensors and actuators. It is also suitable for use in physiological environment. Some promising features of polypyrrole include low actuation voltage, low cost, high force output/weight ratio. Its main drawback is its low speed of response [48].

After polymerization, polypyrrole exists in its oxidized state. Polypyrrole is capable of switching between its oxidized and reduced states under electrical stimulus. The switching processes are often described according to the following manners (Figure 2.5).

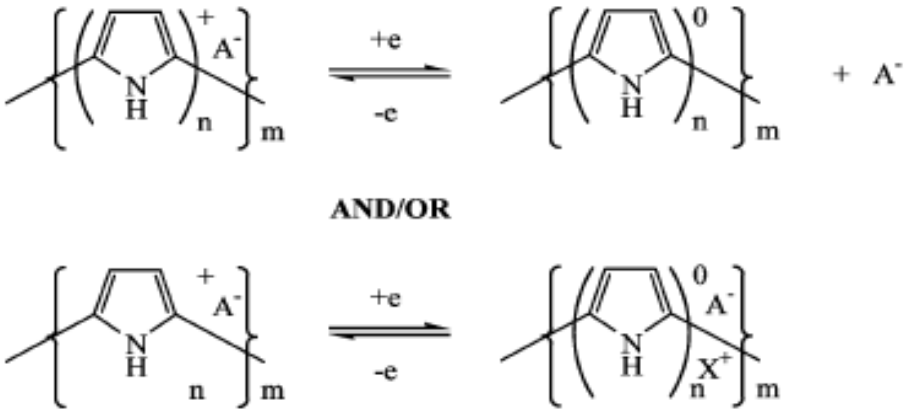

Figure 2.5: Redox switching of polypyrrole [49].

Where A^- is a counterion, which incorporates during polymer growth, X^+ is a cation from the supporting electrolyte, n is the number of pyrrole monomers for each A^- incorporated, and m is the number of pyrrole repeat unit.

The electrolytes used in artificial muscle applications are capable of doping and undoping of polypyrrole. They do not degrade electrical and mechanical properties of polypyrrole. According to Otero et al. [50], when positive charge is applied along the chains and the polymer-solution interface, columbic repulsion between those chains leads to open up enough space in between chains and that allows penetration of ions and solvent molecules. After the conformational change of the structure, ion exchange occurs between the polymer and the electrolyte. It is an established fact that the size of the dopant ions dominates the redox reaction [49]. When polypyrrole doped with small anions is reduced, electrons are injected into the polymer chains and small anions are ejected from the polypyrrole (Figure 2.5) [51]. The polymer then shrinks. On the contrary, during oxidation, electrons are extracted from the polymer chain; positive charges are stored along the chain. Consequently, counterions are incorporated into the polymer and the polymer swells [52]. When polypyrrole is doped with large dopant ions, the anions are entrapped into the polymer chain and remain immobile. As a result, the charge is balanced by the cations from the electrolyte. During the reduction of polypyrrole, the cations are injected into the polypyrrole chain to neutralize the negative charge and results in polymer's (polypyrrole) expansion, while during oxidation cations are expelled from the polypyrrole chain that results in polymer (polypyrrole) contraction (Figure 2.5) [53]. According to Bay et al., [54] the volume change in conducting polymer (polypyrrole) is due to the movement of solvent molecules into the polymer. It can be concluded that the volume changes in conducting polymers (polypyrrole) during redox reactions is mainly due to the insertion of ions

between polymer chains. However, conformational change of the polymer (polypyrrole) backbone and solvent flux may also play a role.

Potential drop (iR) along a freestanding PPy film means that the region remote from the connection point experiences a lower applied potential and may not contribute to the redox reaction in the film. PPy has electric conductivity, but the actuator made from it has series resistance from one end to the other, which hampers the full performance of actuation. When contraction of an actuator occurs with de-doping, the conductivity becomes much lower, and as a result, the iR drop increases drastically. To avoid this type of problem one can provide an electrical contact along the entire length of the film, i.e. the conducting polymer has been placed on a metallized flexible supporting substrate in the form of a bi-layer. Hutchison et al. developed an actuator with increased actuation performance where conducting polymer was deposited on a metallized polymer substrate to get good electrical contact over the entire actuator [2]. However, this poses some problems. For example, the metal may corrode, react in the electrolyte, delaminate, or crack. In addition, it adds processing steps and expense to the production of actuators [55]. Bay and co-workers proved that in the presence of an additional complaint gold electrode a polypyrrole actuator showed actuation strain of 12% [56]. This design was aimed at reducing actuator iR drop and thus increased the performance of the actuator. However, the instability of the conducting polymer actuators is a great challenge for its application.

Polypyrrole-based actuators do not meet the requirements for its potential applications because PPy is neither soluble in common solvents nor thermally processable. Therefore, researchers have attempted to fabricate RC/PPy composites with improved processability and mechanical properties while maintaining the inherent electro-active properties of the

polymer [57]. Recently S. K. Mahadeva and Jaehwan Kim have developed an actuator consisting of regenerated cellulose/polypyrrole/ionic liquid. The actuator shows 1.4 mm bending displacement at 60% humidity [58]. However, the composites are still sensitive to humidity, actuation force is quite low, and the performance degrades with time [4].

In recent years, there has been considerable interest in using in situ chemical polymerization of pyrrole to produce conductive paper composite [59]. Researchers have found that the conductivity stability of cellulose–polypyrrole conductive paper composite depends on the types of dopants used [60]. In general, the conductive PPy composites are less stable in air due to their reactivity with oxygen [61]. This is due to the low oxidation potential of PPy. In addition, the redox reaction of PPy is more sensitive to the oxygen than those polymers that are more difficult to oxidize [7]. Researchers have reported that the conductivity stability of cellulose–PPy conductive paper composite in air depends on the preparation conditions, especially pyrrole concentration, oxidant charge and reaction time [59, 62]. Therefore, conductivity stability is an important parameter for successful industrial application of the paper composite in future. The conductivity stability of the paper composite is related to the oxidation of PPy. At elevated temperatures, there are chemical interactions between counterions and PPy and that lead to block charge carriers paths or shorten conjugated system. As a result, electrical conductivity decreases [7]. The decay of conductivity in air atmosphere is due to the chemical reaction of O_2 with double bonds in conjugated system [7]. In addition, the paper composite prepared from 1.5 g/L pyrrole shows the poorer stability compared to that prepared from 5 g/L pyrrole. This is because of the incomplete encapsulation of the cellulose fibers by the PPy particles that allows more oxygen to penetrate the composite [7].

2.1.3 Carbon nanofibers as fillers of the composites

Carbon nanofibers (CNFs) have experienced considerable interest from the researchers since 1980s because of their potential applications as polymer additives, and similarity in structure to fullerenes and carbon nanotubes. Carbon nanofibers possess a high degree of orientation of their graphitic basal planes parallel to the axes of the fibres [63]. They possess excellent mechanical strength and electrical conductivity [64]. Carbon nanofibers are hollow fibers with diameters ranging from 20-200 nm and lengths below 100 μm. They are produced from the catalytic decomposition of hydrocarbon gases over metal particles at temperatures over the range of 1000±400 °C. Carbon nanofibers are available in the powdered form [65]. The nanofibers possess a hollow core that is surrounded by a cylindrical fiber consisting of highly crystalline, graphite basal planes which are stacked at about 25 degrees from the longitudinal axis of the fiber (Figure 2.6) [36].

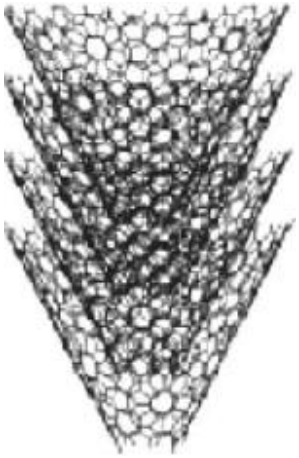

Figure 2.6: Structure of a four-nanocone-stacked CNF [36]

They have excellent mechanical properties, which make them attractive candidates as reinforcing materials [66] for the manufacture of lightweight, high strength composite materials for a wide range of applications such as actuation, sensing, and power generating. There is a difference in fiber structure between CNFs and carbon nanotube (CNT). The

CNFs have relatively linear fiber structure and higher diameter, than CNT [67]. The advantage of CNFs compared to conventional carbon fibers is that their higher aspect ratio, which is important to improve properties of the CNFs-based composites [68].

CNFs are hydrophobic. To improve processability or biocompatibility with a matrix, chemical functionality should be improved and this can be done by a variety of chemical processes. Therefore, in this study, an oxidative treatment of a mixture of boiling nitric acid and sulphuric acid (H_2SO_4/HNO_3) under reflux was applied to introduce carboxylic acid groups to provide sites for grafting different types of molecules to the surface of the nanofibers [69]. In addition, the mixture of concentrated H_2SO_4/HNO_3 has been used to cut nanofibers into shorter lengths [70]. It is generally believed that making the fibers shorter makes them less toxic. Toebes et al. [71] studied the oxidation of carbon nanofibers by HNO_3 and a mixture of HNO_3/H_2SO_4. The results revealed that the graphite-like structure remained intact after oxidation, however, the texture of CNFs changed significantly as indicated by an increment in pore volume. Generally, it is believed that the chemical modification of nanofibers starts from the defect sites. In the presence of strong oxidizing agents, the integrated graphene structure is also attacked to create additional defect sites that can subsequently react with the oxidizing agent [71]. Hence, the oxidation of carbon nanofibers depends on the defects, physical and morphological characters of the starting nanofibers.

In 2004, a carbon nanofibers containing hybrid actuator with increased strength and stiffness was developed, but those properties were inferior to the properties of carbon nanotube-based actuators [72]. Recently, a hybrid actuator consisting of CNF/PMMA (polymethylmethacrylate) has been developed. The actuator works in both aqueous

electrolyte and a solid polymer electrolyte (SPE) [73]. The SPE enables operation in a dry environment. The actuator, as it is not hydrated, shows slower actuation and the amplitude is small compared to the CNFs containing hybrid actuators working in aqueous electrolyte. In addition, dry CNF-based actuators require high voltage for actuation.

A CNF-based dry actuator was fabricated by Y. Yeo-Heung et al. [74] using a solid polymer electrolyte. The actuator shows increased actuation strain with the increase of applied voltage. However, too high voltage degrades the CNF dry actuator, and decreases its lifetime. Therefore, there is a limitation to increase voltage to achieve a high strain rate [74].

In this study, FCNFs are used with RC to improve electrical sensitivity, mechanical strength and compatibility properties of the composites. The main advantages of using carbon nanofibers over carbon nanotubes are that the material can be manufactured in large-scale. In addition to availability, there are also other issues such as cost (single-walled nanotubes still sell at around 100 USD per gram, compared to a few dollars/kg for carbon nanofibers) and compatibility [75]. Moreover, there are a few scalable methods for the synthesis of large-scale carbon nanotubes. Single-walled nanotubes (SWNTs) cannot yet be manufactured in reasonable volume. The amounts are still restricted to gram quantities and that limit their application. In addition, CNFs are smaller than MWCNTs, and incorporating the nanofibers into polymers is easier. Moreover, the toxicity of the functionalized carbon nanofibers was significantly lower than the toxicity of functionalized carbon nanotubes [76].

The charge injected into the valence or conduction band of CNFs causes mechanical deformation. In addition, electrochemical property of CNFs can generate large strains/forces at low voltages. Therefore, electrochemical property of CNFs is considered promising for actuation [77].

2.1.4 Ionic liquids as solvent/electrolyte of the actuators

Molten salts are termed as ionic liquids (ILs**)** as they melt below 100 °C. ILs consist of organic cations, such as alkylimidazolium $[R_1R_2IM]^+$, tetraalkylammonium $[NR_4]^+$, and anions, hexafluorophosphate $[PF_6]^-$, and tetrafluoroborate $[BF_4]^-$. Ionic liquids (ILs) exist in the liquid state below 100 °C because the ions in the ionic liquids are poorly coordinated [78]. Ionic liquids have at least one ion in its delocalized charged form and one component is organic, which prevent the formation of a stable crystal lattice. In addition, ionic liquids have some distinguishing properties such as non-volatility, high stability, suitable polarity, high ionic conductivity, and easy recycle ability [79]. Moreover, their presence causes lower energy consumption in numerous electrochemical processes [80]. Due to their distinguishing properties, ionic liquids are receiving enormous attention as environmentally benign solvents for electrochemical applications. Recently, they have been involved in the development of biopolymers, [81] and actuators [82]. ILs have received intense focus due to their lack of volatility. This non-volatile nature makes them potential alternatives to the conventional volatile organic solvents [80]. Ionic liquids are advantageous for rapid responses in actuation because of their special features such as non-volatile, high ionic conductivities and wide potential windows [21].

All ILs are hygroscopic and are capable of absorbing water from the atmosphere. Suresha et al. [83] worked on the effect of room temperature ionic liquids on the electromechanical behaviour of ionic liquid adsorbed cellulose electro-active paper [22]. He observed that the actuator showed ~62.9 % performance degradation at 50 % relative humidity after activating for 11 h. This might be due to the removal of highly hygroscopic 1-butyl-3-methylimidazolium tetrafluoroborate ($BMIMBF_4$) from the surface of the actuator [22]. Consequently, it limits its application at the highly humid conditions.

The toxicity of ILs increases with increase in the length of the alkyl side chain. This is due to an increase in lipophilicity. Therefore, it is recommended to work with the shorter methyl side chain on the cation core wherever possible [84].

The following review focuses on the different types of drug delivery carriers and the mechanism controlling the drug release from the carriers, structure and biocompatibility of the drug carriers, and future prospects.

2.2 Drug delivery

Drug delivery is a process of administering drugs into our body to obtain a maximum therapeutic effect over desired time. Several possible routes by which drugs can be introduced into our body are the oral route, the injection, and the transdermal route. Oral and injection routes may provide the maximum tolerable dose initially but the dose decreases over a short time period [85]. Transdermal route is advantageous to avoid the first-pass metabolism (a phenomenon of drug metabolism whereby the concentration of a

drug is greatly reduced before it reaches the systemic circulation) and to provide on-demand release of drug to the targeted area of the body. However, Transdermal Drug Delivery (TDD) is suitable for introducing a low amount of drug because of the extremely low drug release rate from the matrices and the low permeability of drug through the skin. Therefore, the use of an electric field on the drug carrier is an effective measure (termed as iontophoresis) to enhance the amount of drug release and the precise control [86]. The advantage of using transdermal iontophoretic technique is that it is capable of administering drugs in a pulsatile pattern by alternately applying and terminating the current input at a programmed rate. As a result, it helps avoiding from chemical burn caused by high current density [87].

The methods of drug delivery include targeted delivery in which the drug is only active in the targeted area of the body and controlled release formulation in which the drug is released over a period of time in a controlled manner from a formulation.

During the last decades polymer based pharmaceutical drug carriers offer numerous advantages such as improved efficiency and reduced toxicity [88] compared to conventionally administrated drugs in dosage forms. Conventional dosage forms have some disadvantages such as [88]

- Difficulty in controlling both the rate of drug delivery and the target area of drug administration
- Provide a rapid and an immediate drug release. Therefore, frequent administration is required in order to maintain a therapeutic level, which in turn causes drug concentration in the blood

It is desirable to an initially high release of drug, followed by a gradual decrease with time over longer period. In addition, in some cases there might be required a slow release of a water-soluble drug or a fast release of low-solubility drugs [88]. Orally administered drugs or injections have limited control on the rate of drug release. In addition, they have harmful side effects and toxicity. The controlled delivery of a drug is a suitable route to eliminate the above drawbacks. In controlled delivery, the drug delivery may commence with first-order kinetics and then followed by zero-order kinetics [89]. This can be achieved if the drug carrier responds well to an electric or magnetic stimulus.

The advantages of localized biodegradable implant include [16]

- High drug concentration at the site of infection
- As the implant is biodegradable, it is not necessary to remove the implant after treatment
- Implant would help minimize toxic side effects and compliance problems that might occur due to prolonged oral antibiotic therapy [90]

An Ideal drug delivery carrier should be biodegradable, biocompatible, mechanically strong, comfortable for the patient, capable of loading drugs in high concentration, and easy to fabricate [16].

Drugs are loaded over the matrices by means of chemical linkage, surface adsorption, and physical entrapment during the preparation of the matrices or after the formation of the matrices by incubating them with the drug. The method of preparation, nature of the drugs,

and carriers play an important role on entrapment of drug. Maximum loading of drugs can be achieved during the time of preparation but the method of preparation, presence of cross-linking agent, and heat of polymerization etc. may affect it. However, it is important that the carrier must be biodegradable and can be eliminated by the physiological processes [91].

Drug delivery systems can be classified according to the mechanism controlling the drug release: [92]

(1) Diffusion-controlled

(2) Chemically controlled

(3) Swelling-controlled

(4) Magnetic field-induced

(5) Electrically responsive

2.2.1 Diffusion-controlled devices for drug delivery

Two types of diffusion-controlled devices are generally used in drug delivery. These are reservoir typed devices and matrix typed devices. In this study, matrix (monolithic) typed devices have been used (Figure 2.7). In matrix typed devices, drug is dispersed as solid particles within the matrices. Matrix typed devices are superior over other design for their low manufacturing costs, and lack of accidental dose dumping [93].

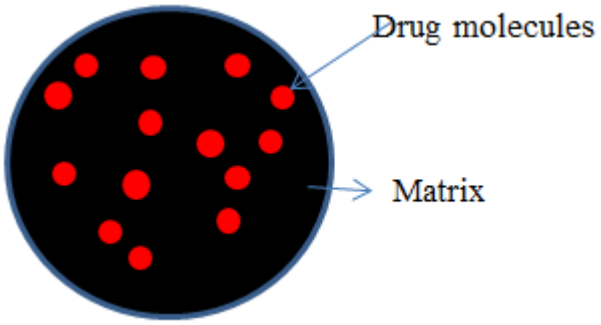

Figure 2.7: A matrix (or monolith) device

The fractional release of a drug from a matrix typed one-dimensional porous system can be described using Fick's second law (2-1). Fick's second law states that how the concentration within the diffusion volume changes with respect to time [88].

$$\frac{\delta c}{\delta t} = D.\Delta c \qquad (2\text{-}1)$$

Where, c is the concentration, D is the diffusion coefficient, and t is the time.

Mathematical models are good tools for understanding drug release from matrix typed devices. In 1961, Higuchi proposed the following equation ((2-2) to predict drug release rate from a matrix typed device with a flat geometry as [94]

$$\frac{M_t}{A} = \sqrt{[DC_S\,(2C_0 - C_s)t]} \ldots for\ C_0 > C_s \qquad (2\text{-}2)$$

Where, M_t is the cumulative absolute amount of drug released at unit time t; A is the surface area of the layer exposed to the drug release medium; D is the diffusion coefficient of the drug in the material and C_0 and C_s respectively represent the initial concentration and the solubility of the drug in the material.

Eq. ((2-2) can be expressed as

$$\frac{M_t}{M_\infty} = k\sqrt{t} \qquad (2\text{-}3)$$

Where, M_∞ is the absolute cumulative amount of drug release at infinite time. It should be equal to the absolute amount of drug incorporated within the system at time t = 0, and k is a constant reflecting the design variables of the system. Thus, the fraction of drug released is proportional to the square-root-of-time. When applying them to controlled drug delivery systems, the assumptions of the Higuchi derivation should be considered [95].

i) The initial drug concentration in the system is much higher than the solubility of the drug
ii) The particles are much smaller in diameter than the thickness of the system
iii) Swelling or dissolution of the polymer carrier is negligible
iv) The diffusivity of the drug is constant
v) Perfect sink conditions are maintained

Korsmeyer and Peppas developed a widely used model for analysing diffusion-controlled release data, comprising a simple empirical equation: [96]

$$\frac{M_t}{M_\infty} = kt^n \qquad (2\text{-}4)$$

Where, M_t is the amount of drug released at time t; M_∞ is the amount of drug released at infinite time; n is the diffusion constant indicating the release mechanism, and k is the kinetic constant. The value of the exponent n provides information regarding the drug transport mechanism. When $n = 0.5$, the drug release mechanism is based on Fickian

diffusion and $n = 1$, the drug release mechanism is swelling controlled. Values of n between 0.5 and 1 indicate anomalous transport. If the glass transition temperature Tg of the polymer is well below the experimental temperature, the polymer chains will have a high mobility that in turn allow easier penetration of the solvent into the drug-loaded film and release of the drug molecules into the release medium. The drug release mechanism corresponds to Fickian diffusion, where drug diffusion rate is slower than the polymer chain relaxation. If the experimental temperature is below Tg, polymer chains are not sufficiently mobile to permit immediate penetration of the solvent into the polymer core. This fact gives rise to a non-Fickian diffusion process [92].

Drug release from hydrophilic matrices involves the following processes [12]:

- Entry of water into the matrices
- Swelling of the matrices
- Dissolution and diffusion of the drug towards the outside of the matrices

Generally, drug release rate varies with the square-root-of-time [93]. Although, matrix swelling favours drug release, it causes strong resistance to drug diffusion through the gel layer. As a result, the drug release rate decreases with time [97]. For water-soluble drugs, the diffusion process controls the release of drug. Matrix typed devices do not usually provide zero-order drug release properties. This is due to the drug molecules in the centre of the device take a longer time to migrate longer distances compared to the drug molecules at the surface of the device. This increased diffusion time that results in a decrease in the release rate from the devices with time [97].

2.2.2 Swelling-controlled devices for drug delivery

In a system controlled by swelling, a swelling-driven phase transition from a glassy state to rubbery state is observed [98]. This happens when glass-rubber polymer transition temperature is lower than temperature of fluid, which surrounds the drug delivery matrix. In the glassy state, entrapped molecules remain immobile whereas in the rubbery state dissolved drug molecules rapidly diffuse to the fluid through the swollen layer of polymer. In these systems, gel swelling controls the rate of drug release [92].

For hydrophilic matrices, in the early phases, polymer swelling rate and drug release are being controlled by Fickian kinetics, and both processes occur rapidly and the rate decreases with time [99].

2.2.3 Chemically controlled drug delivery systems

The release of a drug by the chemically controlled systems generally takes place in the aqueous environment by one or more of the following mechanisms [92]:

- Gradual biodegradation of a drug-loaded polymer system
- Biodegradation of unstable bonds by which the drug is coupled to the polymer system
- Diffusion of a drug from injectable and biodegradable micro-beads

In Bio-erodible and biodegradable systems, the polymer erodes because of the presence of hydrolytically or enzymatically labile bonds. As the polymer erodes, the drug is released to the surrounding medium. The main advantages of such biodegradable systems are the elimination of the need for surgical removal. However, all biodegradable products must be

non-toxic, and non-carcinogenic [92]. These requirements are not easily met. Many anticancer drugs should be released to the affected site only in order to protect normal cells from possible side effects, because of their cytotoxicity. Therefore, their attachment with polymers could be a promising approach to reduce overall toxicity.

2.2.4 Magnetically controlled drug delivery systems

Magnetic field-induced targeted drug delivery is currently gaining significant attention from researchers [100]. There are three types of drug targeting include passive, active or physical. In passive targeting, the properties of drug and carrier are responsible for the distribution of drugs within the body. Active targeting allows drugs and carriers to specific cells through specific recognition mechanisms. In physical targeting, the distribution of drugs occurs through carriers induced by external stimuli, such as magnets in the case of super paramagnetic iron oxide nanoparticles (SPION) [101]. The principle of drug delivery by magnetic carriers is based on the use of both constant and high frequency oscillating magnetic fields. The carriers can be fabricated by one of the two structural configurations: (i) a magnetic particle core coated with a biocompatible polymer or (ii) a porous biocompatible polymer in which magnetic nanoparticles are dispersed inside the pores [102]. A constant magnetic field provides targeted drug delivery, while an alternating current magnetic field is responsible for the controlled release of encapsulated drug. The importance of using magnetic nanoparticles is to use localized magnetic field gradient to hold the particles to the desired location until the therapy is completed [103].

Drug release from polymer/magnetic particles composite under magnetic field is based on the fact that heat produced locally by magnetic particles under alternating current (AC)

magnetic field loosens the polymer strands surrounding the particles at temperatures above the glass transition temperature (Tg) of that particular polymer, resulting in encapsulated drugs released [92]. Magnetic fields are suitable for biological applications because biological fluids do not screen them. In addition, they do not interfere with most biological processes [104].

In recent years, researchers are trying to develop materials that are both magnetic and electrically conductive and can be used as suitable substrates for drug delivery when stimulated by electric and or magnetic fields [105]. Electrically conductive macromolecules such as polypyrrole containing metal oxide nanoparticles have been prepared and investigated [106]. However, these nanocomposites possess low electrical conductivity, low magnetization values and lack of well-defined shape. For drug delivery etc., the nanoparticles must have the combined properties of high magnetic saturation, biocompatibility and interactive functions at the surface. These particle surfaces could be modified by coating a few atomic layers of organic polymer suitable for further functionalization by conjugating with various bioactive molecules [107].

Local inflammatory processes characterize many of the diseases in the musculoskeletal system. They can be treated with anti-inflammatory drugs [108]. However, these oral drugs have some side effects such as gastric ulcers or bleeding tendencies. Maintaining drug concentrations is another problem. Magnets in association with carriers containing super paramagnetic iron oxide nanoparticles (SPION) help delivering drug to inflammatory sites to maintain appropriate concentrations and allow magnetic field with on and off switching, thus targeting the particles at the local site [109]. Gamma ferric oxide nanoparticles having diameter < 50 nm is termed as SPION. They have magnetic properties because of the

presence of aligned unpaired electron spins. They show magnetism even in the absence of external magnetic field [110].

2.2.5 Electrically/electro-chemically controlled drug delivery systems

The migration of charged molecule from a hydrated membrane is performed by the combined effect of the electrical forces on the solutes and counterions from the adjacent electrolyte solution. It is a different approach of drug delivery based on polymers, which bind and release bioactive compounds in response to electrical signal. The polymer, which has two redox states, shows electro-chemically controlled drug release. Under electric field, drug ions bound in one redox state of the polymer are released from the other. The electrode attached with the film acts to switch the redox states and the amount of drug ions released depends on the amount of current passed [111].

2.2.5.1 Transdermal drug delivery by iontophoresis

Recently iontophoresis has been developed as a physical skin penetration enhancing method for delivering high molecular weight drugs through skin [112]. This technique facilitates movement of ions across the membrane under the influence of an externally applied electric field. It has an advantage over passive diffusion, as it is capable of delivering drugs across the dermal barrier by 3 to 4 orders of magnitude [113]. Transdermal device acts as a drug reservoir and controls the rate of drug transfer instead of skin. This technique is capable of administering drugs in a pulsatile pattern by alternately applying and terminating the current input at a programmed rate [87].

Nicotine Patch is the America's first commercially marketed transdermal patch. It uses a passive mode of drug delivery that permits drugs to diffuse through a vascular dermis to the deep dermis. This approach depends on the physicochemical properties of the drug's, which facilitates transport drug molecules through the skin by using a simple concentration gradient as a driving force. All the available transdermal delivery systems use passive technology. In addition, few drugs are available with the right physicochemical properties. Even with these limitations, passive transdermal patches are gaining worldwide acceptance. Drugs with large molecular weight, such as, proteins and peptides, cannot be transported through this technique [112]. While delivering a negatively charged drug across a biological matrix, the drug-loaded matrix is placed between the negative electrode (cathode), and the skin (Figure 2.8) [114]. The drug ion is then attracted through the skin towards the positive electrode (anode) placed elsewhere on the body by the electromotive force provided by the cell. Similarly, cationic drugs enter the skin when the matrix is attached with a positively charged electrode. Iontophoresis helps in achieving enhanced transport of solutes by three additional mechanisms besides the pure diffusion. First, the ion-electric field interaction that drives ions through the skin; secondly the electrical flow that increases permeability through the skin; thirdly the electro-osmosis that carries ionic or neutral solutes with the blood stream [115]. Iontophoresis may have potential application for the effective delivery of peptide and protein drugs, since these compounds exist in a charged form at physiological pH. Without iontophoresis charged species are incapable of transdermal penetration because of the skin's lipophilic nature [112].

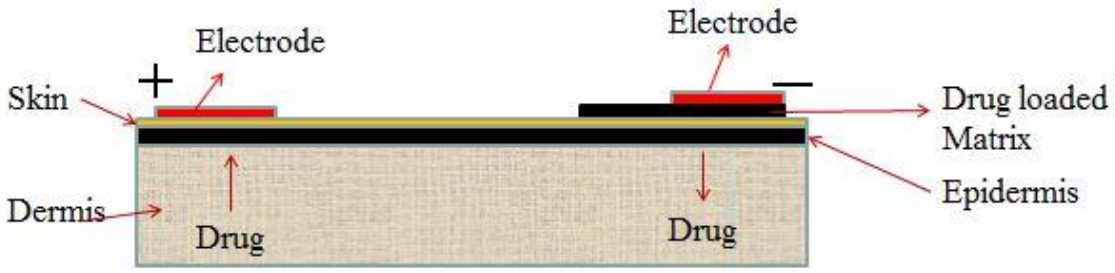

Figure 2.8: Transdermal iontophoretic technique [116]

The advantages offered by the iontophoretic technique can be summarized as follows [112]:

i) Delivery of both ionized and neutral drugs
ii) This technique is capable of administering drugs in a pulsatile pattern by alternately applying and terminating the current input at a programmed rate
iii) Restoration of the skin barrier functions without producing severe skin irritation
iv) Charged as well as high molecular weight drugs can be delivered
v) Reduce frequency of dosages
vi) Self-administration is possible

The disadvantages of iontophoretic technique can be summarized as follows**:**

- There is a possibility of chemical burn caused by the high current density and time of application as that generate extreme pH [111]
- High current density causes electric shocks at the skin surface [117]

2.3 Factors that impact the performance of implantable devices

This chapter will review on the several major factors that have impact on the performance of implantable devices such as, (i) drug reservoir size and loading volume (ii) effective delivery method, (iii) operating time, (iv) controllability of the device and (v) biocompatibility of the device [118-120]. Small sized devices are suitable as minor surgery (local anaesthesia) is required for implantation.

Actuation-less methods are based on diffusion to release drug. However, this approach depends on external stimuli. Li et al. [121] have developed an electrochemical micro pump in which electrolysis of water builds up pressure within the reservoir and helps transporting drug solution to the target site. However, electrolysis of water may cause degradation of the drug within the reservoir [122].

Powering small sized implants for a long time is an issue [123]. Najafi et al. [124] developed an magnetic field induced actuator. The drawback of this device is, as it is remotely controlled, it increases the operating time of the device. However, since the implant situated deep within the body, may not be magnetically induced perfectly [125].

The biocompatibility of the implant is an important factor as they interact with the tissues in the body [126]. Coating around the implants is required in order to prevent biofouling. Consequently, it increases the size of the device [127]. In addition, rigid implants with increased size can cause inflammation [128] at the implant site. Therefore, flexibility is an important parameter while choosing materials for implant. Cellular adhesion on coating material is also important. An ideal implant must be small sized, capable of holding large

enough drugs and long device lifetime to reduce the complications associated with replacing these implants [125].

2.4 Summary

The existing actuators fabricated from regenerated cellulose have several drawbacks such as: [129]

- Sensitive to environmental humidity
- They show little displacement output at ambient humidity
- Force output and frequency are also small
- Low conductivity limits the speed and amount of actuation
- The polymer actuates in region closest to the contacts where the voltage is the largest
- Performance of the actuators degrades with time

To overcome these drawbacks, the following strategies can be undertaken

- Layer-by-layer structure with outer layers act as electrodes; gold or platinum coating is not required to make the material electro-active
- Using conductive fillers- to improve their electrical sensitivity, mechanical strength and compatibility properties
- Built-in ionic liquid electrolyte layer may provide the durability of the actuators
- Improve the capacitance of the material in order to increase the bending displacement of the actuators

The currently available drug delivery techniques have a number of shortcomings. The controlled drug delivery through an implant may be an appropriate route to eliminate the above drawbacks. In controlled drug delivery, the drug is released initially to the targeted region with first-order kinetics followed by zero-order kinetics. This can be achieved if the drug carrier responds well to an electric or magnetic stimulus. This thesis proposed a method of developing drug delivery carriers working under external stimuli such as electric and alternating current magnetic field to achieve kinetics of zero order. In addition, this thesis proposed an alternative method of iontophoretic technique, where, the drug-loaded matrix can be implanted subcutaneously (Figure 2.9). Moreover, this research aimed at investigating electro-chemically controlled release system developed from regenerated cellulose-based electro-conductive composite matrices. It is a different approach of drug delivery based on polymers (polypyrrole), which bind and release drugs in response to electrical signal.

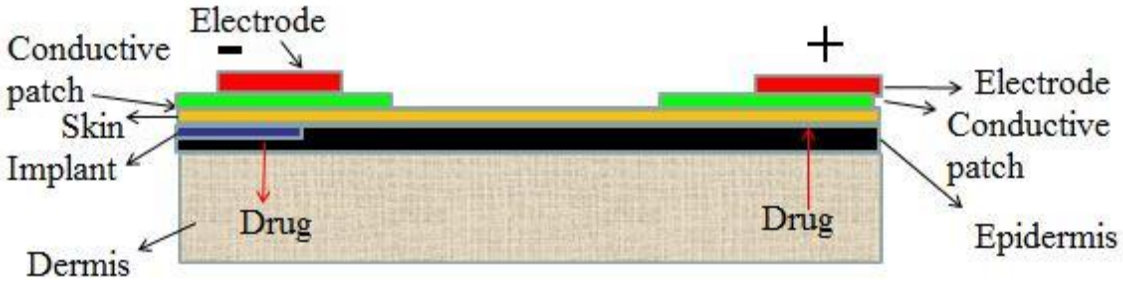

Figure 2.9: Transdermal iontophoretic technique on implants

The applications of this technique may help in enhancing the drug release rate compared to the other techniques. This approach is expected to offer the significant benefits in terms of zero-order drug delivery, as zero-order drug delivery maintains a safe and constant concentration of drugs inside the body.

2.5 Specific objectives

Although the general objectives of this work are spelled out in chapter 1, the specific objectives may be summarized as follows:

- Develop regenerated cellulose-based electro-conductive composites with improved conductivity and mechanical strength using functionalized carbon nanofibers as fillers
- Investigate the properties of the materials which are developed by different preparation processes
- Test the actuation performance of these materials in terms of bending displacement, actuation force, mechanical strength, and power consumption
- Design layer-by-layer structure where electrode and electrolyte layers are seamlessly connected with one another to improve the actuation performance
- Using non-volatile ionic liquids as electrolytes to enhance the durability of the actuators
- Develop drug carriers which respond well under both electric and magnetic fields to precisely control the drug release rate
- Investigate the feasibility of using iontophoretic technique to facilitate the drug release rate from the matrices
- Investigate the feasibility of using alternating current magnetic field to control the drug release rate from the matrices, as contactless actuation is superior to the electric field induced actuation
- Analyse the results and give final recommendations

Chapter 3 **Regenerated cellulose-based actuators**

3.1 Introduction

Actuators that can be operated at low voltages are highly desirable for better biological compatibility and higher safety standards. The main objective of this work is to develop regenerated cellulose-based actuators with improved electrical conductivity and durability. Consequently, they can be operated at lower voltages compared to the other electro-active actuators. In this study, regenerated cellulose/ ionic liquid/ polypyrrole (RC/IL/PPy blend) actuators are developed with a view to compare the performance of the actuators with the actuators consisting of RC/PPy/IL (nanocoating) developed by Suresha et al [130]. In addition, regenerated cellulose/ functionalized carbon nanofibers/ polypyrrole (RC/FCNF/PPy coated) and RC/FCNF/PPy (blend) actuators are developed with different preparation processes to compare their performances in terms of electrical conductivity and bending displacement. This chapter presents the theory of actuation mechanisms, and preparation processes of regenerated cellulose-based electro-active composites by combining carbon nanofibers, conducting polymers, and ionic liquids (through blending, doping, or coating). This chapter also presents the assessment of the performance of the actuators in terms of bending displacement, actuation force, and power consumption. Further, the techniques used for characterization of the composites are presented.

3.2 Actuation Mechanism

The RC/IL/PPy actuator consists of electrolyte layer sandwiched by electrode layers. The outer polypyrrole layers act as electrodes. Ionic liquid dispersed regenerated cellulose acts as the electrolyte layer.

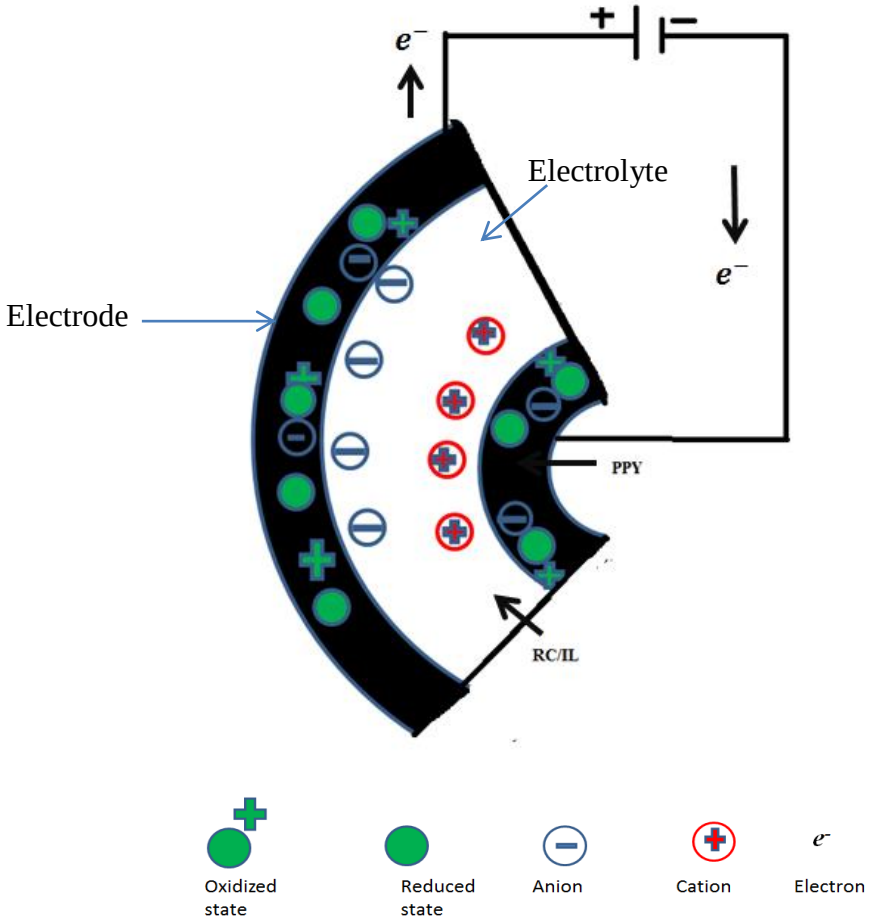

Figure 3.1: Bending of the RC/IL/PPy actuator upon application of an electric potential

The actuation mechanism in RC/IL/PPy (coated) actuator is based on ion migration (see Figure 3.1). Two additional factors are also contributed towards the actuation behaviour. An electric field applied across the actuator creates an electric double layer at the electrode-electrolyte interface on the anode side. That can be treated like a double-layer capacitance. Then the anions (from the electrolyte) driven into oxidize the PPy layer, and cause it to

expand, while the other PPy layer on the cathode side are reduced and contract. This differential expansion results in bending actuation (Figure 3.1.)

The actuation principle of RC/FCNF/PPy (coated) actuators can be divided into two parts. The first part is the combined effect of piezoelectricity and ion migration associated with cellulose EAPap. The second part includes two additional effects associated with PPy layers. The first additional factor is the dimensional changes due to applied voltage causing adsorption and desorption of water molecules in the film structure. The second factor is the structural changes in conducting polymer films due to the application of electric field.

RC/FCNF/PPy actuators (blend) operate through different mechanisms. It is well known that actuation of FCNFs depends on the non-faradaic electrochemical charging of the FCNFs, while the actuation of polypyrrole depends on the redox reactions. The actuation of RC/FCNF/PPy actuators governs by the loading of FCNFs and PPy in the composites. The ratio of FCNF and PPy in the composite is 3: 2. The actuation principle of the composite is based on mainly ion migration. In a humid condition, carboxylic group containing FCNFs enhances water retention of RC, and that results in movement of Cl^- ions in the composite.

In this research, coating of PPy on RC/IL and RC/FCNF films was proposed to enhance the performance of the actuators. The polypyrrole coating has several advantages [131]:

- The conductive state of PPy that can exert its contraction and expansion to enhance the bending actuation of the actuators
- PPy coating can absorb moisture that would also improve the performance of the actuators

- Coating enhances the mechanical stiffness of the actuators, consequently, it increases the force output of the actuators

In this study, sonication process was employed to disperse FCNFs in RC solution. Sonication is a process of sound energy to agitate particles in a sample. Sonication process plays an important role in improving the interaction between FCNFs and RC by disentangling agglomerated FCNFs, which occur due to the Van der waals force between them. Improved interaction may reduce the electrical conductivity of the composites. However, sonication causes aggregated FCNFs disentangled and makes them well covered with the PPy [131].

Generally, carboxyl groups are introduced on the surface of CNFs by acid treatment. The groups on FCNFs can form hydrogen bonds with hydroxyl groups of cellulose (Figure 3.2). As a result, FCNFs can be dispersed in the layered structure of cellulose [34].

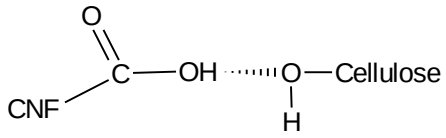

Figure 3.2: H-bonding between –OH group of cellulose and –COOH group of CNF

3.3 Actuators structure

The structures of the RC/FCNF/PPy (blend), RC/FCNF/PPy (coated) and RC/IL/PPy (coated) actuators are shown in Figure 3.3. Each of the actuators was clamped with two copper electrodes at one end of the actuator strip. The thickness of the RC/FCNF/PPy (blend) actuators is 40 μm. For RC/FCNF/PPy (coated) actuators, the thickness of the RC/FCNF layer is 30 μm. RC/IL/PPy (coated) actuator, the electrolyte layer in the middle is RC/IL with a thickness of 30 μm. The total thickness of the two-polypyrrole layers for the actuators (b) and (c) is 10 μm.

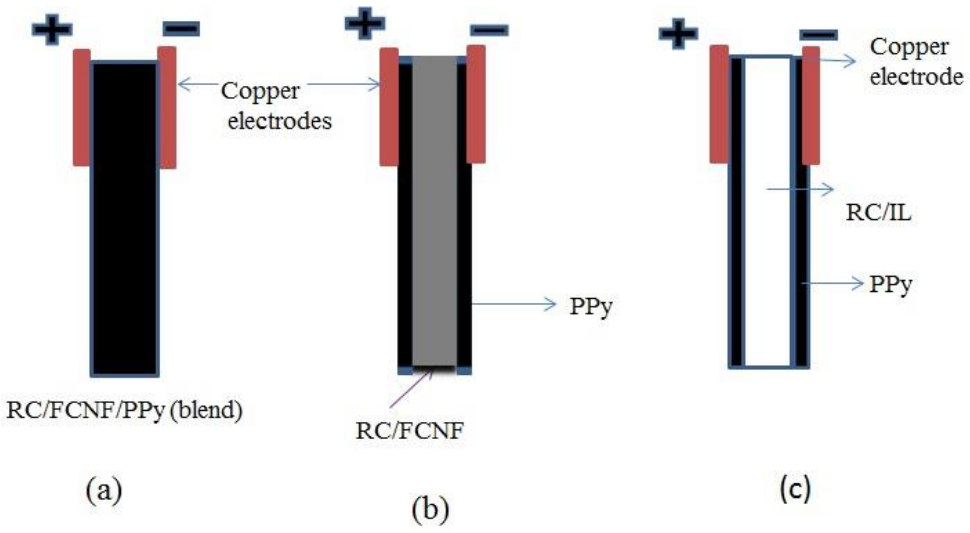

Figure 3.3: Structure of (a) RC/FCNF/PPy (blend) actuators, (b) RC/FCNF/PPy (coated) actuators, and (c) RC/IL/PPy (coated) actuators

3.4 Preparation of regenerated cellulose-based composites

In this study, three different types of regenerated cellulose-based composite films were prepared by different preparation processes.

(1) Regenerated cellulose/ionic liquid/polypyrrole (RC/IL/PPy) composite actuator films were prepared by

- Solution blending to disperse ionic liquid in regenerated cellulose solution and casting films
- The composite films were coated with polypyrrole electrode by chemical polymerization-induced adsorption process

(2) Regenerated cellulose/functionalized carbon nanofibers/polypyrrole (RC/FCNF/PPy) composite actuator films were prepared by

- Blending FCNFs in RC solution and casting films
- The composite films were coated with polypyrrole electrode by chemical polymerization-induced adsorption process

(3) RC/FCNF/PPy (blend) actuator films were prepared by blending FCNFs and PPy in RC solution and casting films.

3.5 Composite films preparation

3.5.1 Reagents and materials

1-butyl-3-methylimidazolium chloride (99 %, HPLC) is from Fluka, USA. Dimethylacetamide (DMAC) (Anhydrous 99.8 %), 2-propanol, lithium chloride, cotton linter (DPW 4580), carbon nanofibers, pyrrole, anthraquinone-2-sulfonic acid sodium salt monohydrate, 5-sulfosalicylic acid dihydrate, and ferric chloride hexahydrate were purchased from Sigma Aldrich, USA. All the chemicals were used as received except pyrrole. Freshly prepared pyrrole was used during polypyrrole synthesis.

3.5.2 Preparation of regenerated cellulose solution

2 g cotton linter and 8 g lithium chloride were heated under reduced pressure at 110 ^{0}C for an hour before use. In a two neck round bottomed flask, 90 mL dimethylacetamide heated at 65 ^{0}C. Lithium Chloride was then added and the mixture was heated to 100 ^{0}C until dissolved. Cotton Linter was then added and the mixture was heated at 155 ^{0}C for 30 min, followed by cooling to 40 ^{0}C for 2 h. From this process, a transparent solution was obtained [25].

3.5.3 Preparation of ionic liquid dispersed RC films

Ionic liquid dispersed cellulose films were prepared using a solution blending technique. Ionic liquid (20 % w/v) was mixed with 10 mL previously prepared RC solution under mechanical stirring for 24 h. 4.5 g of the clear mixture solution was then poured in a 10 cm petri dish. The films were allowed to cure for 24 h in an ambient atmosphere. The films

were then washed in a mixture of deionized water and isopropyl alcohol of ratio 40:60 for 24 h. Finally, the films were soaked in DI water for 6 h and dried in air.

3.5.4 Coating of polypyrrole on ionic liquid dispersed RC films

Conductive polymer (polypyrrole) electrodes were deposited on both sides of the films by an adsorption-induced chemical polymerization technique. First, 9.3 g anthraquinone-2-sulfonic acid, sodium salt monohydrate, 5.34 g 5-sulfosalicylic acid dihydrate and 16.21 g ferric chloride hexahydrate ($FeCl_3.6H_2O$) were dissolved in 100 mL distilled water. 2.1 mL pyrrole was then dissolved in 100 mL distilled water and was poured into the above solution. Ionic liquid containing regenerated cellulose films were then immediately immersed in the polymerizing pyrrole solution for 40 min allowing in situ deposition of conductive polypyrrole on both sides of the films under ambient laboratory conditions. The films were then removed from the polymerizing solution, rinsed with distilled water, and dried in vacuum. The resultant polypyrrole electrodes were smooth, and adhered well to the ionic liquid containing cellulose films [132].

3.5.5 Functionalization of carbon nanofibers (CNFs)

Functionalized carbon nanofibers were synthesized by the following procedure. 240 mg carbon nanofibers were added to a mixture of 100 mL HNO_3 [2.4 M] and 100 mL H_2SO_4 [7.6 M] and sonicated for 10 min. The mixture was then refluxed for 3 h at 100 °C. After filtering through 0.2 μm glass-fiber filter, the acid treated nanofibers were washed with deionized water until pH ~ 7. The resulting nanofibers were dried under vacuum for 12 h at 60 °C [34].

3.5.6 Fabrication of RC/FCNF/PPy (blend films)

RC/FCNF/PPy films were fabricated as follows. 0.31 g polypyrrole was dispersed in 20 mL DMAC (Dimethyl acetamide) by ultrasonication for 1 h to make the stock solution. 0.12 g FCNFs were then dispersed in 50 mL previously prepared regenerated cellulose solution. From the stock solution, 5.5 mL solution was mixed with the FCNFs dispersed regenerated cellulose solution. The mixture was then sonicated for 5 hours for homogenisation. After that, the mixture was poured on a glass petri dish to cast films. The films were left 24 h in an ambient atmosphere to remove solvent. The films were then washed in a mixture of deionized water and isopropyl alcohol of ratio 40:60 for 24 h. Finally, the films were soaked in DI water for 1 h and dried in air.

3.5.7 Fabrication of RC/FCNF/PPy (coated)

First, 0.21 g FCNFs were dispersed into 10 mL dimethylacetamide. The resulting solution was added to 20 mL previously prepared RC solution. After ultrasonic dispersion (125 W) for 4 h, the RC/FCNF mixed solution (3.5 g in a 10 cm petri dish for each film) was poured on a glass petri dish. The solvent was evaporated and the films were dried in air. The films were then coated with polypyrrole similar to the method described in subheading 3.5.4.

3.6 Techniques used for polymer characterization

The actuation mechanism is mainly based on material properties. Characterization of these properties with respect to actuation has been one of the focuses of the current work. Electrical, chemical, mechanical, and morphological properties of the composite films were analysed by conductivity measurement, infrared absorption spectra (FTIR), vertical tensile

tester, and scanning electron microscope (SEM). In the following sections, the functions of these equipment and devices are briefly explained.

3.6.1 Electrical conductivity measurements

Electrical conductivity (σ_s) of the films was calculated using the following equation:

$$\sigma_s = \frac{\Delta I}{\Delta V}\frac{l}{wd} \tag{3-1}$$

Where, $\Delta I/\Delta V$ denotes the slope of the current versus voltage curve, l is the length, w is the width and d is the thickness of the samples. Prior to measurement, silver paste was painted at the ends of the rectangular sample to ensure good electrical contact. The voltage (V) was swept between 2-5 V and the resulting dc current (I) was measured.

3.6.2 Thermo-Nicolet iS10 Fourier transform infrared spectrometer

The Thermo-Nicolet iS10 (Thermo Scientific) (Figure 3.4) is a research-grade Fourier transform infrared spectrometer. It has both transmission and attenuated total reflectance (ATR) accessories. It can provide data in both transmission and absorbance modes using a standard transmission accessory. Attenuated total reflectance (ATR) accessory, which can be used for acquiring spectra of liquids and solids for a variety of applications.

Figure 3.4: Nicolet iS10 FTIR Spectrometer

The attenuated total reflectance (ATR) accessory consists of a diamond crystal in the centre of the plate through which an IR beam is focused from underneath, bouncing off the crystal face (internal reflectance). A sample pressed on the face of a crystal can be examined because the IR beam that is bounced through the crystal penetrates a few microns past the surface of the crystal and into the sample. Thus, an IR spectrum can be acquired for a sample.

The FTIR spectra were obtained by using spectrometer with KBr beam splitter, detector with resolution 8 cm^{-1}, in the spectral region from 4000 to 525 cm^{-1}, and 32 scans per sample. Data acquisition and analysis were performed using standard software (Omnic).

3.6.3 Scanning electron microscopy (SEM)

To study the morphological difference of the composite films, scanning electron microscopy (SEM) images of the films obtained from a scanning electron microscope [Hitachi SU-70 FE SEM (field emission scanning electron microscope)] (Figure 3.5) were used. The technique involves scanning an electron beam across the sample surface and

secondary electrons are ejected from the surface. When interact with a solid, secondary electron images are generated by synchronizing the optical output of the detector system with the raster of the electron probe across the solid surface. SEM images are used to examine the surface morphology and fracture cross section.

Figure 3.5: Hitachi SU-70 FE SEM (field emission scanning electron microscope)

3.6.4 Measurement of Tensile strength and elongation at break

Tensile strength and elongation at break are the two most important mechanical properties of regenerated cellulose-based composite films. Tensile strength (TS) is a measure of the maximum stress developed in a film during elongation. Elongation at break is the maximum change in length of a film before breaking. Factors, such as the composition of the film, temperature, and relative humidity can affect tensile properties.

Tensile test specimens were prepared by cutting the RC/FCNF/PPy (blend) films into 8 mm wide and 70 mm length strips using a precise cutter. The tensile test was conducted using

Vertical Tensile Tester: Tinius Olsen, Model: H50KS, according to ASTM D-882-97 as a standard method used. Two ends of the specimen were fixed between upper and lower jaws of the instrument, (Figure 3.6) leaving a length of 50 mm of the film in between the two jaws. The extension speed was 3.0 mm / minute. Three samples were tested for each case and average values were used.

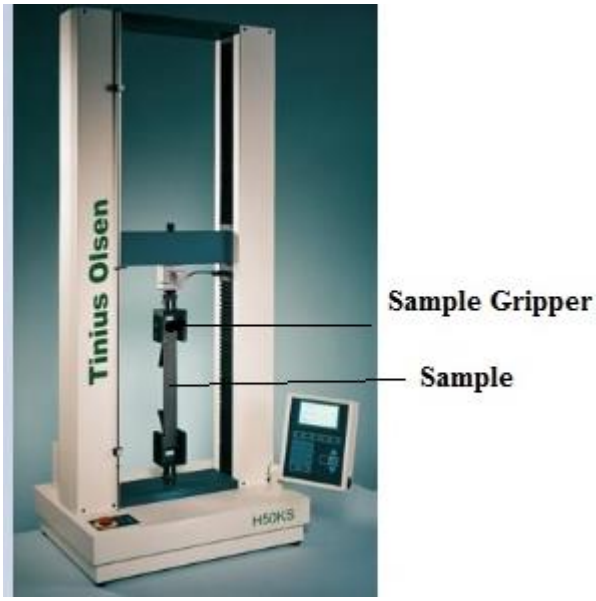

Figure 3.6: Vertical Tensile Tester: Tinius Olsen, Model: H50KS

3.7 Material characterization

Structural, morphological, electrical, and mechanical properties of the composite films were investigated in this study.

3.7.1 Investigation of surface modification of the film by FTIR spectra

In this study, a boiling mixture of nitric acid and sulphuric acid was used to functionalize CNFs. As a result, polar carboxylic acid groups were introduced on the surface of the nanofibers and the nanofibers were cut to shorter lengths. Ros et al. [133] surveyed several

methods of surface oxidation and found that a mixture of concentrated nitric and sulphuric acids would be the most effective method for developing polar carboxylic acid groups on the surface of carbon nanofibers [133]. The reactive carboxylic acid sites are useful for further functionalization.

Figure 3.7 shows FTIR spectra of carbon nanofibers (sample 1) and functionalized carbon nanofibers (sample 2). In sample 2, C=O stretch of carboxylic acid group appears from 1760-1690 cm^{-1} and O-H stretch appears at 3300 cm^{-1}.

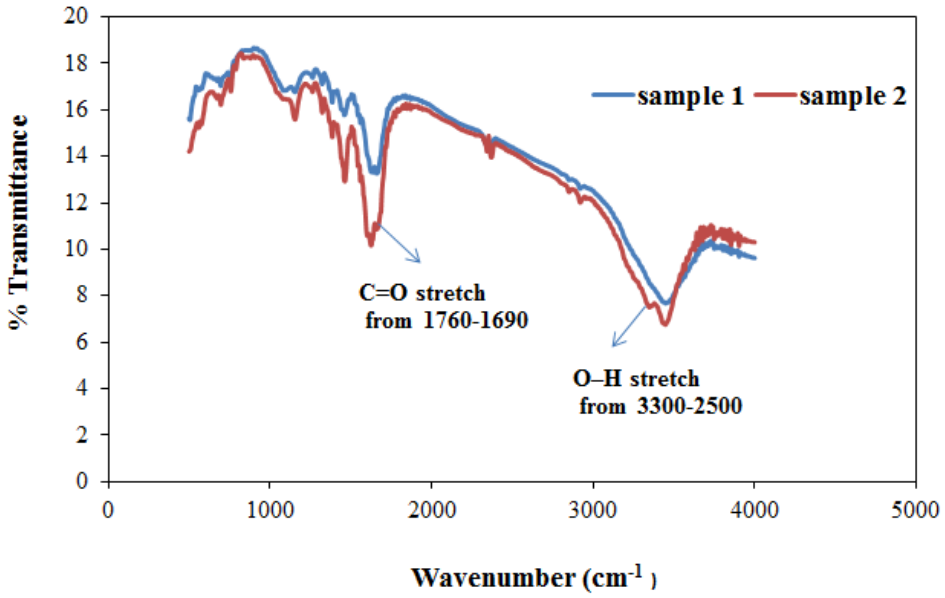

Figure 3.7: FTIR spectra of CNF (sample 1) and FCNFs (sample 2)

The presence of FCNF in the RC/FCNF/PPy (Coated) films results in the appearance of a band at 1144 $cm^{-1.}$ The band at 1540-1550 cm^{-1} is due to the N-H bond, [134] and that confirms the presence of PPy in the composite (Figure 3.8).

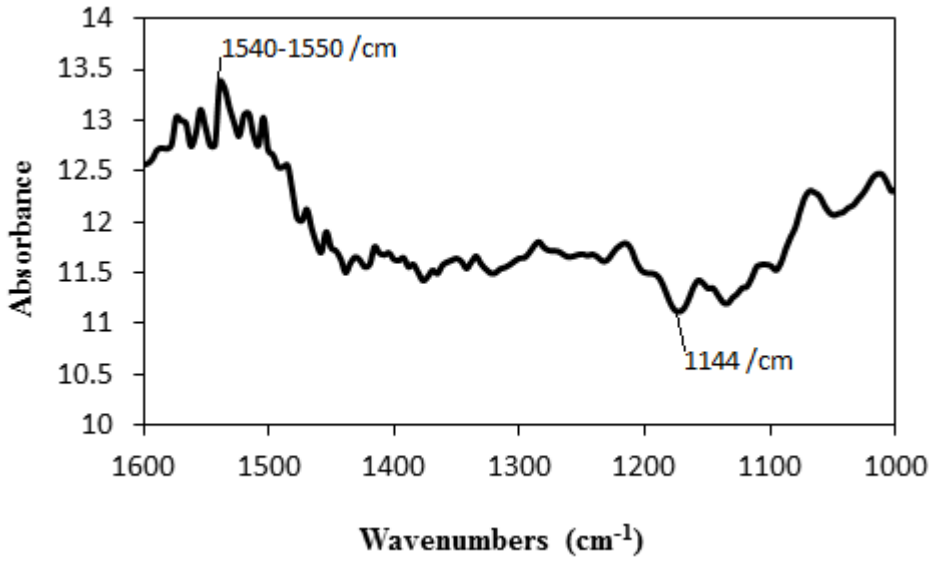

Figure 3.8: FTIR spectra RC/FCNF/PPy (coated)

3.7.2 Morphological studies of CNF, FCNF, and RC/FCNF

The SEM images after treatment in 1:3 HNO_3/$H2SO_4$ mixtures display a partial destruction of the fibres. The macro-porous skeins of long and interwoven fibres are broken into short fibre fragments (Figure 3.9). In addition, the fragments have about the same average diameter as that of the untreated fibres, (Figure 3.10) which strongly suggests that the original long fibres are broken up perpendicular to the length axis. Treatment of the fibres with a strong oxidizing agent ultimately leads to complete oxidation and consumption of defect-rich regions in the CNF, leaving the short fragments.

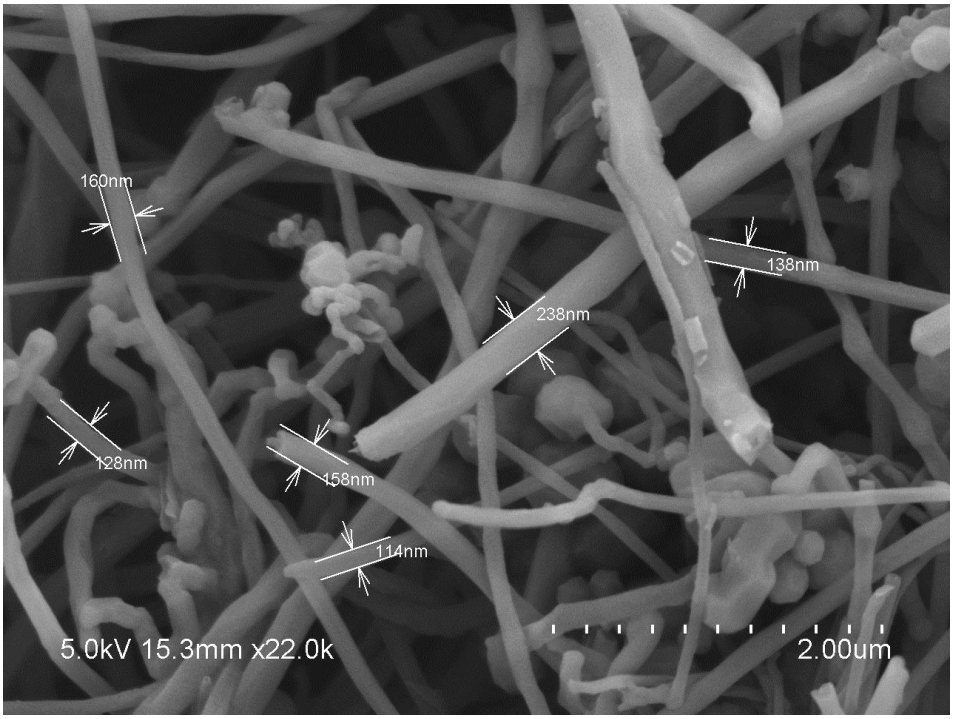

Figure 3.9: SEM image of FCNFs

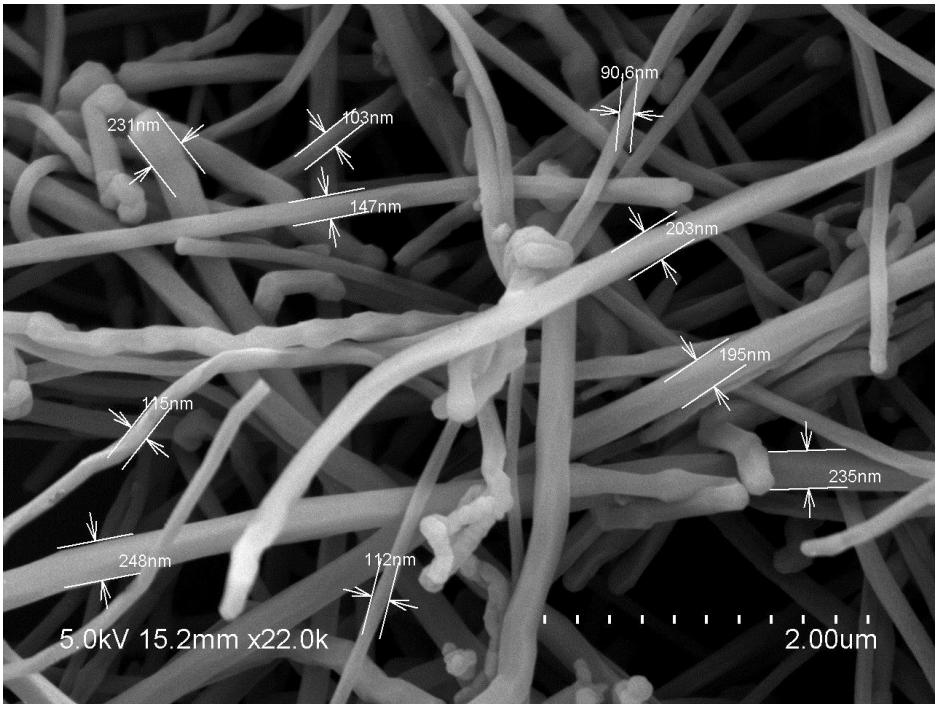

Figure 3.10: SEM image of untreated CNFs

SEM examined the overall structure and distribution of FCNFs in the RC/FCNF films. The homogeneous dispersion of nanoscaled particles in the polymer matrix is very difficult because these particles have a tendency to aggregate. This is because of the strong van der waals force among the nanoscaled particles [131]. Figure 3.11 shows a good dispersion of FCNFs in the RC/FCNF matrix. The dispersion of FCNFs is possible due to the good dispersability of FCNF in dimethylacetamide and enough sonication treatment. As a result, the aggregative force between FCNFs becomes weak in RC solution, and FCNFs do not entangle during solvent evaporation.

The combined effect of blending and sonication, a good distribution (Figure 3.11) as well as interaction between cellulose and FCNFs is made. This gives a reinforced mechanical behaviour related to an output force improvement of the actuators. Generally, oxidation process of CNFs by acid treatment can decorate CNFs with oxygen containing groups, such as hydroxyl groups and carboxyl groups [135]. The groups on FCNFs can form hydrogen bonds with hydroxyl groups of cellulose.

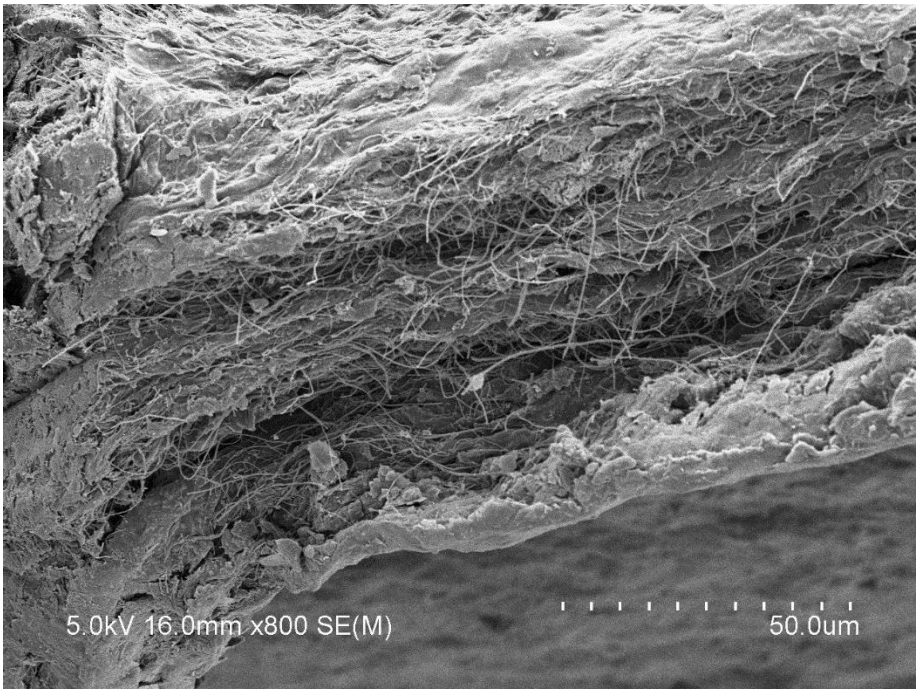

Figure 3.11: Cross-section image of RC/FCNF film

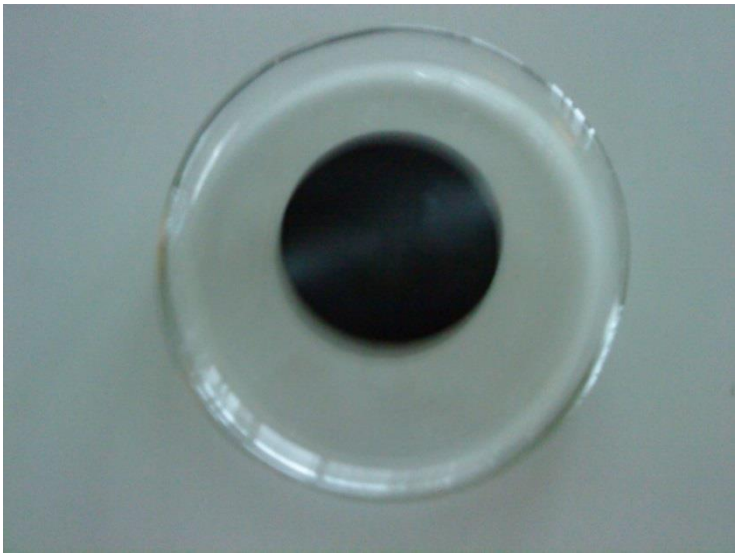

Figure 3.12: PPyAQSA coated RC/FCNF film

Figure 3.12 shows a smooth and coherent polypyrrole electrode coating on the FCNFs containing cellulose film.

3.7.3 Effect of morphology on electrical properties of the composites

RC/FCNF/PPy (coated) films showed electrical conductivity 0.54 S/cm. This value is seven orders of magnitude higher than pristine cellulose (8.22 X 10^{-8} S/cm at 50 percent relative humidity) [58]. This may be due to the presence of 2.0 % FCNFs. It is clear that high electrical conductivity and high aspect ratio of FCNFs and their good dispersion (Figure 3.11) in the composite help in achieving high electrical conductivity. In addition, the dopant has significant effect on the conductivity of the composite films. In this study, polypyrrole electrodes were deposited on both sides of the films by an in situ deposition technique using ferric chloride as an oxidant and anthraquinone-2-sulfonic acid sodium salt (AQSA-Na) as a dopant. AQSA-Na possesses an anthraquinone ring, and that gives good electrical conductivity of the composite films. The RC/IL/PPy (coated) and RC/FCNF/PPy (coated) films show good electrical conductivity because of the presence of AQSA-Na as a dopant, along with suitable polymerization conditions. In addition, electrical conductivity of PPy depends on the conjugation length and inter-chain packing [114]. Moreover, PPy doped with AQSA-Na has a well-packed structure and the sulfonate may serve as a nucleus for PPy formation [115].

Scanning electron microscope (SEM) was used to evaluate the microstructure of the RC/IL/PPy (coated) films. The polypyrrole doped with AQSA-Na shows very dense granule morphology and some become aggregated into clusters. The sizes of PPy particles are estimated to be around 200-300 nm (Figure 3.13).

RC/FCNF/PPy (blend) films show considerably lower electrical conductivity than the composites prepared by chemical deposition of PPy on RC/FCNF membrane. This is due to

the mix-composite (blend) where the amount of PPy is below the critical volume for percolation, which results in a low conductivity value. In addition, the randomly distributed ball-like particles in the mix-composite (blend) have difficulties to form conductive paths (Figure 3.14) [136].

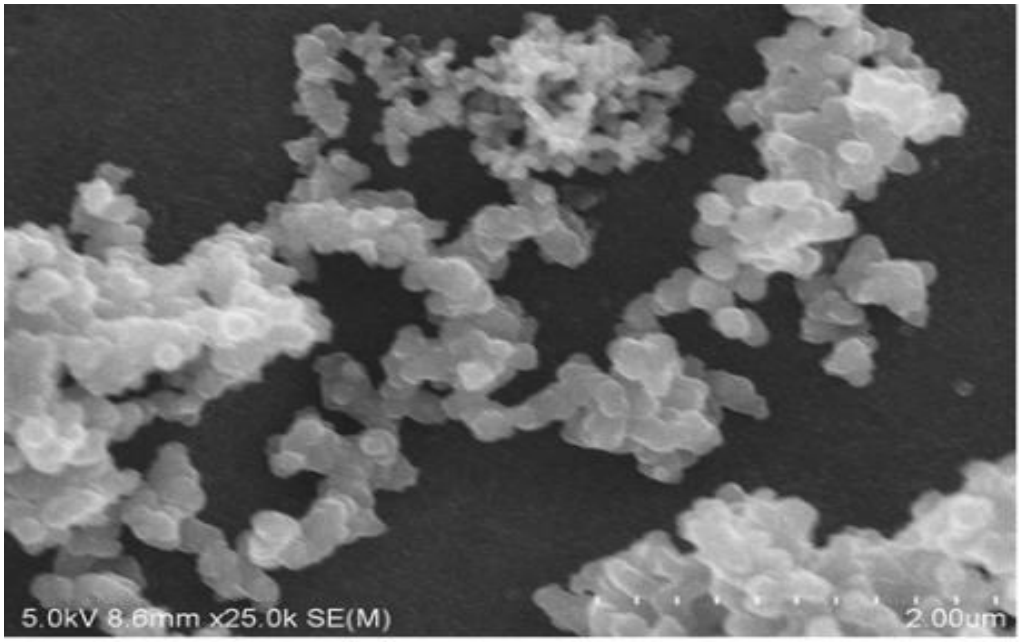

Figure 3.13: Surface image of RC/IL/PPy-AQSA (coated) film

Figure 3.14: Surface image of RC/FCNF/PPy-AQSA (blend) film

3.7.4 Tensile strength and elongation at break

To measure Young's modulus of the RC/FCNF/PPy (blend) films, tensile test was carried out in ambient conditions. Figure 3.15 shows stress–strain curves of the films. The slope of the stress–strain curve shows the Young's modulus of the films. The RC/FCNF/PPy (blend) films show tensile strength of 9.97 MPa, this decreased value compared to the pristine cellulose (13.8 MPa) [137] is due to the decreased crystallinity of cellulose. Decreased crystallinity of cellulose is caused by the introduction of PPy in the structure of cellulose and trapped air bubbles during processing.

Table 3-1: Sample's dimension and distance between grips

	Sample's Name	Width (mm)	Thickness (mm)	Distance between grips (mm)
1	RC/FCNF/PPy (blend)	6.0	0.12	50
2	RC/FCNF/PPy (blend)	6.0	0.12	50
3	RC/FCNF/PPy (blend)	7.0	0.12	50
Mean		6.33	0.12	50
Std. Dev		0.03	0.00	0.00

Table 3-2: Tensile Strength and Tensile Strain of the samples used

	Maximum Load (N)	Extension at Break (mm)	Tensile Strength (MPa)	Tensile Strain at Break (%)
1	7.5	1.43	10.01	2.98
2	6.6	1.35	9.25	2.82
3	8.2	1.40	9.75	2.92
Mean	7.4	1.39	9.67	2.90
Std. Dev	0.43	0.004	0.09	0.01

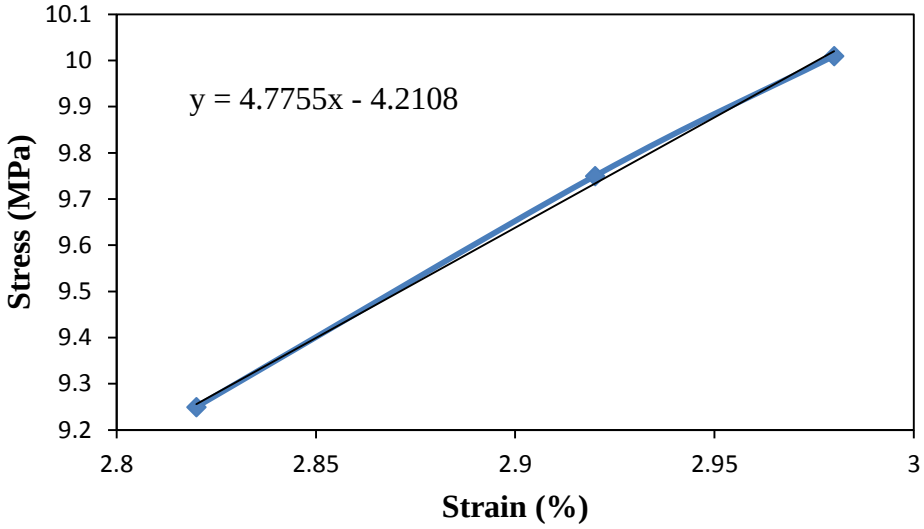

Figure 3.15: Young's moduli of RC/FCNF/PPy (blend) films, y = Stress, x = Strain (%)

The samples failed rapidly after experiencing the maximum load showing induced brittle nature of failure due to the addition of FCNFs. FCNF has high aspect ratio, which can prevent crack generation and propagation in the film. The Young's modulus of the RC/FCNF/PPy (blend) films is larger (4.87 GPa) than the RC/fMWNTs films (4.16 GPa) [34]. This is due to the dispersion of FCNFs in cellulose matrix and interaction between cellulose and FCNFs.

3.8 Techniques used for actuator's performance assessment

The techniques used to assess the performance of the actuators are given below.

3.8.1 Bending displacement, current consumption, and blocked force measurement

The bending displacement was measured using a setup drawn in Figure 3.16

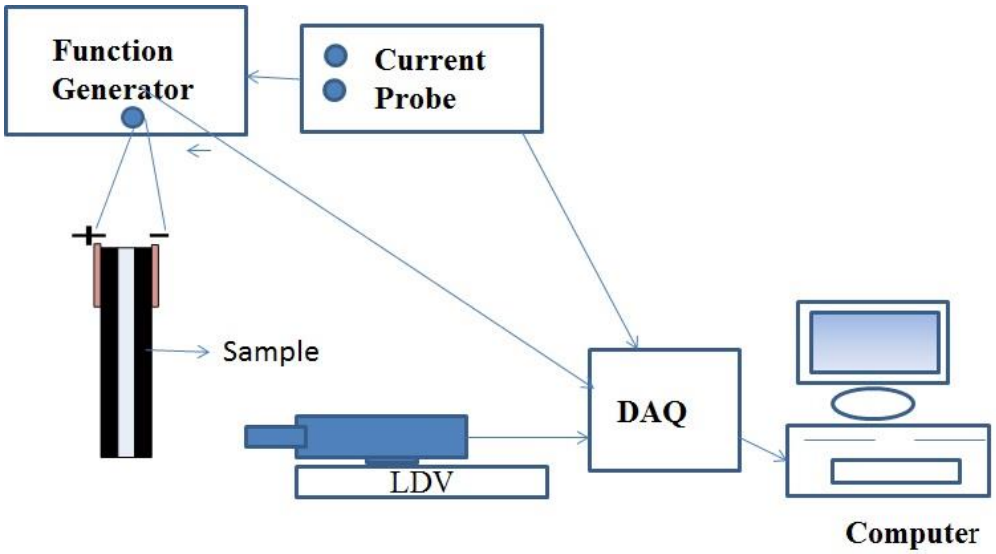

Figure 3.16: Bending displacement measurement setup

The setup consists of two laser displacement sensors (Keyence, LK-G85 and LK-G15), a current probe (Tektronix, TCP 300), a personal computer and a function generator (Agilent, 33220A). Copper electrodes attached with the samples worked to get good electrical contact with the function generator and the current probe. When the function generator sent out the electrical signal to the sample, the laser vibrometer sensors captured the tip velocity of the actuator. Lab view software in the computer converted the tip velocity into

displacement by integrating it over time. Current probe measured the current passing through the actuator during actuation and the electrical power consumption was calculated thereby. The performance of the actuators at 90 % relative humidity was evaluated to perform the actuation tests in an environmental chamber.

Blocked force is the maximum force generated at the tip of the samples when the movement of the tip is blocked. The blocked force was measured using a setup drawn in Figure 3.17.

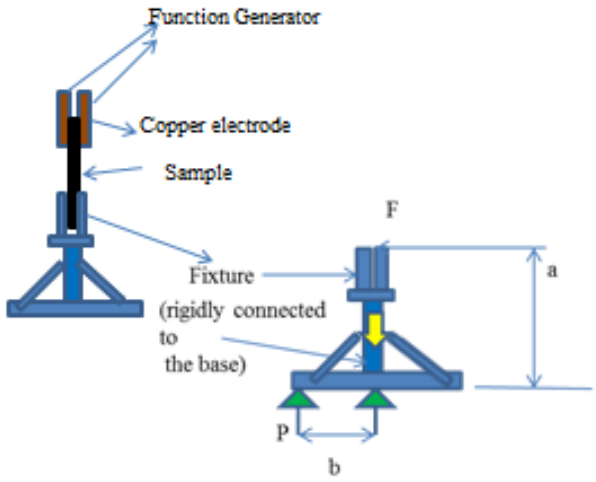

Figure 3.17: Blocked force measurement setup

When the actuator was activated under an alternating current electric field, a bending motion of the actuator was initiated. Since the top of the fixture constrained the actuator's movement, a horizontal blocked force (F) acting at the top of the fixture was converted to the vertical force (P) because of the moment equilibrium of the fixture. As a result, the balance experienced the force vertically as the weight of the fixture was nullified from the

balance. The force was measured in gram/kilogram and converted it to Newton by multiplying it with Earth's gravitational field of 9.81 N/Kg.

3.9 Actuator characterization

This section investigates the electromechanical performance and durability of the actuators.

3.9.1 Electromechanical properties of the actuators

When the actuators were excited with an electric field of 0.1V μm^{-1}, the RC/IL/PPy (coated) actuator, because of its lower stiffness, had a maximum force output of 1.49 mN and the RC/FCNF/PPy (blend) actuator had a maximum force output of 0.9917 mN at the tip. The blocking force of the composite actuators was higher than that of the electro-active paper actuators [33] because of the presence of ionic liquid and FCNF in the composites. Well-dispersed FCNFs in the composite films give additional mechanical stability and conductivity that result in less creep and faster actuation. Blocked force is generally determined by the stiffness and the displacement of the actuator. Dispersed ionic liquid in regenerated cellulose reduces the ordered domains of cellulose. As a result, ion mobility increases within the actuators, and an electric double layer is formed at the electrode-electrolyte interface on the anode side which accounts for large bending displacement showed by the RC/IL/PPy (coated) actuators (1.9 mm) compared to the RC/PPy/BMIMCL nanocomposite actuator (1.4 mm) developed by Suresha et al. [130].

Table 3-3below shows that the actuators developed in this study have better actuation performance in terms of bending displacement because of higher electrical conductivity

values compared to the RC/PPy/IL (coated) actuators developed by Suresha et al. [130].The difference between the RC/PPy/IL (coated) and RC/IL/PPy (coated) actuators besides the thickness includes:

- An intermediate layer of polypyrrole in RC/PPy/IL (coated) actuator that securely holds IL on RC
- Different types of dopant agents are used
- Can be operated up to 70% RH

Table 3-3: Voltage, displacement, and electrical conductivity of the actuators

Name of the samples	Thickness (μm)	Voltage (V)	Relative humidity (%)	Displacement (mm)	Electrical conductivity (S/cm)
RC/IL/PPy (Coated)	40	4	50	1.9	1.6×10^{-3}
RC/PPy/IL (Coated)	14-17	4	50	1.4	1.7×10^{-4} [130]
RC/FCNF/PPy (blend)	40	4	90	4.0	2.7×10^{-3}
RC/FCNF/PPy (Coated)	40	4	90	5.0	5.4×10^{-1}

Electrical power consumption was measured during the actuation test by measuring the current used. The RC/FCNF/PPy (coated) actuators consumed higher electrical power (0.19 mW cm^{-2}) compared to the RC/FCNF/PPy (blend) actuators (0.10 mW cm^{-2}). The

decreased electrical power consumption is due to the decreased electrical conductivity of the RC/FCNF/PPy (blend) actuators.

3.9.2 Durability of the actuators

In order to evaluate the influence of the polypyrrole coating on the durability of the actuators, the actuators were actuated continuously for more than 5 h and the data were provided in Figure 3.18. Many EAPap actuators showed nearly 50 % performance degradation because of the damage of the gold electrode caused by the trapped DMAc and reactive Li^+ ions into the EAPap [6]. However, the actuators developed here exhibit very stable performance up to 5 h. The low surface resistivity and environmental stability of the actuators were achieved when the molar ratio of dopant AQSA-Na (anthraquinone- 2-sulfonic acid sodium salt) to pyrrole was 1:1 and AQSA-Na bearing an anthraquinone ring, which seemed to inhibit the reaction of PPy with oxygen. X-ray photoelectron spectroscopy (XPS) analysis reveals that paper samples doped with AQSA-Na possess higher sulphur/nitrogen (S/N) ratios, but lower oxygen/nitrogen (O/N) ratios [138]. Results from Figure 3.18 show that the dopant has significant effect on the environmental stability of the composite actuators.

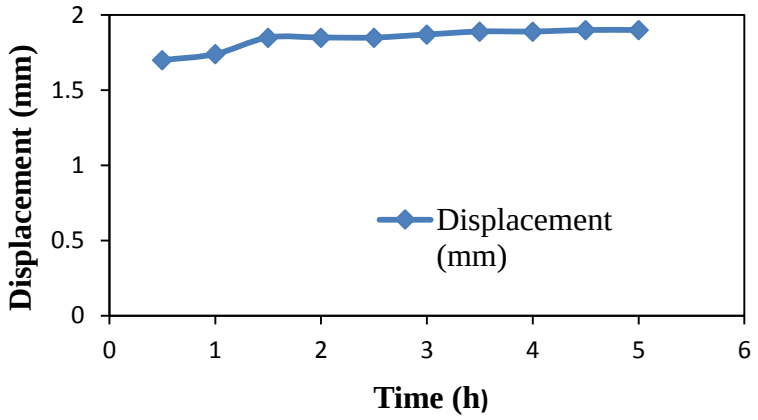

Figure 3.18: Durability of RC/IL/PPy (coated) actuators

3.10 Summary

The results suggest that preparation process and dopants have great impact on the electrical, electrochemical, mechanical and morphological properties of the actuators. Actuators coated with polypyrrole doped with AQSA dopant showed improved electrical conductivity and durability compared to that of using ClO_4^- as the dopant [139]. This is due to the good redox performance of AQSA and the porous submicron/ nanosized structure of polypyrrole on the composite film. The durability of the EAPap composite actuators was improved in this project as AQSA-Na bearing an anthraquinone ring, which seemed to inhibit the reaction of PPy with oxygen. The RC/FCNF /PPy (coated) and the RC/FCNF /PPy (blend) actuators showed their maximum performance at 90 % relative humidity. This result reveals that water molecules play an important role during actuation. The RC/FCNF /PPy (coated) actuators consumed higher electrical power compared to the RC/FCNF /PPy (blend) actuators due to their higher electrical conductivity values. RC/IL/PPy (coated) actuators work well at ambient humidity because of the built-in electrolyte layer. However, the actuators are not capable of generating sufficient amount of forces.

The next chapter will focus on the layer-by-layer casting actuators developed in this research, in order to improve the actuation force at ambient humidity.

Chapter 4 Layer-by-layer casting actuators

4.1 Introduction

In this study, to improve the actuation performance, two actuators were developed through layer-by-layer casting. Often traditional multilayer capacitor can contain internal stress due to in-homogeneities generated by the internal electrodes which in turn leads to reduced life time of the multilayer capacitor [140]. This chapter presents the influence of electrode design on the properties of the actuators such as capacitance, which in turn increases the extents of the bending displacement and actuation force at lower voltages compared to the other CNF- based actuators. This chapter also presents how to improve the durability of the actuators. Further, the electro-magnetic nature of the actuators is investigated.

4.2 Theory and actuation mechanism

To improve the actuation performance, two approaches (electric and magnetic actuation) are presented in this section.

4.2.1 Electrode and electrolyte layers

Baughman et al. developed an electrochemical actuator consisting of singled walled nanotube (SWNT) sheets laminated together with double-sided Scotch tape, where SWNT sheets not only serve as electrodes but also undergo elongation/contraction upon charge injection into the nanotubes in aqueous electrolyte solution [141]. In the current research, functionalized carbon nanofibers were used instead of SWNTs as they have structural

similarities. The actuators developed here have bimorph configuration with regenerated cellulose-supported internal ionic liquid electrolyte layer sandwiched by electrode layers consisting of regenerated cellulose/functionalized carbon nanofibers/ionic liquid. Regenerated cellulose-supported internal ionic liquid electrolyte layer was proposed with a view to operate the actuators without external electrolytes. In addition, Ionic liquids are not volatile, have high ionic conductivities and wide potential windows, which are favourable for rapid response in actuation and stable performance [142]. Moreover, reacting with ionic liquid, entangled nanofibers are exfoliated by a possible cation-π interaction [143]. When an electric potential is applied to the actuator, cations and anions of the built-in ionic liquid may be transported to the cathode and anode sides, thereby develop electric double layers with negatively and positively charged carbon nanofibers. These movements of ions may cause swelling of the cathode layer and shrinkage of the anode layer, as the former ions are larger than the latter. Consequently, may generate a large bending motion toward the anode side [144].

4.2.2 Magnetism in carbon nanofibers

Carbon nanofibers possess paramagnetic properties because of the presence of large amount of defects in the graphene layers of the nanofragments. In addition, the carbon atoms neighbouring to defects adjust their bonds to accommodate the defects and produce a dangling sp^2 orbit, which in turn generates a magnetic moment [145]. According to the electronic structure calculations with density functional theory, magnetic moment and ferromagnetic interaction can be enhanced by including H-atoms to zigzag edge in nanographite system and a combination of vacancy defects and impurities (H, or N atoms)

[146]. In the current research, the paramagnetic nature of functionalized carbon nanofibers was used to make the actuators magnetically induced.

4.3 Actuators fabrication

4.3.1 Materials

1-butyl-3-methylimidazolium chloride (99 %) and 1-butyl-3-methylimidazolium tetrafluoroborate (98 %) were received from Fluka, USA. Dimethylacetamide (DMAC) (Anhydrous 99.8 %), 2-propanol, lithium chloride, cotton linter (DPW 4580), and carbon nanofibers were purchased from Sigma Aldrich, USA. All the chemicals were used as received.

4.3.2 Fabrication method of actuator films by layer-by-layer casting

The actuators (Figure 4.1) were fabricated simply by adopting a bimorph configuration with an internal electrolyte layer consisting of regenerated cellulose and ionic liquid sandwiched by electrode layers. The electrode layers were prepared by blending FCNFs in ionic liquid dispersed regenerated cellulose solution.

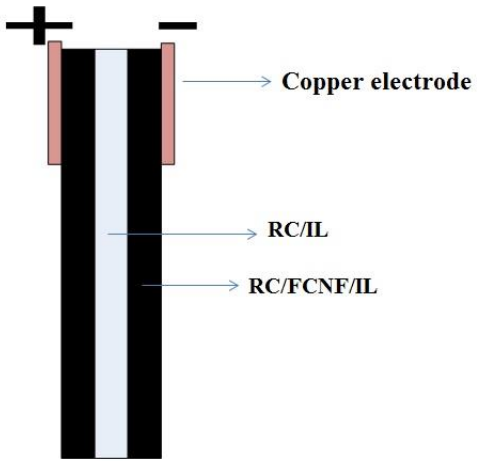

Figure 4.1: Configuration of layer-by-layer casting actuator

Typically, 100 mg FCNFs and 500 mg ionic liquid were ground for 15 min with an agate mortar and pestle. The mixture was then dispersed in 10 mL regenerated cellulose (RC) solution prepared by the method of McCormick et al [25] by ultrasonication at 50 ºC for 2 h. The electrode layer was fabricated by pouring a portion of the resultant gelatinous material (3.4 g) on an aluminium mould with a diameter of 50 mm and 0.18 mm depth. It was then left in an oven at 50 ^{0}C for 1 h for coagulation and solvent evaporation. Following that, 1.0 g ionic liquid was dispersed by blending in 10 mL RC solution at 50 ºC. A portion of this mixture 2.4 g was poured onto the surface of the first layer, and allowed to put in an oven at 50 ^{0}C to let the solvent evaporated. Finally, another 3.4 g of RC solution containing FCNFs and ionic liquid was poured onto the second layer and the solvent let evaporated. A mixture of isopropanol and deionized water was poured on to the film and left it for 24 h for curing the film. The films were then dried in air followed by hot pressing at 50 ^{0}C. The finished films thus obtained have thickness 150-230 μm.

4.4 Material characterization

Structural, morphological, electrical, and mechanical properties of the composite films were investigated in this study.

4.4.1 Effect of morphology on the electrical properties of the composites

The conductivity (σ_s) of the RC/FCNF/BMIMCL and RC/FCNF/$BMIMBF_4$ layer-by-layer films was calculated by the following equation [147]:

$$\sigma_s = \frac{\Delta I}{\Delta V}\frac{l}{wd} \tag{4-1}$$

Where, $l =$ length, $w =$ width, $d =$ thickness, and $\frac{\Delta I}{\Delta V} =$ slope of the current *vs* voltage curve.

Sample's Name	$l\ (cm)$	$w =$ (cm)	$d =$ thickness (cm)	$\frac{\Delta I}{\Delta V}$
RC/FCNF/BMIMCL	2.2	1.2	0.015	0.0011
RC/FCNF/$BMIMBF_4$	1.0	1.0	0.014	0.0018

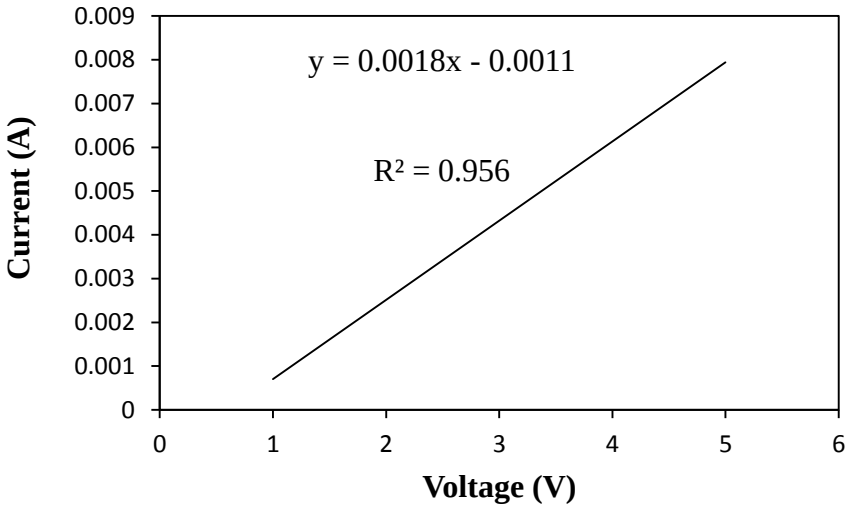

Figure 4.2: Current *vs*. Voltage curve for RC/FCNF/$BMIMBF_4$ layer-by-layer film, y = Current, x = Voltage, R^2 = Correlation coefficient

Figure 4.2 shows the typical current-voltage sweep curve. Electrical conductivity of the composites (RC/FCNF/BMIMCL) was found 0.134 *S/cm*. These values are seven orders of magnitude higher compared to the pristine cellulose [58]. This may be due to the presence of 1.0 % FCNF. It is clear that high electrical conductivity and high aspect ratio of FCNFs and their good dispersion in the composite (Figure 4.3) help in achieving high electrical conductivity.

4.4.1 Morphological studies of the composites

SEM images were used to examine the overall structure and distribution of FCNFs in the layer-by-layer structure. Figure 4.3 shows that FCNFs can be dispersed in the polymer matrix. The dispersion of FCNF is possible due to the good dispersability of FCNF in dimethylacetamide (DMAC) with sonication. As a result, the cohesive forces between FCNFs become weak in the RC/$BMIMBF_4$ solution, and they do not entangle during solvent evaporation.

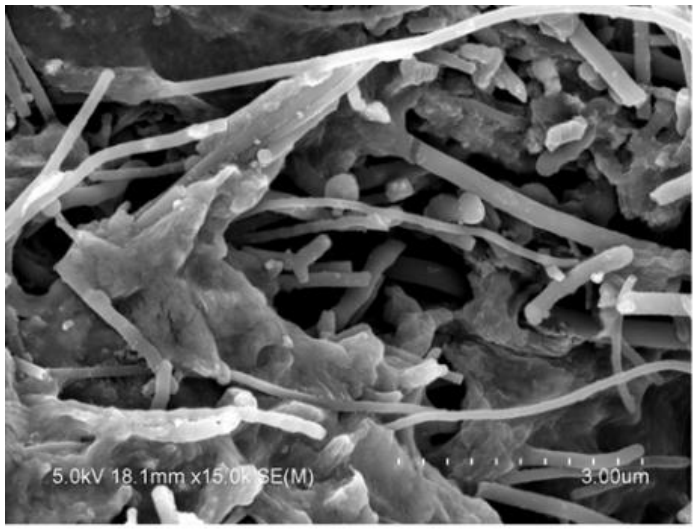

Figure 4.3: SEM image of FCNFs dispersed RC/$BMIMBF_4$ matrix

A scanning electron microscope image of a cross-section of the layer-by-layer film shows that the electrode and electrolyte layers are seamlessly connected with one another (Figure 4.4). As a result, intra- and interlayer ion transport are facilitated, which is essential for quick response.

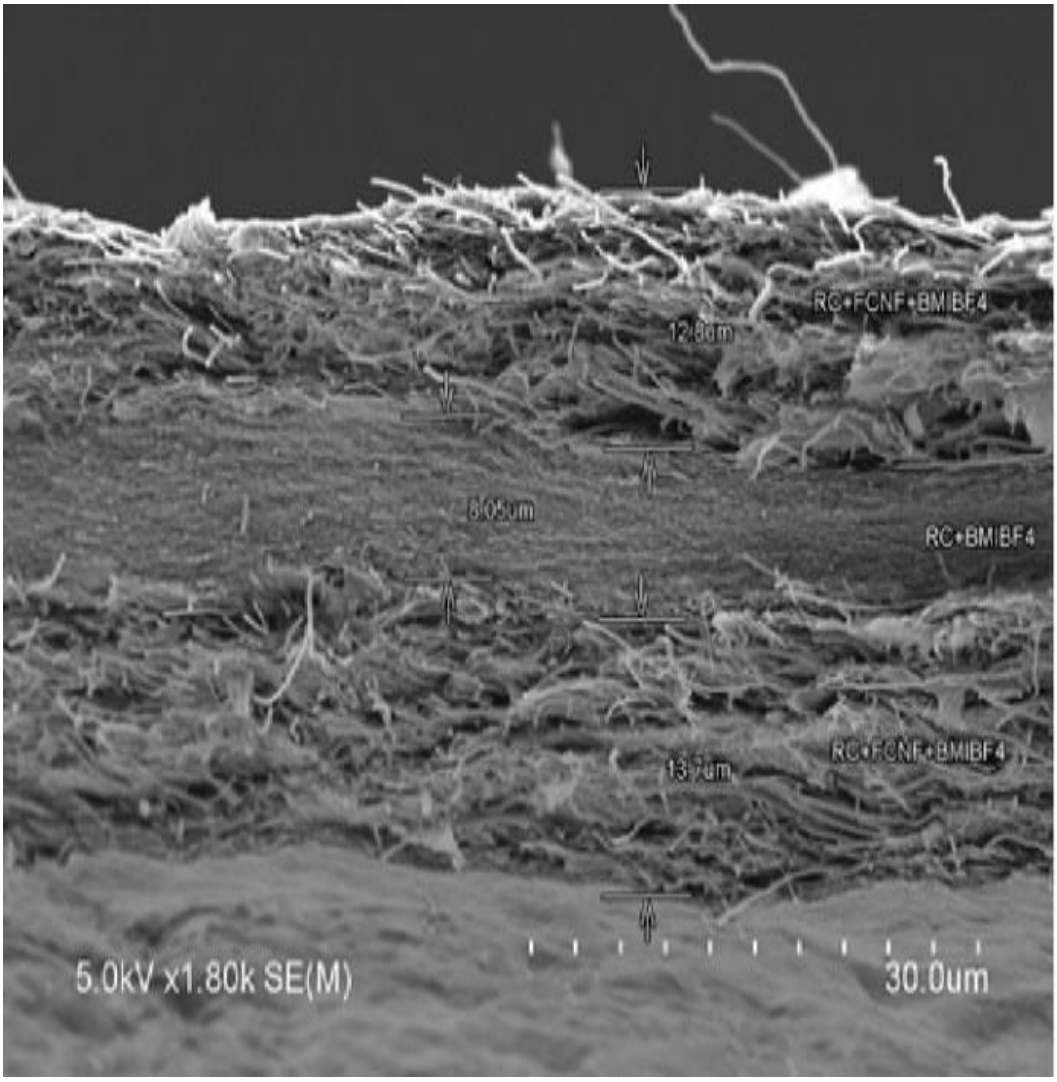

Figure 4.4: SEM image of a cross-section of the layer-by-layer film

4.5 Actuators characterization

The performance of the actuators was evaluated in terms of bending displacement, current consumption (charge density) during actuation, and blocked force. Bending displacement was measured using a setup given in Figure 3.16 and blocked force was measured using a setup given in Figure 3.17. To study electro-magnetic nature of the actuators, a magnetic field was produced using a magnet with a diameter of 35 mm at 10 V DC and 0.1 A.

4.5.1 Electro-mechanical properties of the actuators

When an electric potential of 7.0 V_{pp} with a frequency of 0.75 Hz was applied to a layer-by-layer actuator strip clipped to copper electrodes (2.4 cm x 0 .1 cm x 0.023 cm sized), the RC/BMIMBF$_4$/FCNF actuator experienced a bending motion of 5.0 mm toward the anode side (Figure 4.5). However, the RC/BMIMCL/FCNF actuator showed a maximum displacement of 3.2 mm at 1.0 Hz. The increased frequency is due to the actuator's stiffness.

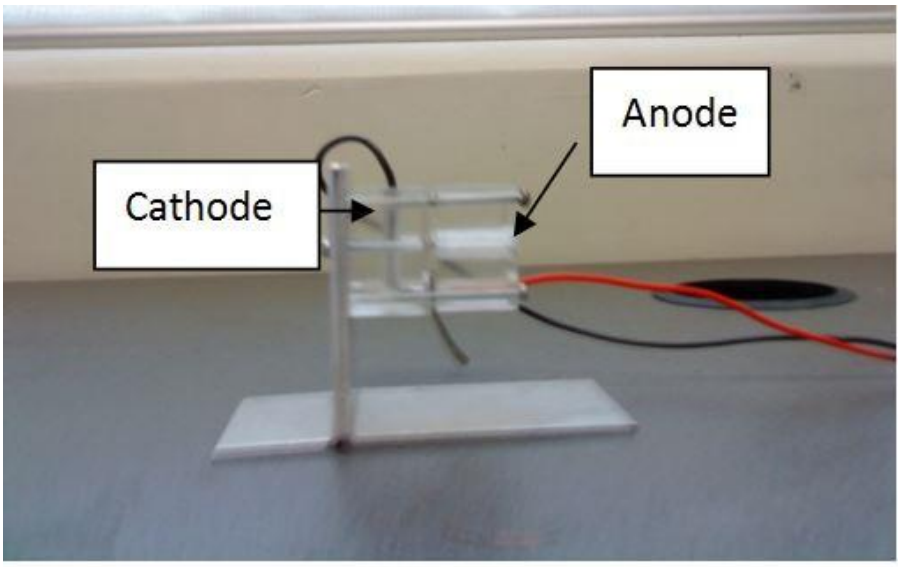

Figure 4.5: Bending motion toward the anode side

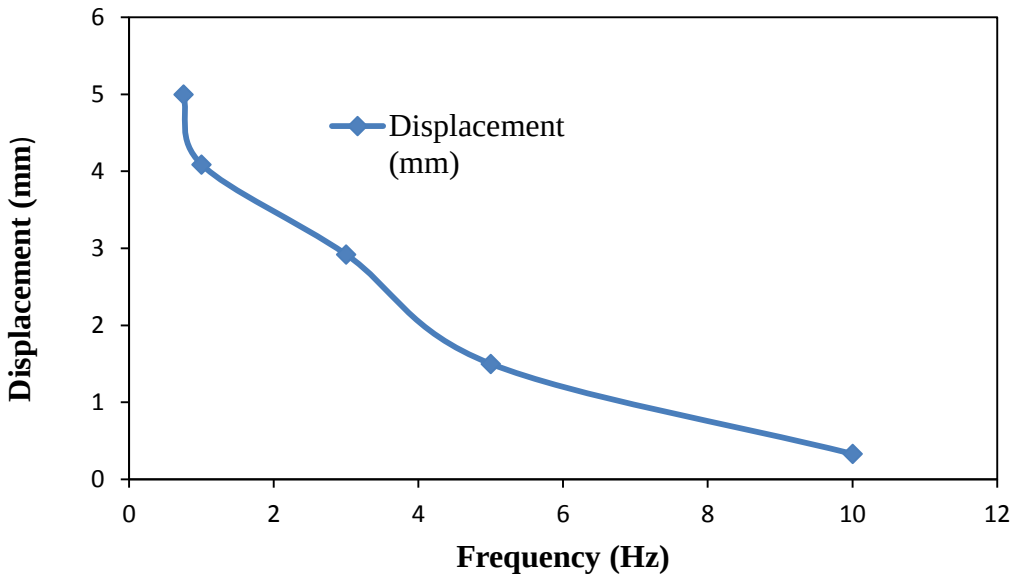

Figure 4.6: Actuated displacement with increasing frequency at a 7.0 V_{pp} sine wave

RC/BMIMBF$_4$/FCNF actuators show decreased bending displacement with increasing frequency (Figure 4.6). This is due to the amplitude of the accumulated charge that decreases with the increase in the frequency.

Figure 4.7 shows that bending displacement increases with increasing applied voltages to 7 V_{pp}. This is due to the higher potentials that increase the charge accumulation at the electrode-electrolyte interface, and cause the faster response and higher displacement. At 10 V_{pp}, the actuators start degrading and the performance was dropped. Both types of the layer-by-layer actuators show stable performance at 7 V_{pp} at ambient humidity because of the built-in ionic liquid electrolyte layer. During actuation, cations and anions of the ionic liquids move towards the cathode and anode sides and swell the cathode layer and shrink the anode layer, as the cations are larger (size) than the anions. As a result, the actuator bends toward the anode side.

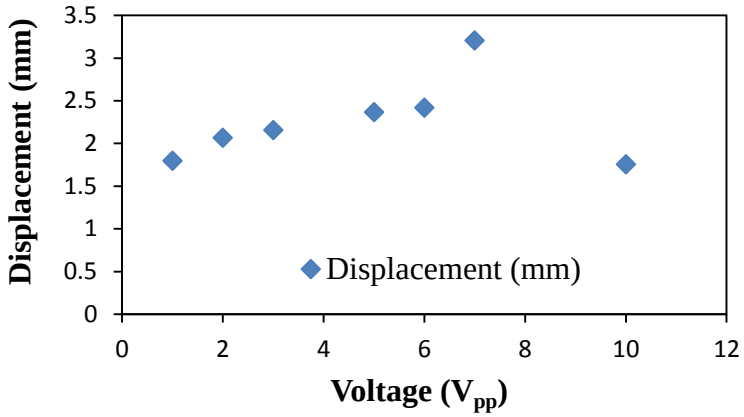

Figure 4.7: Actuated displacement with increasing voltage at a 0.75 Hz sine wave

When the actuators were excited with an electric field of 0.03V μm^{-1}, the RC/$BMIMBF_4$ /FCNF actuator, because of its lower stiffness, had a maximum force output of 2.49 mN and the RC/BMIMCL/FCNF actuator had a maximum force output of 1.70 mN at the tip. The blocked force of the composite actuators was higher than that of the electro-active paper actuators [33] because of the presence of ionic liquid and FCNF in the composites. Blocked force depends on the stiffness and the bending displacement of the actuator. Dispersed ionic liquid in regenerated cellulose reduces the ordered domains of cellulose. As a result, it increases the mobility of the ions within the matrix. In addition, electric double layers are formed at the electrode-electrolyte interface, which in turn enhances bending displacement. Moreover, the presence of FCNFs provides mechanical stiffness of the composite actuators.

Table 4-1 below shows the mechanical power output, power consumption, and efficiency of the composite actuators. The electrical power consumption was measured during the actuation test. When 7 V_{pp} was applied at their resonance frequencies, the RC/$BMIMBF_4$/FCNF actuator consumed 0.32 mW cm^{-2} electrical power, whereas the

RC/BMIMCL/FCNF actuator consumed 0.14 mW cm^{-2} electrical power. As the materials consume low power, therefore, they may be suitable to develop microwave driven actuators. Mechanical power of the composite actuators was calculated using the following equation [33]:

$$Mechanical\ power = \frac{1}{4} Fmax.Xmax.2\pi f \quad (4\text{-}2)$$

Where, F*max* is the blocked force, X*max* is the maximum displacement, and f is the resonance frequency. The RC/$BMIMBF_4$/FCNF actuator showed mechanical power output 0.01 mW while the RC/BMIMCL/FCNF actuator showed 0.0064 mW. The $BMIMBF_4$ ionic liquid containing actuator consumed 0.32 mW cm^{-2}, whereas the BMIMCL ionic liquid containing actuator consumed 0.14 mW cm^{-2} because of its decreased electrical conductivity. The efficiency of the actuators is defined as the ratio of the mechanical power and the electrical power consumption. BMIMCL ionic liquid containing actuator consumes low power, as a result, it showed higher efficiency compared to the other actuator.

Table 4-1: Mechanical power output, power consumption, and efficiency of the composite actuators

Sample's name & thickness	RC/BMIMBF$_4$ /FCNF (0.023 cm)	RC/BMIMCL/FCNF (0.023 cm)	EAPap (0.004 cm)
Maximum displacement (mm)	5.0	3.2	1.5
Frequency (Hz)	0.75	1.0	8.0
Blocked force (mN)	2.49	1.70	1.64
Mechanical power (mW)	0.01	0.006	0.031
Power consumption (mW cm^{-2})	0.32	0.14	55
Efficiency (%)	3.0	4.0	0.056

4.6 Electro-magnetic actuation of the composite actuators under magnetic field

The composite actuators were tested in air under a magnetic field for (a) S→N and (b) N→S directions using a set up drawn in Figure 4.8. The magnetic force direction was changed, when the current polarity was switched from positive to negative. The composite actuators as they possess magnetic properties move to the magnetic force directions (a) S→N and (b) N→S (Figure 4.8).

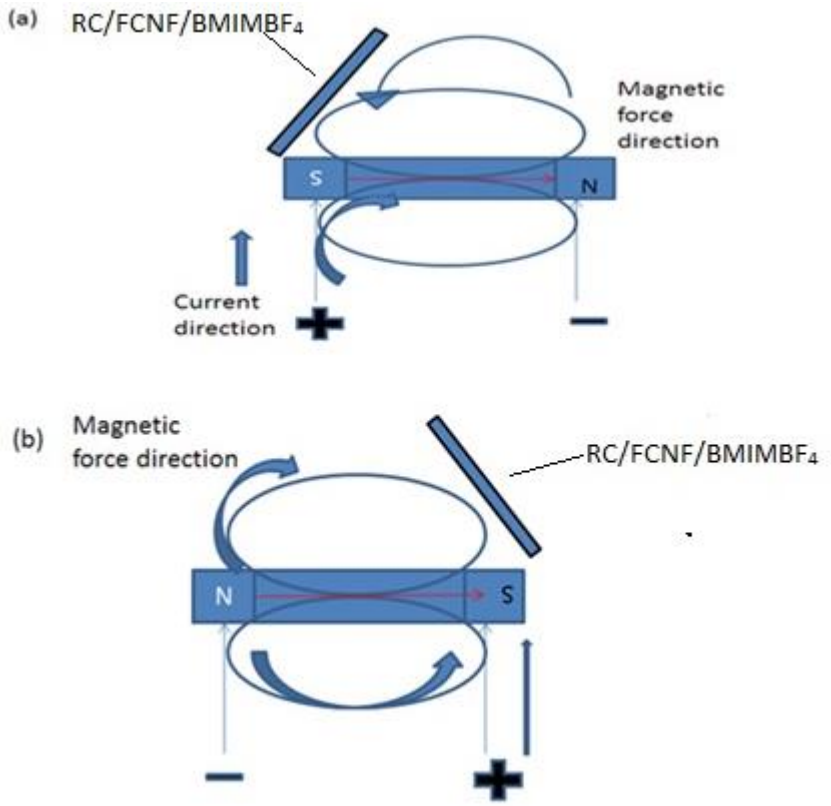

Figure 4.8: Outline of experimental scheme for investigation of electromagnetic actuators under magnetic fields for: (a) S→N and (b) N→S

Functionalized carbon nanofibers have paramagnetic properties [145] because of the presence of large amount of defects in the graphene layers of the nanofragments. In addition, the carbon atoms neighbouring to defects produce a dangling sp^2 orbit, which in turn generates a magnetic moment. As a result, actuators composed of functionalized carbon nanofibers respond strongly under magnetic field (Figure 4.8).

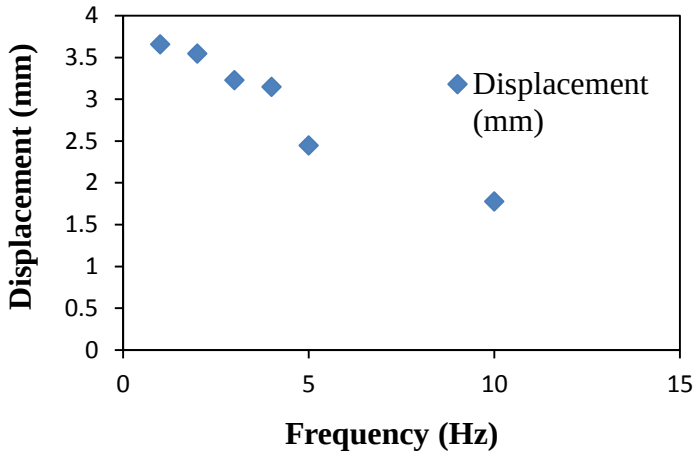

Figure 4.9: Actuated displacement of RC/BMIMBF$_4$/FCNF actuators with increasing frequency at a 7.0 V_{pp} sine wave

RC/BMIMBF$_4$ /FCNF actuators show 3.0 mm bending displacement at 4 Hz and the displacement decreases with the increase of frequency (Figure 4.9).

4.7 Summary

This work can be summarized as:

- FCNFs were well-dispersed in the layer structure of cellulose
- The layer-by-layer structures showed larger displacement and actuation force at lower voltages compared to the CNF-based actuators.
- The built-in ionic liquid electrolyte layer in the layer-by-layer structure helps achieving stable performance at ambient humidity
- The actuators can be operated remotely by microwave as they consume low power.
- BMIMCL ionic liquid containing actuator showed higher efficiency compared to the other actuators
- They did not require any external electrolyte for operation

- They were actuated magnetically and responded well at higher frequencies (4Hz) compared to the actuators working under electric field

The main advance of these functionalized carbon nanofibers (FCNFs) impregnated actuators compared to previously described actuators is that they can be actuated magnetically. This is due to the paramagnetic characteristics originated from a large amount of defects in the graphene layers of the nanofragments [148].

The next chapter will focus on drug delivery through conductive regenerated cellulose-based matrices. The layer-by-layer casting actuators developed in this research were not used for controlled drug delivery, as they are suitable for fabricating reservoir typed devices. Reservoir typed devices can provide constant drug release with time (zero-order release kinetics) [93], but there is a possibility of accidental dose dumping. Generally, matrix typed devices provide decreasing rate of drug release with time [93]. Therefore, the next chapter will be focusing on how to achieve zero-order drug release kinetics from matrix typed devices.

Chapter 5 Conductive regenerated cellulose-based matrices: Controlled drug delivery systems

5.1 Introduction

Matrix based delivery systems usually show first order or square-root-of-time release kinetics [93]. This is due to the matrix swelling. This chapter presents the methods of developing drug delivery carriers, which respond well under external stimuli such as electric and magnetic field. This chapter also presents several techniques (iontophoresis, electro-chemically and magnetically induced) to reduce burst effect and to achieve zero-order release kinetics from the drug-loaded matrices. Further, this chapter presents electrical and swelling behaviour of the composite matrices, morphology, electro-active composite-drug interaction, in vitro drug release behaviour of the matrices, and a comparison between electrically and magnetically induced drug delivery as the later method of drug delivery is safer than the former one.

5.2 Drug release mechanism

Under the influence of an electric field electro-responsive matrices deswelled when the matrices lies perpendicular to the electrodes. Electrically-induced gel deswelling and other responses (expansion of conductive polymer chain and the electrostatic force between electron and drug) cause movement of drug molecules out of the matrices [149].

Drug release from polymer/paramagnetic particles composite under magnetic field is based on the fact that heat produced locally by magnetic particles under alternating current (AC)

magnetic field loosens the polymer chain surrounding the particles at temperatures above the glass transition temperature (Tg) of that particular polymer, resulting in drug ions released through the chain [92].

5.2.1 Analysis of in vitro drug release kinetics of model drug from matrices

The drug release data (in vitro) are normally fitted with various kinetic models such as zero-order, first-order, Higuchi, and Korsmeyer-Peppas to investigate the kinetics and drug release mechanism from the RC-based matrices [150-154]

Zero order: A system follows zero-order rate equation (5-1), when the drug release rate is independent of its concentration.

$$M_t = K_o t \tag{5-1}$$

Where, M_t is the rate of drug released at time t, K_o is the zero-order rate constant and t is the time. The drug-loaded matrices release the same amount of drug by unit time.

First order: Gibaldi first applied the first order kinetics for drug dissolution studies and Feldman in 1967 and later Wagner in 1969 [155, 156]. A system follows first order equations (5-2 and (5-3), when the drug release rate is dependent of its concentration.

$$logM_t = logM_o - \frac{k_1 t}{2.303} \tag{5-2}$$

And

$$logM_o - logM_t = \frac{k_1 t}{2.303} \quad (5\text{-}3)$$

Where, M_t is the amount of drug released in time t, M_o is the initial concentration of drug and k_1 is the first order constant. In first order drug release kinetics, there is a linear relationship between the *log* cumulative of % drug remaining, *log* % ($M_t - M_0$) versus time.

In 1961, Higuchi proposed the following equation to predict drug release rate from a matrix system by correlating drug release rate with square-root-of-time [152].

$$\frac{M_t}{A} = k_H t^{1/2} \quad (5\text{-}4)$$

Where, M_t is the cumulative absolute amount of drug released at time t; k_H is a kinetic constant. According to Higuchi, the release of drug is a diffusion process, which is based on the Fick's law. He observed a linear relationship between $\frac{M_t}{A}$ versus square-root-of-time ($t^{1/2}$).

Korsmeyer and Peppas developed a model comprising a simple empirical equation below [96]:

$$\frac{M_t}{M_\infty} = kt^n \quad (5\text{-}5)$$

Where, M_t is the cumulative absolute amount of drug released at time t; M_∞ is the amount of drug released at infinite time; n is the diffusion constant indicating the release mechanism, and k is the kinetic constant. The value of the exponent n provides information

regarding drug release mechanism. n = 1 shows swelling controlled drug release. Values of n between 0.5 and 1, show anomalous transport. According to Korsmeyer-Peppas models, the drug release is diffusion controlled when the values of $n \leq 0.45$.

For each model, the values of slope (n), correlation coefficient (R^2) and rate constant (k) are graphically determined and are used to predict the kinetics and mechanisms of drug release from the matrices.

In section 5.6 , the above models will be used to analyse the drug release data obtained in this chapter.

5.3 Fabrication of regenerated cellulose-based matrices

5.3.1 Materials

Cotton linter (DPW 4580), lithium chloride, dimethylacetamide (DMAC) (Anhydrous 99.8 %), 2-propanol, and carbon nanofibers were purchased from Sigma Aldrich, USA. 5-sulfosalicylic acid (Fluka) was used as a model drug. Pyrrole, 5-sulfo-salicylic acid dihydrate, and ferric chloride hexahydrate (Fluka), acetone (Fluka, AR grade), methanol (Fluka, AR grade) were used without further purification except pyrrole.

5.3.2 Matrices fabrication

0.21 g FCNFs were dispersed into 10 mL dimethylacetamide and added to 20 mL RC solution [25]. After ultrasonic dispersion under 125 W for 4 h, the RC/FCNF mixture (3.5 g in a 10 cm petri dish for each film) was poured into a glass petri dish. Finally, the solvent was evaporated and the films were dried in air.

5.3.3 Loading of drug into the RC/FCNF matrices

Drug was loaded into the matrices in two different ways. In the first method, drug was loaded by incubating the matrices with the drug. The drug loading process is as follows. The matrices were immersed in 1.5 %, 3 %, and 10 % (w/v) aqueous solution of 5-sulfosalicylic acid dihydrate for 3 days at 37 °C to swell to an equilibrium position. The fully swollen matrices removed from the drug solution were blotted with filter paper to eliminate the surface water. The matrices were then dried in air. The amount of drug loaded was determined from the weight difference of matrices before and after drug loading.

In the second method, drugs were loaded into the matrices by chemical linkages during coating of the matrices with polypyrrole. The method of synthesis is as follows. RC/FCNF matrices were coated with polypyrrole by the adsorption induced chemical polymerization using $FeCl_3$/5-sulfosalicylic acid at 2:1 ratio as oxidant/dopant in aqueous solution. 5-sulfosalicylic acid dihydrate acts as a model anion drug as well as a dopant. 0.03 mol freshly distilled pyrrole monomer and 0.015 mol model drug were dissolved in 50 mL distilled water. The mixture was stirred vigorously for 20 min at 0 ^{0}C in an ice bath. 0.03 mol $FeCl_3$ dissolved in 50 mL distilled water was slowly added to the mixture at a rate of 5

mL/min and the temperature was maintained at 0 ^{0}C. RC/FCNF matrices were then immersed in 50 mL of the mixture in a glass petri dish and were left for 24 h at 0 ^{0}C. Polypyrrole was formed slowly, and was deposited on the surface of the matrices. Finally, polypyrrole coated matrices were washed with water, methanol and acetone and dried in a vacuum environment for 24 h.

5.4 Drug release experiments

5.4.1 Preparation of acetate buffer solution

150 g sodium acetate was dissolved in distilled water in order to prepare 1000 mL acetate buffer solution with pH 5.5. 15 mL glacial acetic acid was then added very slowly into the aqueous sodium acetate solution.

5.4.2 Development of calibration curve of sulfosalicylic acid

2.18 mg of sulfosalicylic acid was taken into 10 mL volumetric flask, dissolved in a buffer solution, and diluted up to the mark with buffer solution to make a stock solution. Further dilutions were prepared from 0.001-0.0001 moles/L (Table 5-1) with buffer solution and the absorbance was measured at 298 nm. The drug solution after scanning in the UV range showed maximum absorbance at 298 nm and hence, the calibration curve was developed at this wavelength. The calibration curve for sulfosalicylic acid is shown in Figure 5.1.

Table 5-1: Concentration Vs Absorbance of sulfosalicylic acid at 298nm

Concentration (moles/L)	Absorbance
0.001	2.196
0.0075	1.35
0.0005	0.85
0.0001	0.065

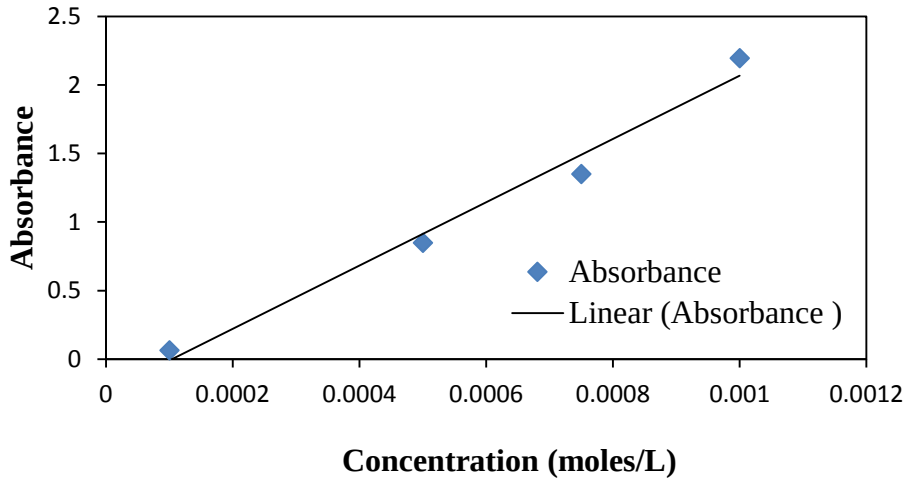

Figure 5.1: Calibration curve of sulfosalicylic acid

5.4.3 Actual drug content

The actual amounts of drug in the RC/FCNF/SSA and RC/FCNF/PPySSA matrices with the dimension of 1.1 cm X 1.0 cm X 105-110 µm were determined by dissolving the drug in the samples in 2 mL dimethylsulfoxide (DMSO) and after that 0.5 mL of the solution was added to 3 mL of the acetate buffer solution. The amount of drug in the buffer solution was measured with the UV/Visible spectrophotometer at 298 nm.

5.4.4 Diffusion studies under electric field

Diffusion studies in in vitro were carried out using a set-up shown in Figure 5.2 [16]. A drug-loaded matrix attached with negative electrode was placed in 5 mL acetate buffer solution of pH 5.5 at 37 °C. Electric potentials (0, 1, & 3 V) were applied through a carbon electrode, the attached membrane, acetate buffer solution, and another carbon electrode. The drug was diffused through the matrix into the buffer solution. The total diffusion period was 5 h. A sample of 1 mL of the buffer solution was withdrawn and an equal amount of fresh buffer solution was added to the cell. The UV–Visible spectrophotometer was used to measure the drug concentrations in the samples at the wavelength of 298 nm.

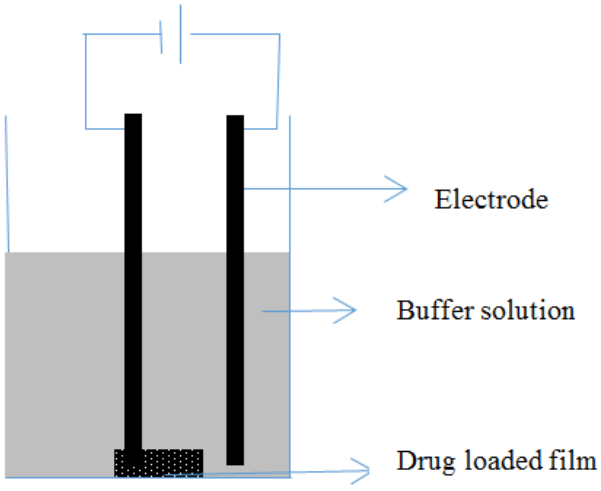

Figure 5.2: Experimental set-up used to study electro-responsive drug delivery from implants

The set-up in Figure 5.2 was used to study the response of the RC-based matrices to electric field strength of 0, 1, and 3 volts. Negative electrode was attached with the matrices placed in the acetate buffer solution.

5.4.5 Spectrophotometric analysis of model drug

The maximum absorption spectra of the model drug were recorded using a Shimadzu UV-2101PC scanning spectrophotometer. The wavelength at the maximum absorption was used to determine the amount of drug released from the predetermined calibration curve.

5.4.6 Diffusion studies under alternating current magnetic field

To study drug release behaviour under an alternating current (AC) magnetic field an electromagnetic field was produced using a magnet with a diameter of 35 mm at approximately 0.1 A and 1.15 KHz.

5.5 Matrices characterization

The degree of swelling, structural, morphological, and electrical properties of the composite films were investigated in this study.

5.5.1 The degree of swelling of RC/FCNF matrices

The degree of swelling was measured by immersing the matrices in acetate buffer solution of pH 5.5 at 37 ^{0}C for 72 h [157]. The matrices were then removed, pressed between a tissue paper and weighed. Finally, the matrices were dried at room temperature and weighed again. The degree of swelling was expressed as a relative weight increase.

The (%) degree of swelling of the matrices was calculated by the following equation:

$$degree\,of\ swelling\ (\%) = \frac{M - M_d}{M_d} \times 100 \qquad (5\text{-}6)$$

Where, M, weight of the sample after submersion in the acetate buffer solution, M_d, weight of the sample after removing the solvent.

RC/FCNF matrices showed degree of swelling of 159 %. This result indicates the porous structure of the matrices, which is suitable for developing drug delivery systems. The presence of –OH, and –COOH functional groups in the structure of the matrices help swelling considerably in an aqueous medium and imbibing water into the network structure. This hydrophilic network can retain a large amount of water that not only contributes to its good blood compatibility but also maintains a certain degree of structural integrity and elasticity [158]. In the drug-loaded matrices drug diffuses through the gel layer formed by the swelling of the matrices because of the entry of water. Although matrix swelling favours drug release, it causes strong resistance to drug diffusion through the gel layer. As a result, amount of drug released decreases with time [12]. In this study, to get rid of this problem, the matrices were coated with polypyrrole doped with drug.

5.5.2 Structural and morphological analysis

The absorption infrared spectra of RC/FCNF and RC/FCNF/SSA matrices are shown in Figure 5.3. For RC/FCNF matrices, C=O stretch of carboxylic acid group appears at 1632.7 cm^{-1} and –OH stretch appears at 3333.5 cm^{-1}. For RC/FCNF/SSA matrices, the sulfonate group (SO_3^-) stretching is observed at 1025 cm^{-1} along with a gradual shift of the

–OH stretching (3000–3600 cm^{-1}). These results indicate the H-bonding between the sulfonate groups of sulfosalicylic acid and the hydroxyl group of RC (in Figure 5.4) [159].

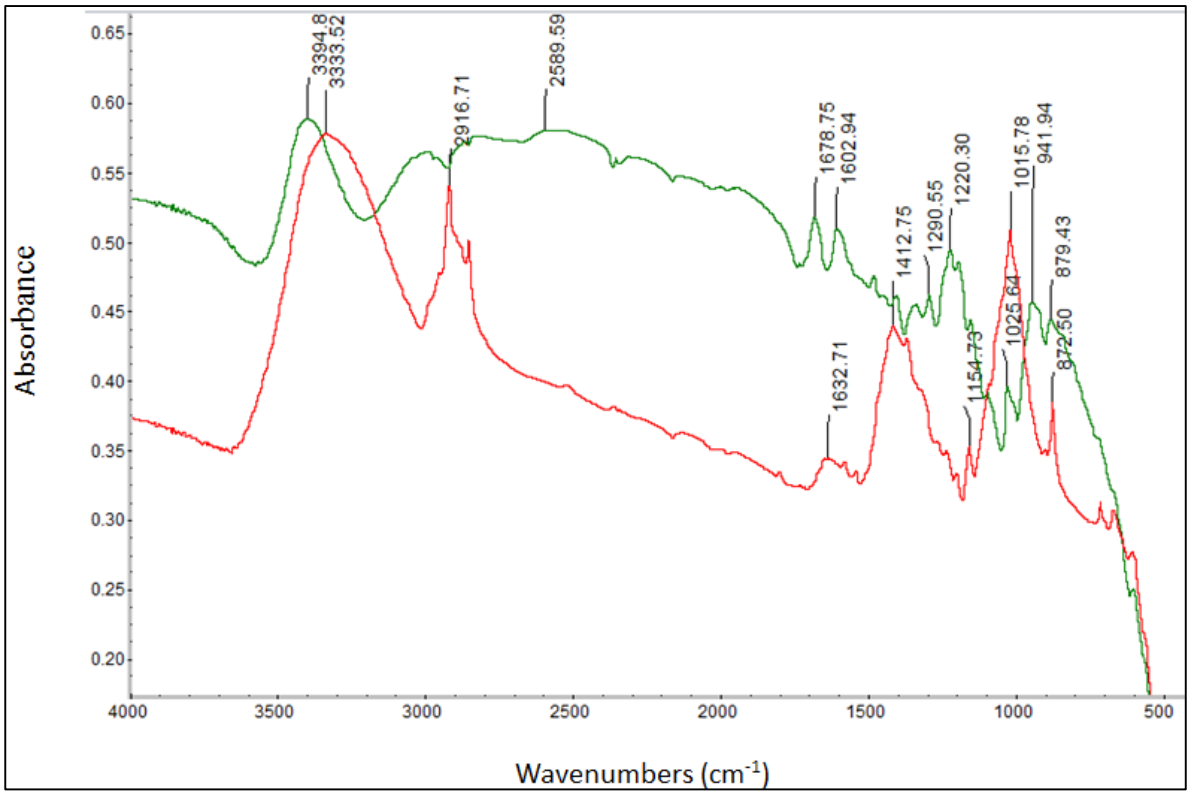

Figure 5.3: Absorption infrared spectra of: RC/FCNF film (Red line); RC/FCNF/SSA film (Green line)

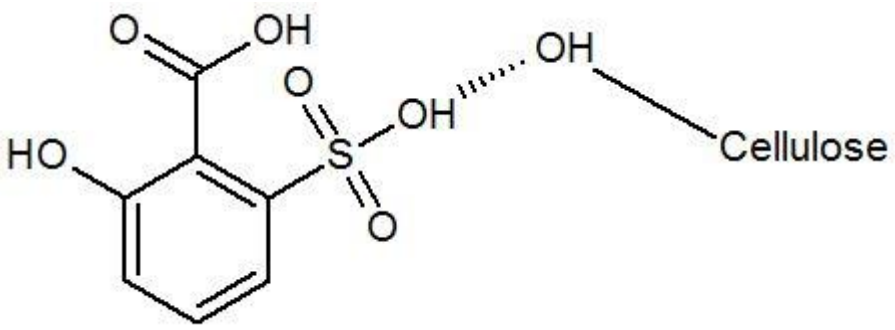

Figure 5.4: H-bonding between the sulfonate groups of sulfosalicylic acid and the hydroxyl group of RC

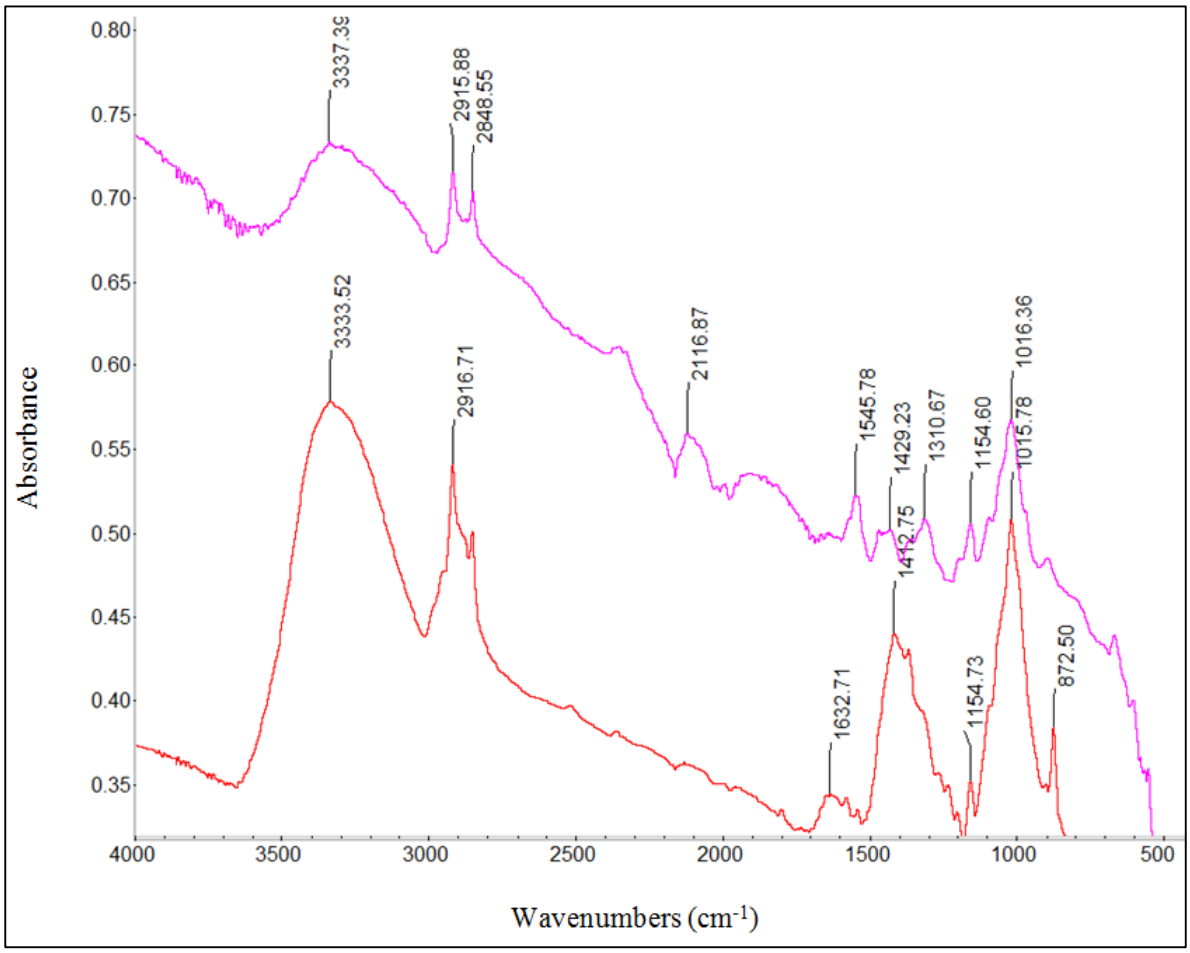

Figure 5.5: Absorption infrared spectra of: RC/FCNF/PPySSA matrix film (purple line) and RC/FCNF matrix film (red line)

The absorption infrared spectra of RC/FCNF, RC/FCNF/PPySSA matrices are shown in Figure 5.5. For RC/FCNF/PPySSA matrices, five-membered PPy ring-stretching and conjugated C–N stretching vibration bands are observed at 1545 and 1429 cm^{-1}, respectively [134]. C- H in-plane vibration is observed at 1310 cm^{-1}. In addition, the peaks at 2915 and 2848 cm^{-1} are associated with five membered ring C–H stretching [160]. These spectral features indicate that the PPy layer is successfully introduced onto the surface of the RC/FCNF matrices. In addition, the sulfonate groups (SO_3^-) stretching is observed at

1016 cm^{-1} and the –OH stretching peak has a slight shift between 3000 and 3600 cm^{-1} because of the H-bonding between the sulfonate groups of sulfosalicylic acid and the amine group of pyrrole unit of PPy (Figure 5.6).

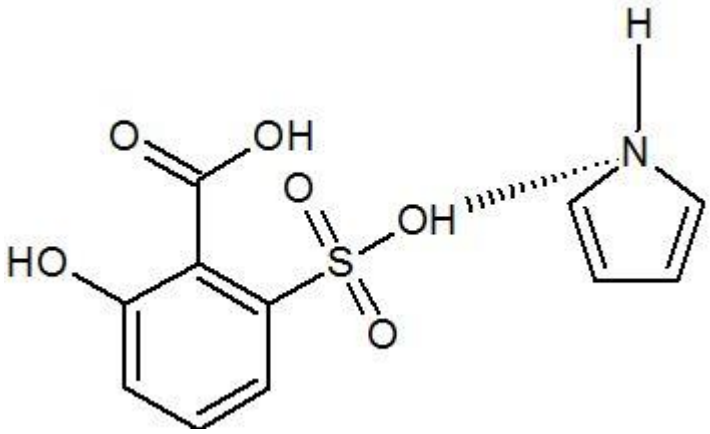

Figure 5.6: H-bonding between the sulfonate groups of sulfosalicylic acid and amine group of pyrrole unit of polypyrrole

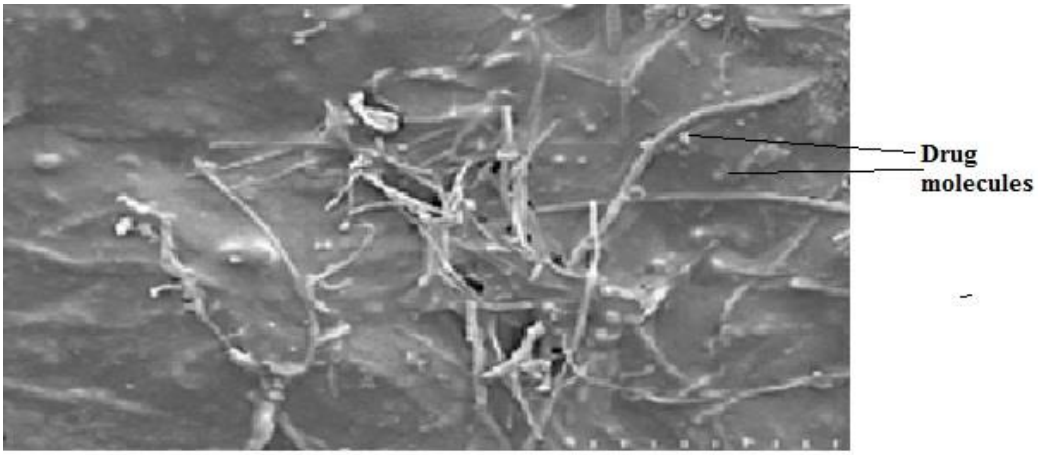

Figure 5.7: SEM image of drug loaded RC/FCNF matrix

The distribution of drug molecules in the RC/FCNF matrix was examined by the images of SEM. SEM images (Figure 5.7) show that drug molecules are well dispersed into the

RC/FCNF matrix. Figure 5.8 shows that polypyrrole is successfully introduced on the surface of the RC/FCNF matrices.

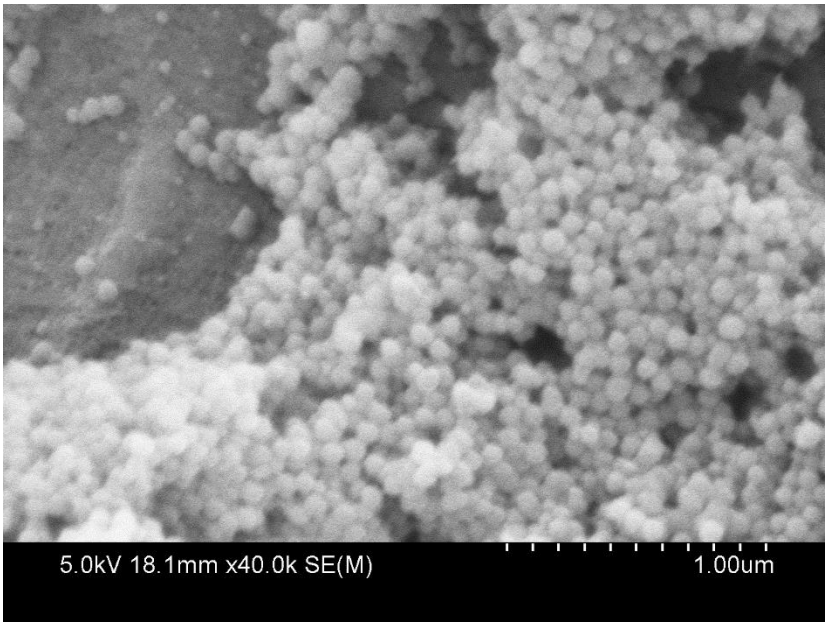

Figure 5.8: SEM image of PPySSA coated RC/FCNF matrix

5.5.3 Electrical conductivity measurement of RC/FCNF and RC/FCNF/PPySSA matrices

Electrical conductivity (σ_s) of the matrices was calculated using the equation (4-1). Figure 5.9 and Figure 5.10 show the typical current-voltage sweep curve. The conductivity of the matrix follows the Ohm‘s law. The electrical conductivity of the RC/FCNF matrix film is 1.1 S/cm. This value is eight orders of magnitude higher compared to the pristine cellulose [58]. This may be due to the presence of 1.0 % FCNFs.

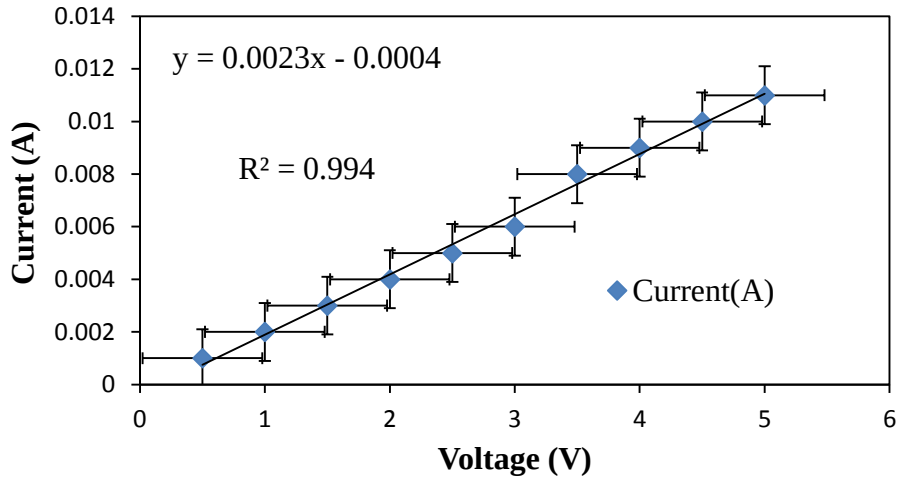

Figure 5.9: Current *vs*. Voltage curve for RC/FCNF film, y = Current, x = Voltage, R^2 = Correlation coefficients

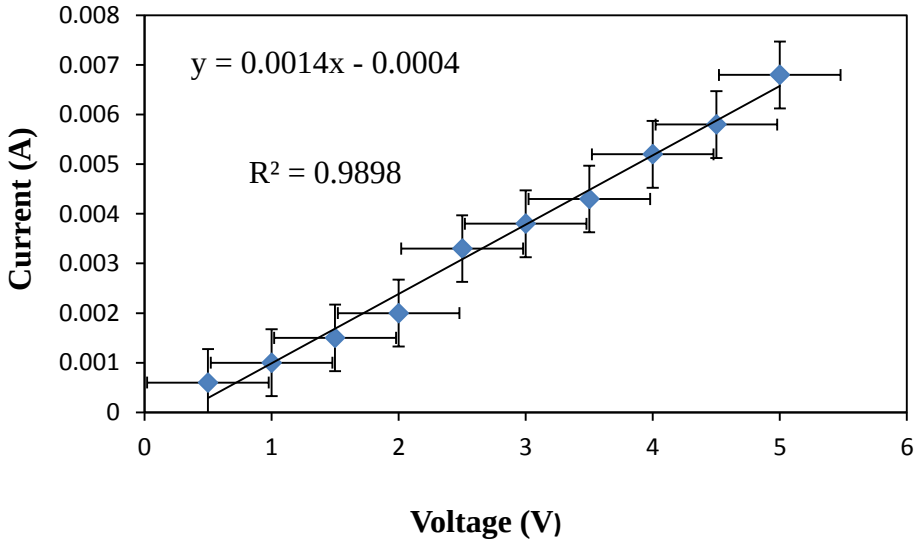

Figure 5.10: Current *vs*. Voltage curve for RC/FCNF/PPySSA film, y = Current, x = Voltage, R^2 = Correlation coefficients

The electrical conductivity of the RC/FCNF/PPySSA matrix film is 0.54. This is due to the presence of FCNFs. In addition, low polymerization temperature (0 °C) that leads to higher polymerization degree and hence to better electrical conductivity compared to the pristine cellulose [58].

5.6 Kinetic modelling of drug release profile

Initially, the actual amounts of drug within the matrices were measured. The amounts of drug present in the RC/FCNF/SSA and RC/FCNF/PPySSA matrices are about 96 ± 1.0 and 90 ± 1.0 % respectively. The in vitro release data from RC/FCNF/SSA (3%) and RC/FCNF/PPySSA were fitted to various kinetic models such as zero order, first order, and Higuchi release in order to determine the kinetics of drug release. The rate constants (k) were calculated from the slope of the respective plots and high correlation value was obtained for the zero-order drug release (Table 5-2). The data were also put in Korsmeyer-Peppas model in order to determine n values. The value of the exponent n determines the type of drug release mechanism. Each data point in the plots (figure 5.11-figure 5. 24) is an average value from two samples.

Table 5-2: Fitting parameters of the in vitro release data to various release kinetic models for (a) RC/FCNF/SSA and (b) RC/FCNF/PPySSA matrices

Samples	Order	Electric field strength (Voltage)	Slope	K	R^2
(a) RC/FCNF/ SSA (3%)	First	0	0.051	0.051	0.9695
		3	0.006	0.006	0.9873
	Zero	0	4.47	4.47	0.9754
		3	0.6129	0.6129	0.9892
	Higuchi	0	16.469	16.462	0.9704
		3	2.11	2.11	0.9721
	Korsmeyer-Peppas	0	0.1706		0.9013
		3	0.0178		0.9147
(b) RC/FCNF/ PPySSA	First	0	0.013	0.013	0.8587
		3	0.027	0.027	0.9828
	Zero	0	0.831	0.831	0.8690
		3	2.249	2.249	0.9845
	Higuchi	0	2.81	2.81	0.8182
		3	7.30	7.30	0.9758
	Korsmeyer-Peppas	0	0.035		0.7147
		3	0.064		0.9428

Matrix based delivery systems usually show first order or square-root-of-time dependent drug release kinetics. Figure 5.11 below shows square-root-of-time dependent drug release kinetics from the RC/FCNF/SSA (10 %) matrices in the process of passive release characteristic (E = 0 V). This result suggests that the drug release is diffusion controlled. However, the amount of drug release decreases with the square-root-of-time.

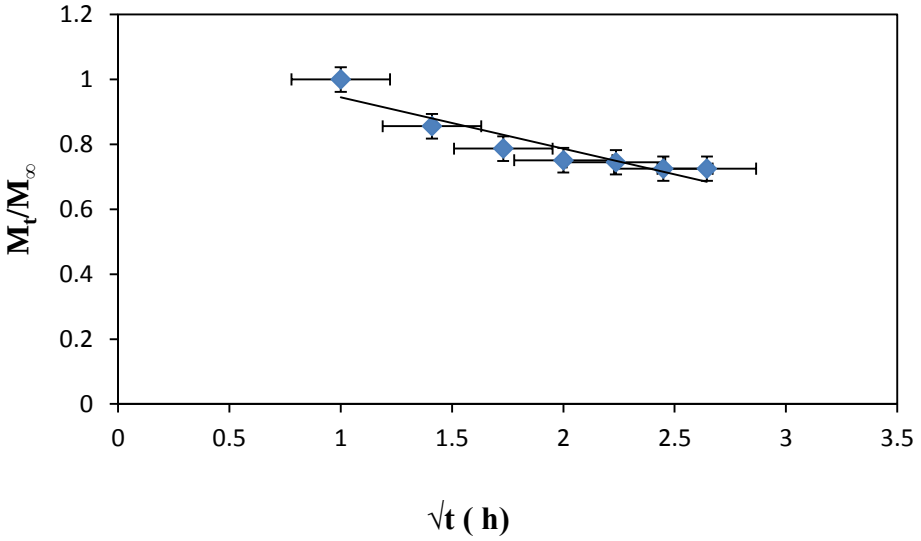

Figure 5.11: Square-root-of-time dependent drug release kinetics from the RC/FCNF/SSA (10 %) matrices film, E= 0 volt, pH = 5.5, 37 °C

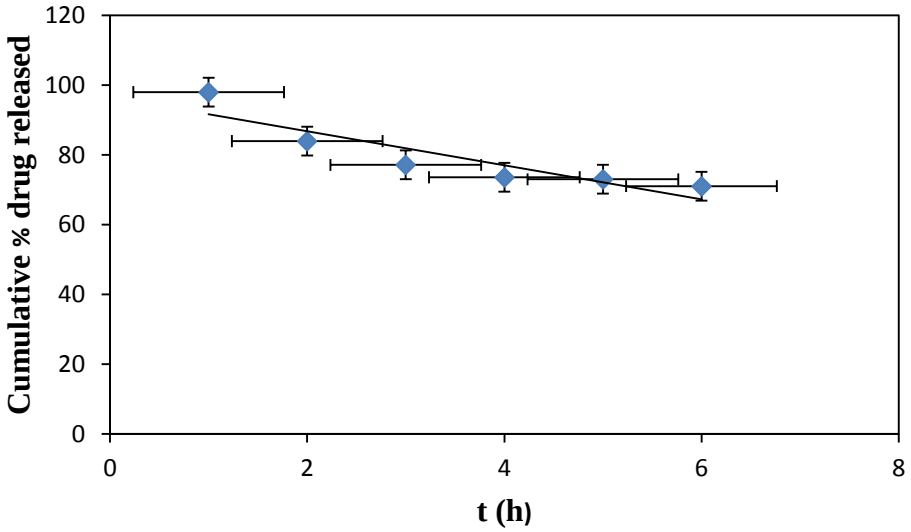

Figure 5.12: Plot of release rate of SSA from RC/FCNF/SSA (10 %) matrices film, E = 0 V, pH 5.5, 37 °C

Figure 5.12 shows that the drug release rate from the RC/FCNF/SSA (10 %) matrices film with the dimension of 1.1 cm X 1.0 cm X 105-110 µm at E = 0 V decreases with time, t. An initial burst effect followed by a slow release of drug is observed. The initial fast release of drug is probably due to the dissolution of surface-bound drug. In addition, for matrix typed drug delivery devices, burst effect is a common phenomenon as molecules of regenerated cellulose take time to form a hydrogel. After the burst release of SSA drug, the rest of the drug entrapped into the matrices is released slowly because of the swelling of the matrices. Although matrix swelling increases the surface area of the system, which favours drug release, the resistance to drug diffusion through the gel layer becomes stronger. Consequently, the amount of drug released decreases with time [161].

Figure 5.13 shows that the rate of drug release from the RC/FCNF/SSA (10 %) matrices attached with the cathode is higher than that with the anode. This is due to the electrostatic repulsion between the negatively charged drug and negatively charged electrode driving the

charged drug through the matrices into the buffer solution [162]. In addition, the positively charged electrode tends to retard the drug diffusion through the matrices. This study establishes the fact that the rates of drug release can be altered to be higher and lower than that under no electric field.

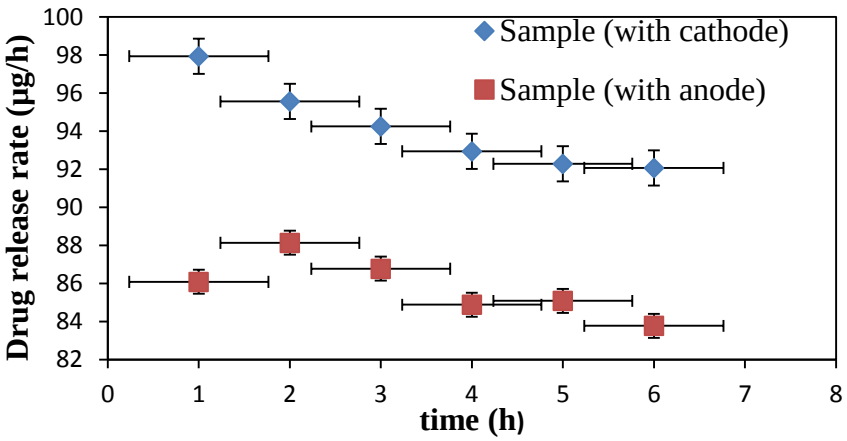

Figure 5.13: Plot of release rate of SSA from RC/FCNF/SSA (10 %) matrices attached to the anode or the cathode, E = 1 V, pH 5.5, at 37 °C

The plots given in Figure 5.14 show that the RC/FCNF/SSA (3%) matrices with the dimension of 1.1 cm X 1.0 cm X 105-110 µm at E = 0 V follow zero order drug release kinetics. High correlation value is obtained for the zero-order model. However, the amount of drug released decreases with time.

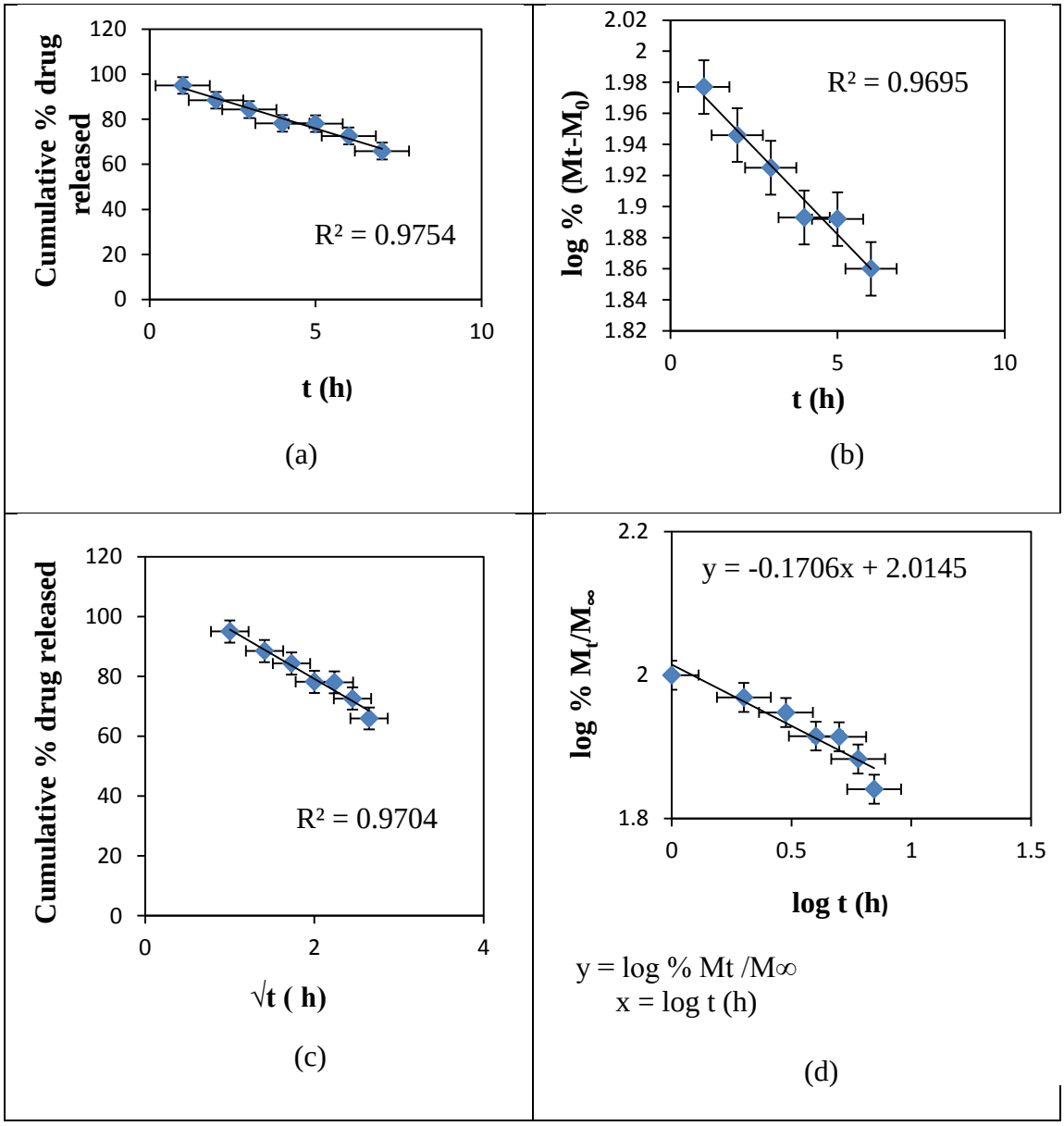

Figure 5.14: Plots of (a) Zero, (b) First, (c) Higuchi, and (d) Koresmeyer- Peppas Release Kinetics of SSA from RC/FCNF/SSA (3%) matrices at E = 0 V, pH 5.5, 37 °C, R^2 = Correlation coefficients

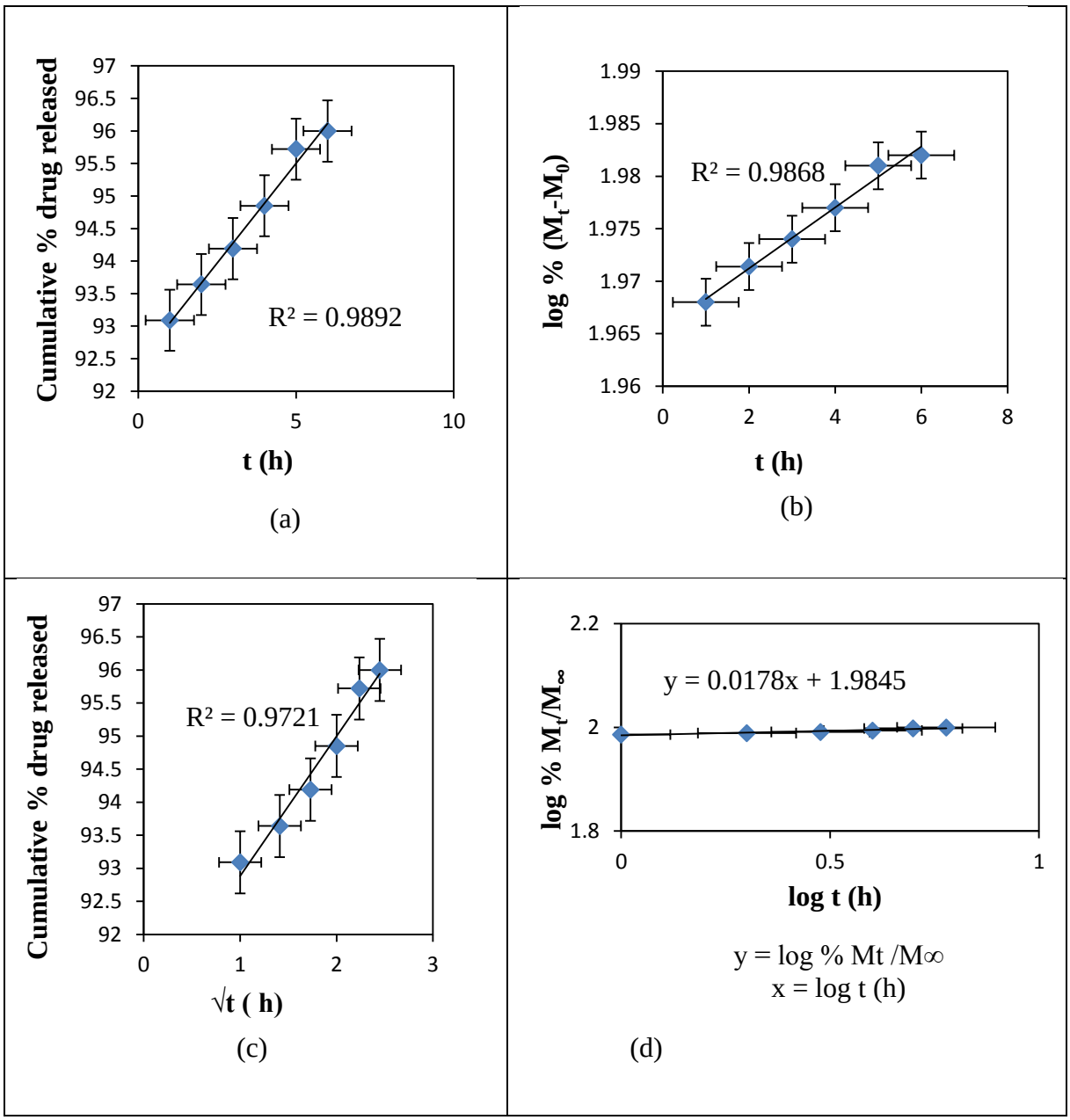

Figure 5.15: Plots of (a) Zero, (b) First, (c) Higuchi, and (d) Koresmeyer- Peppas Release Kinetics of SSA from RC/FCNF/SSA(3%) matrices at E = 3V, pH 5.5, 37 °C, R^2 = Correlation coefficients

The plots given in Figure 5.15 show that the RC/FCNF/SSA (3 %) matrices with the dimension of 1.1 cm X 1.0 cm X 105-110 µm under electric field follow zero-order drug release model. Simultaneous swelling and diffusion through matrices may provide an almost constant release rate. However, it has been observed working with matrices

containing different percentages of drug, that the release rate from matrix system can be controlled by the amount of drug in the matrix. Matrices containing 10 % drug show square-root-of-time dependent drug release kinetics (Figure 5.11), whereas matrices containing 3 % drug show drug release kinetics of zero order at 0 volt (Figure 5.14). However, for both types of the actuators the amount of drug released decreases with time at 0 V.

In this study, to increase the rate of drug release, RC/FCNF matrices were coated with polypyrrole doped with the drug. The plots given in Figure 5.16 show that the RC/FCNF/PPySSA matrices under electric field follow the model for zero-order drug release. The release mechanisms of drug from the RC/FCNF/PPySSA matrices include expansion of polypyrrole chain and the electrostatic force between electron and the drug. As the external electric field is applied, the PPy is reduced. As a result, PPy chains are expanded, and a free space in the PPy matrix is generated, thus electric field pushing the ionic drug out by the electrostatic force. Consequently, it increases the amount and the release rate of drug.

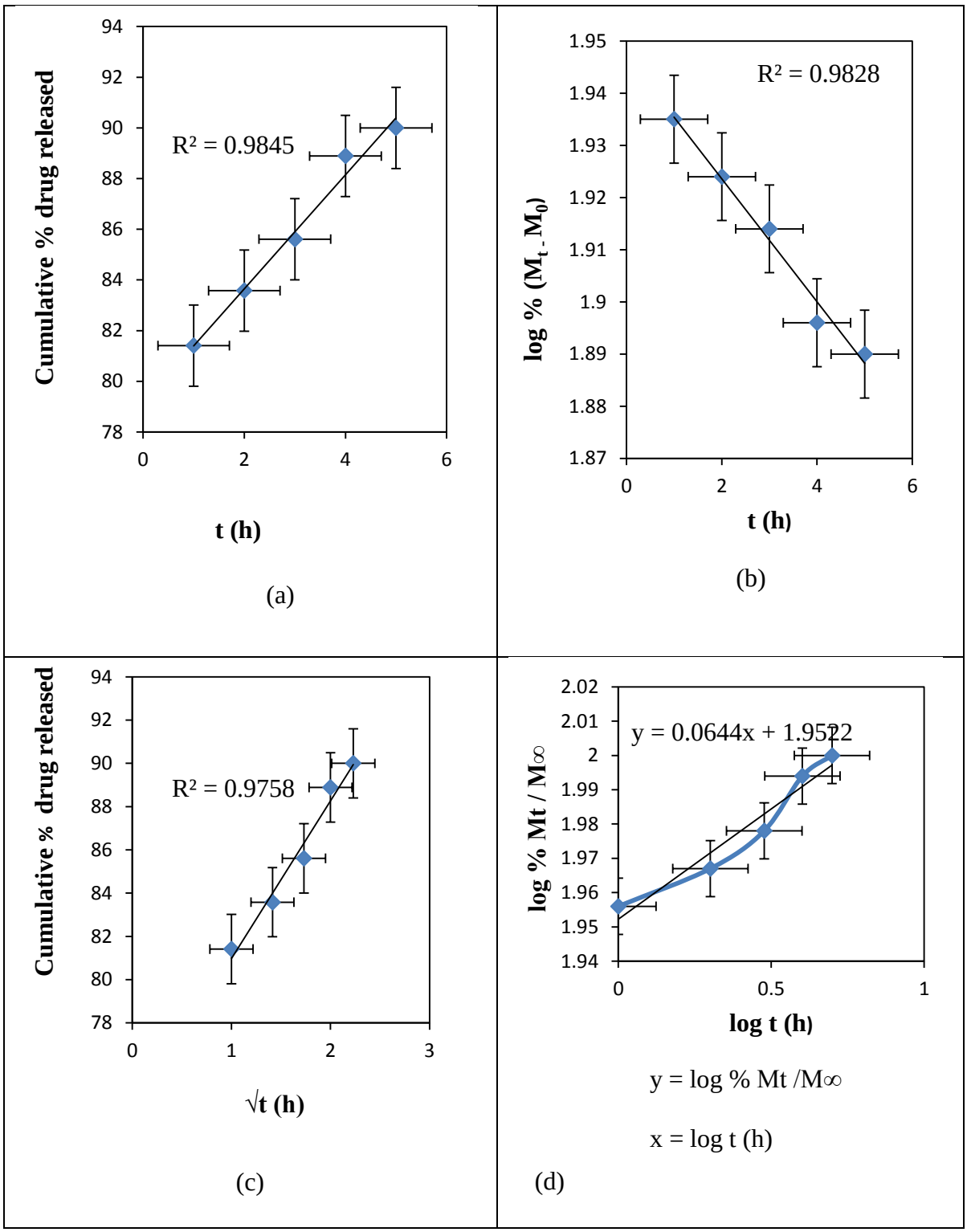

Figure 5.16: Plots of (a) Zero, (b) First, (c) Higuchi, and (d) Koresmeyer- Peppas Release Kinetics of SSA from RC/FCNF/PPySSA matrices at E = 3V, pH 5.5, 37 °C, R^2 = Correlation coefficients

Figure 5.17 shows that conductive polypyrrole has great impact on the release rate of SSA (drug) from the RC/FCNF/PPySSA matrices. The diffusion of SSA from sample-1 (RC/FCNF/PPySSA) is less than that of the sample-2 (RC/FCNF/SSA) initially due to the ionic interaction between the anionic drug and polypyrrole. In RC/FCNF/PPYSSA matrices, drug molecules are chemically bonded with polypyrrole. Here polypyrrole bind and release drug in response to electrical signal. Polypyrrole has two redox states. Drug ions bound in one redox state are released from the other under electric field. The attached electrodes act to switch the redox states. For sample-2, drug molecules come out from the matrices due to the electro-static repulsion between the negatively charged drug and the negative electrode. These results suggest that the drug release rate can be controlled by coating the RC/FCNF matrices with polypyrrole (sample-1) perfectly compared to the RC/FCNF/SSA (sample-2), which shows fast release.

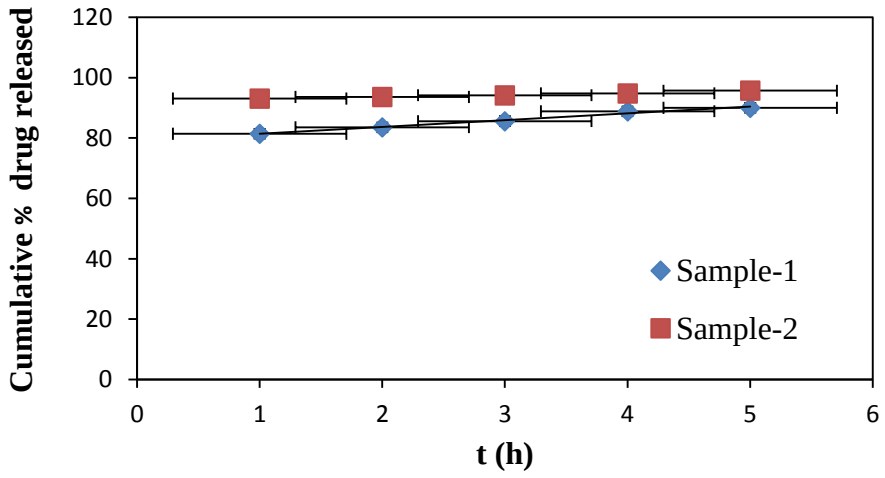

Figure 5.17: Plots of cumulative % drug released *vs* t (h) for RC/FCNF/PPySSA film (Sample-1), and RC/FCNF/SSA film (Sample-2), E = 3V, pH 5.5, 37 °C

In this study, the rate of drug release is increased by increasing the applied electric field (Figure 5.18). For RC/FCNF/SSA matrices, electrophoresis of charged drugs towards oppositely charged electrodes causes drugs to be released [11]. The amounts of drug released are effectively increased with the increase of the applied electric voltages due to the excellent conductivity of the carbon additives. Matrices have deswelled to a certain extent at voltages higher than 3 V, as a result, their resistivity to the passage of charge increases as the content of free water decreases. Consequently, charge passes through the matrices is proportionally smaller [16]. Therefore, 3 V is the optimum voltage for increasing the rate of drug delivery.

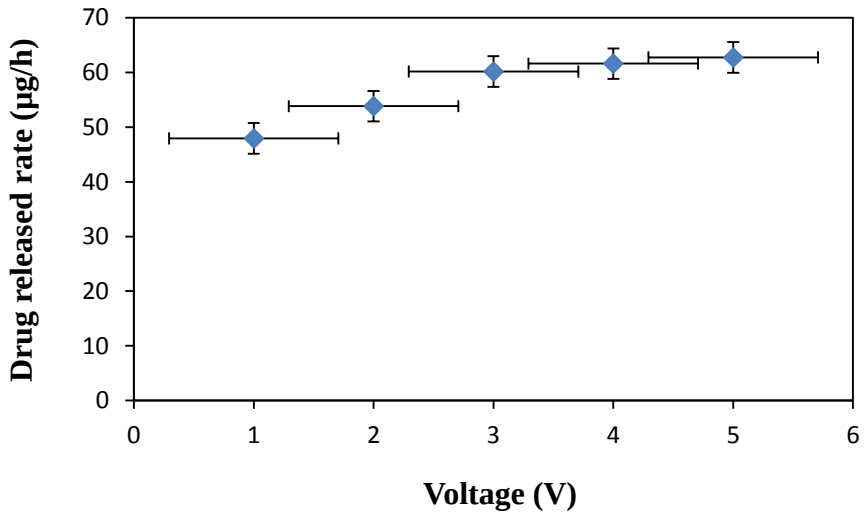

Figure 5.18: Plot of drug release rate *vs*. voltage from RC/FCNF/SSA matrices, V = 1-5 V, pH 5.5, 37 °C

RC/FCNF/PPySSA matrices (1.1 cm X 1.0 cm X 105-110 µm) show a constant rate of drug release at E = 0 V. The drug is released through the matrices due to the concentration gradient effect (Figure 5.19). Coating of polypyrrole physically restricts the RC/FCNF matrix swelling, as a result, the drug release mechanism is changed and a close to constant

drug release profile is obtained (Figure 5.19). The initial fast release rate of drug may be due to the some loosely held drug on the surface of the matrices.

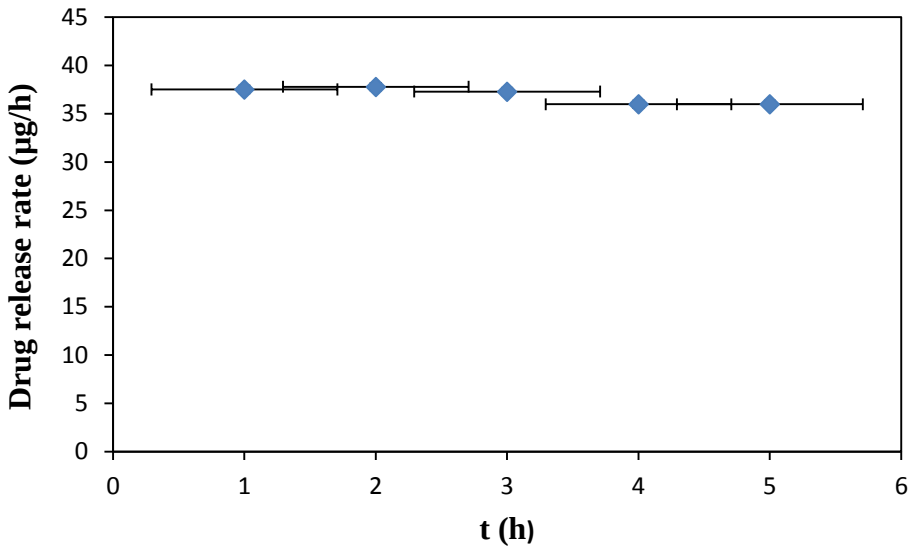

Figure 5.19: SSA release rate *vs.* t (h) from RC/FCNF/PPySSA matrices at E = 0 V, pH 5.5, 37 °C

The results given in Figure 5.19 can be analysed by the plots given in Figure 5.20. It is observed that RC/FCNF/PPySSA matrices at E = 0 V follow zero-order drug release.

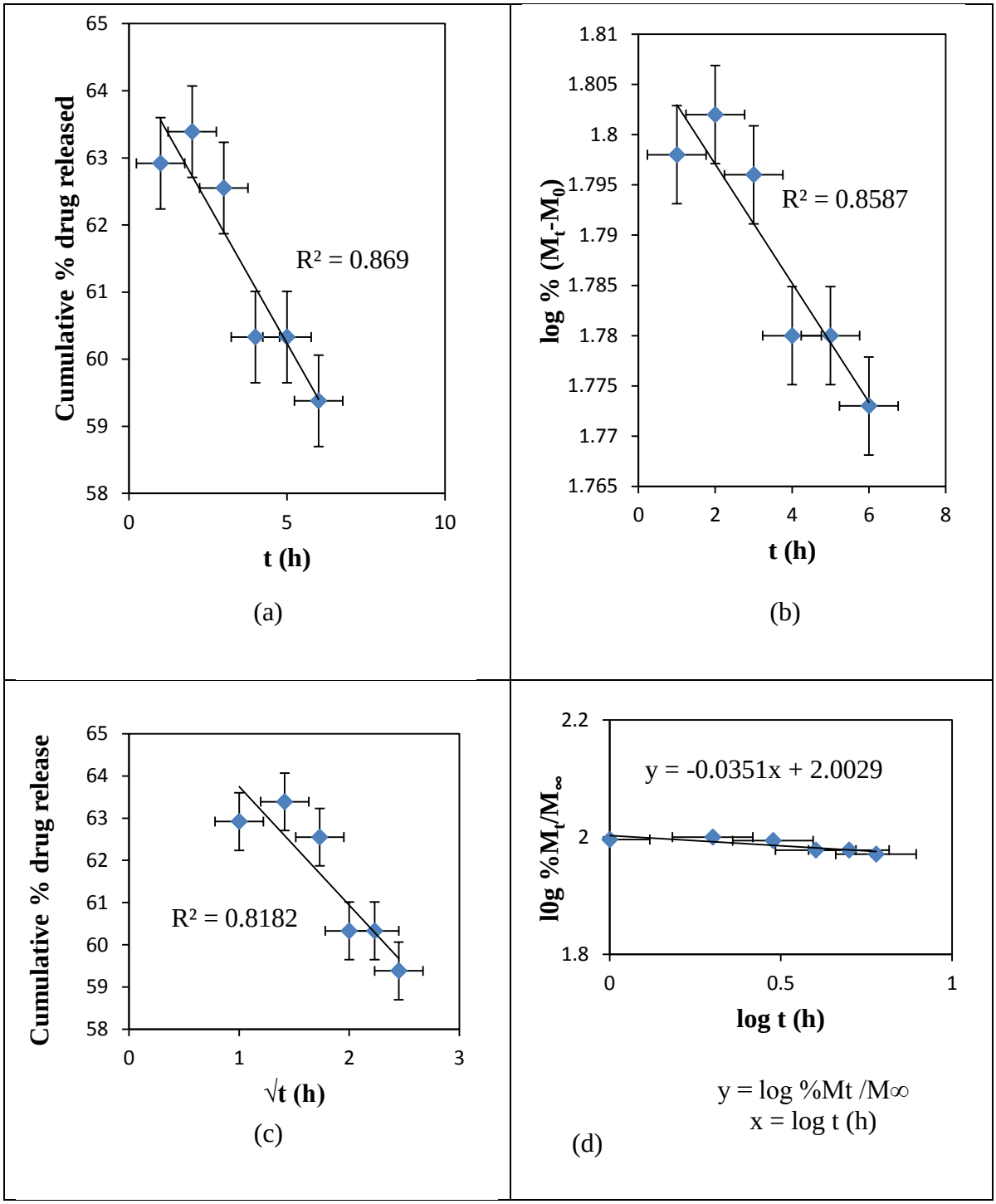

Figure 5.20: Plots of (a) Zero, (b) First, (c) Higuchi, and (d) Korsmeyer- Peppas Release Kinetics of SSA from RC/FCNF/PPySSA matrices, E = 0 V, pH 5.5, 37 °C, R^2 = Correlation coefficients

The diffusion coefficients of sulfosalicylic acid from the matrices are calculated according to the following equation [8]:

$$\sqrt{(\frac{M_t}{M_0 \times 2})} = (\frac{Dt}{\pi h^2}) \quad (5\text{-}7)$$

Where, M_t is the amount of drug released at time, t; M_0 is the initial drug concentration in the matrices; D is the diffusion coefficient of the drug; and h is the thickness of the matrices. The diffusion coefficient of the drug from RC/FCNF/SSA matrices is higher (4.2 X 10^{-8} cm^2 s^{-1}) than that of the RC/FCNF/PPYSSA (1.4 X 10^{-8} cm^2 s^{-1}) matrices. The presence of polypyrrole can hold quantities of drug within the nanoporous coatings, while at the same time regulating drug transport.

Drug release mechanism under AC magnetic field is based on the fact that heat produced locally by functionalized carbon nanofibers in AC magnetic field loosens the polymer chain surrounding the particles and lets the entrapped drug molecules to be released.

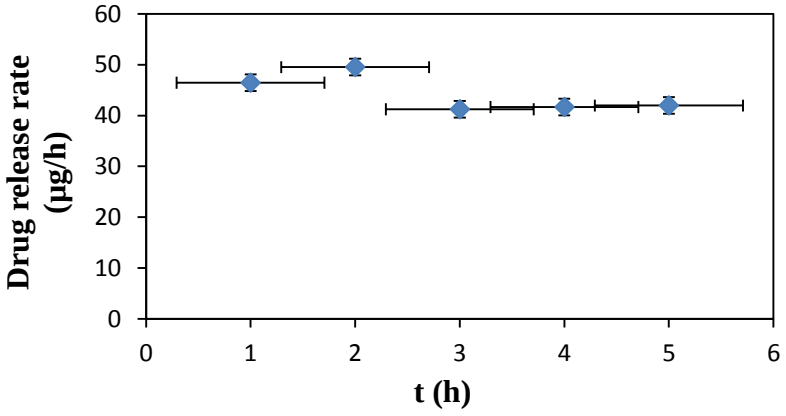

Figure 5.21: Plots of release rate of SSA from RC/FCNF/SSA (1.5 %) matrices at ACMF 1.15 KHz, 0.1 A, pH 5.5

Figure 5.21 shows release rate of SSA from the RC/FCNF/SSA (1.5 %) matrices under magnetic field. The release rate of SSA increases with time up to 2 hours. This is due to the burst effect. After that, the release rate dropped and a zero order drug release is observed because of the swelling and diffusion of the matrices (Figure 5.21). Zero-order, first-order, Higuchi, and Korsmeyer-Peppas models are used to estimate the kinetics of drug release (Figure 5.22).

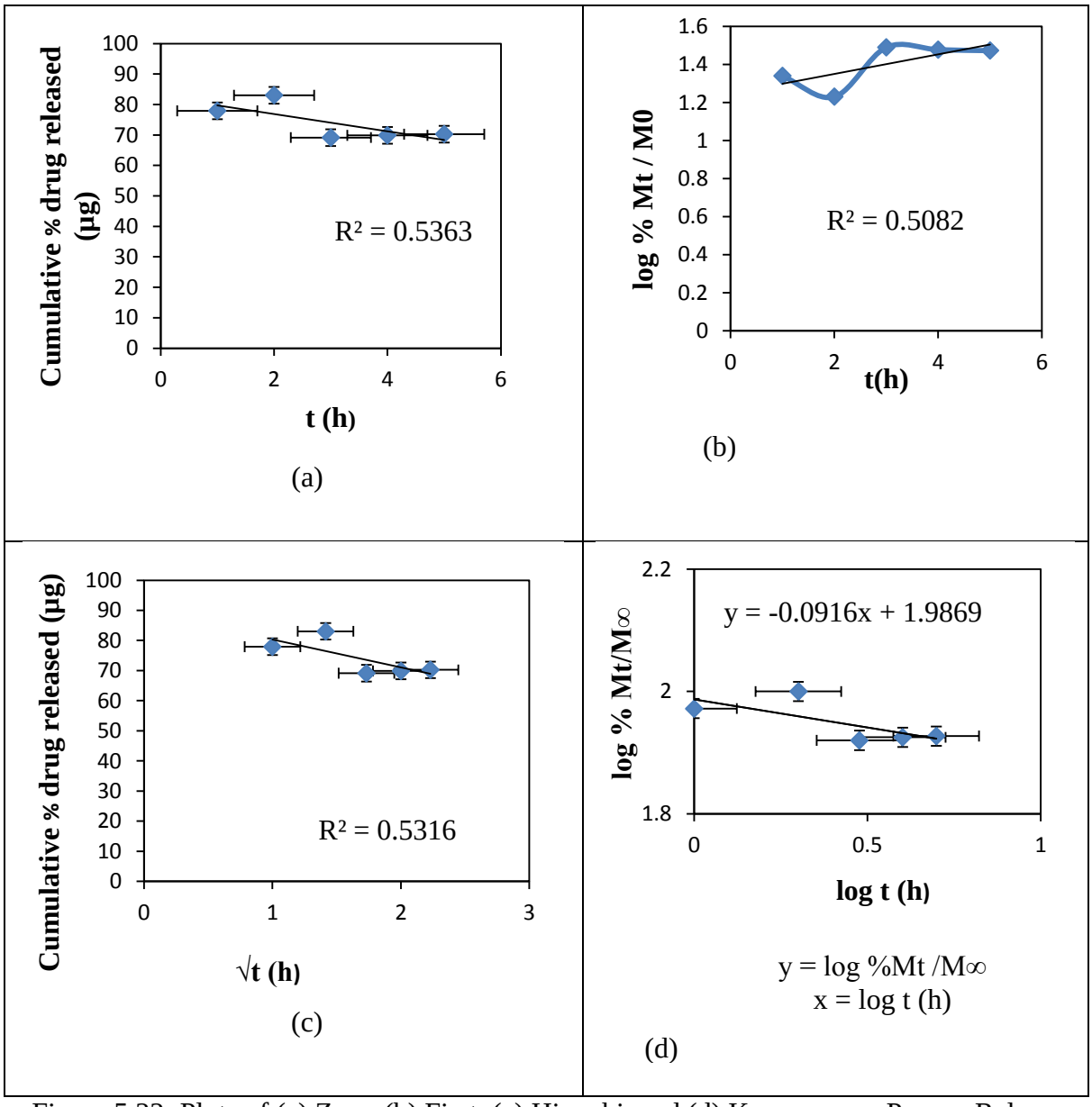

Figure 5.22: Plots of (a) Zero, (b) First, (c) Higuchi, and (d) Koresmeyer- Peppas Release Kinetics of SSA from RC/FCNF/SSA matrices at ACMF 1.15 KHz, 0.1 A, pH 5.5, R^2 = Correlation coefficients

Figure 5.23 shows release rate of SSA from the RC/FCNF/PPySSA matrices under magnetic field. The release rate of SSA increases with time up to 2 hours. This is due to the some loosely held drug molecules attached with the matrices. After that, the release rate dropped and a zero-order drug release is observed because of the nanocoating of polypyrrole on the RC/FCNF matrices that holds some drug molecules within the matrices (Figure 5.23). Zero-order, first-order, Higuchi, and Korsmeyer models are used to estimate the kinetics of drug release (Figure 5.24).

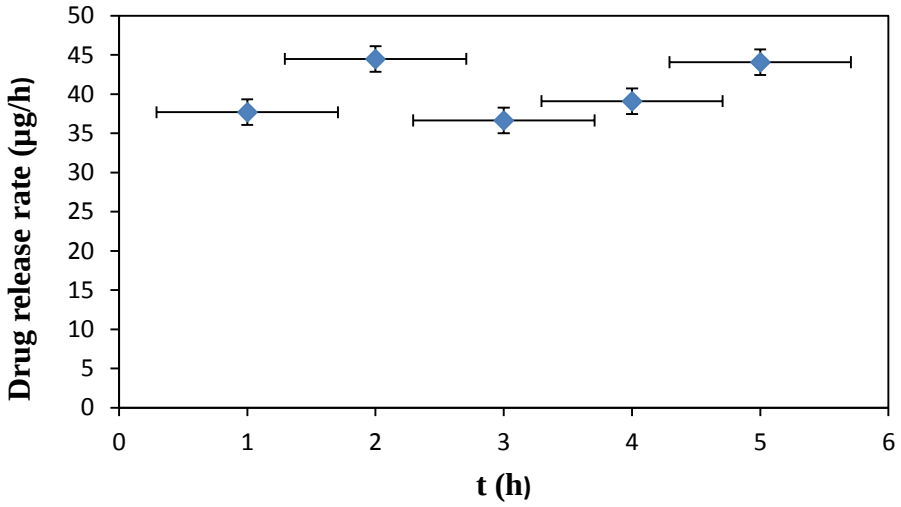

Figure 5.23: Plots of release rate of SSA from RC/FCNF/PPySSA matrices at ACMF 1.15 KHz, 0.1 A, pH 5.5

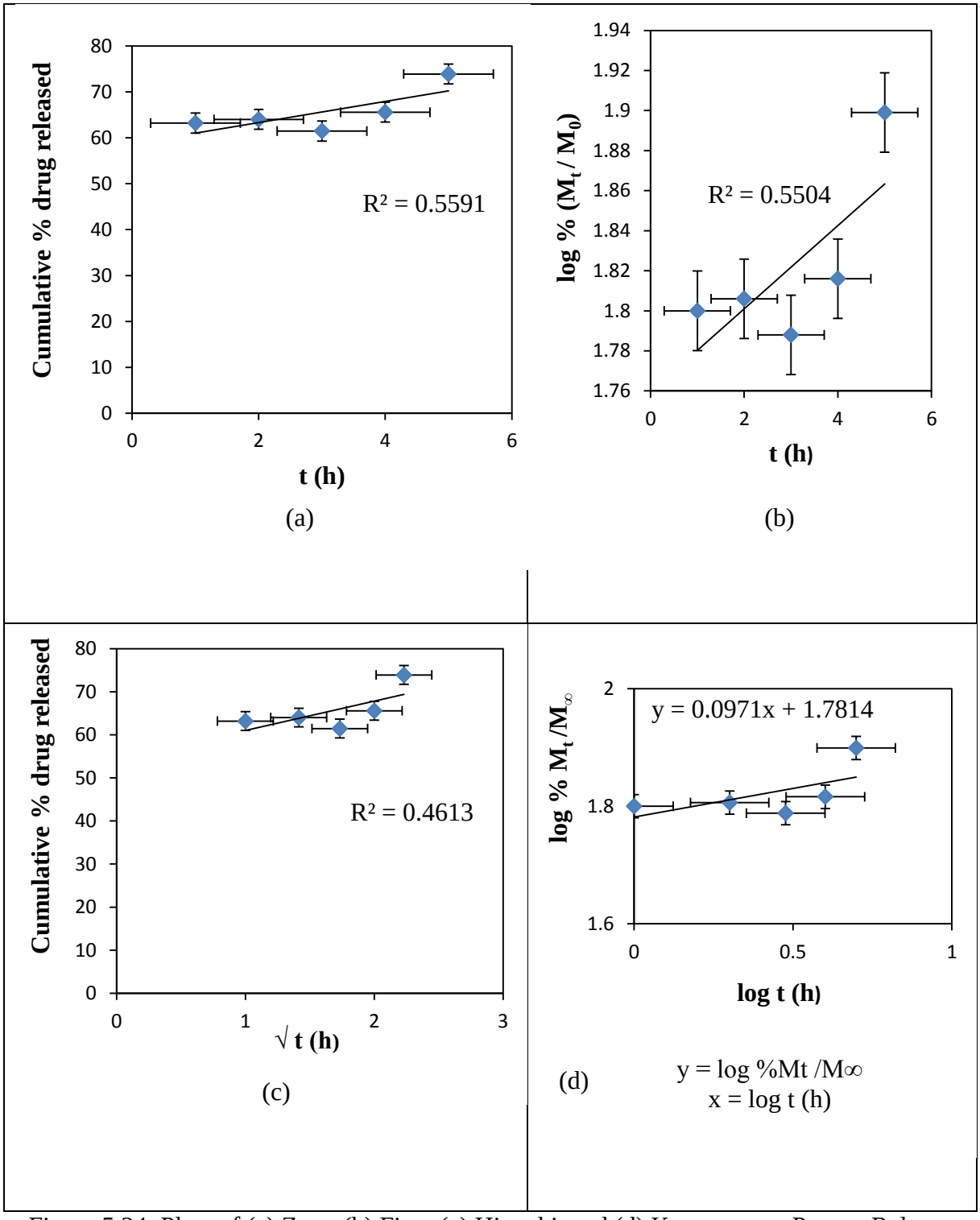

Figure 5.24: Plots of (a) Zero, (b) First, (c) Higuchi, and (d) Koresmeyer- Peppas Release Kinetics of SSA from RC/FCNF/PPySSA matrices at ACMF 1.15 KHz, 0.1 A, pH 5.5, R^2 = Correlation coefficients

5.7 Summary

The present study gives importance on the initial concentration distribution of a drug in the drug delivery carriers. The comparison of the release mechanism of sulfosalicylic acid from the RC/FCNF/SSA and RC/FCNF/PPYSSA matrices in the passive release characteristic (E = 0 V), and under electric field was investigated in this study. At E = 0 V, for RC/FCNF/SSA matrices, the rate of drug release was decreased with time due to the matrix swelling. Therefore, in this study, the rate of drug release was controlled by varying the electric field strength. The rate of drug release was effectively increased with increasing applied electric potential due to the excellent conductivity of the carbon additives. In addition, the release rate of drug was controlled by changing the electrode polarity.

For RC/FCNF/PPYSSA matrices, at E = 0V, the drug release rate decreases with time. The drug release rate was increased by applying electric field of 3 volts. The drug release rate was controlled by coating the RC/FCNF matrices with polypyrrole perfectly compared to the RC/FCNF/SSA matrices, which shows fast release. The materials also responded under alternating current (AC) magnetic field, even though the correlation coefficient is less than 0.56. They can be actuated remotely. Magnetically induced drug delivery is superior to the electrostatic one, as it does not damage healthy tissue. Another important characteristic is that the material is biodegradable [163]. Therefore, they have potential application as subcutaneous implants. The advantage of biodegradable implant includes high drug concentration at the site of infection, and as the implant is biodegradable, it is not necessary to remove the implant after treatment.

The next chapter will focus on the controlled drug delivery from γ-ferric oxide containing regenerated cellulose-based matrices, as magnetically induced drug delivery is safe compared to the electrostatic one. In addition, γ-ferric oxide nanoparticles are more paramagnetic (γ-ferric oxide nanoparticles with sizes less than 50 nm possess super paramagnetic properties) compared to the functionalized carbon nanofibers.

Chapter 6 Magnetic carriers for controlled drug delivery systems

6.1 Introduction

The principle of controlled drug delivery by magnetic carriers is based on the use of alternating current (AC) magnetic field. This approach requires magnetic nanoparticles with adequate magnetic strength, biocompatibility and interactive functions on the surface [164]. Magnetic nanoparticles themselves may not be very useful in practical applications because they tend to form large aggregates and can undergo rapid biodegradation when they are directly integrated in a biological system [165]. This chapter presents suitable methods of how to (i) make the particles fully dispersed in a polymer matrix and (ii) coat the particles for practical applications. This chapter also presents in vitro drug release behaviour of the drug-loaded matrices under electric field and an alternating current (AC) magnetic field. Further, this chapter presents electrical and swelling behaviour of the composite matrices, morphology, and electro-active composite-drug interaction.

6.2 Mechanism of drug release under magnetic field

The principle of controlled drug release from regenerated cellulose/magnetic particles composite under magnetic field is based on the fact that heat produced locally by magnetic particles under alternating current (AC) magnetic field loosens the polymer chain surrounding the particles at temperatures above the glass transition temperature (Tg) of that particular composite, resulting in encapsulated drugs released [92]. Magnets in association with carriers containing super paramagnetic iron oxide nanoparticles (SPION) help

delivering drug to inflammatory sites at a desired rate and allow switching on and off the magnetic field, thus targeting the particles at the local site [109]. Gamma ferric oxide nanoparticles having diameter < 50 nm is termed as SPION. They have magnetic properties because of the presence of aligned unpaired electron spins. They show magnetism even in the absence of external magnetic field. Their moments align to the direction of the magnetic field while placed under magnetic field. As a result, it enhances magnetic flux and the rate of drug release [110].

6.3 Fabrication of regenerated cellulose-based matrices

6.3.1 Materials

Fe $(NO_3)_3$ •$9H_2O$ (Ferric nitrate nonahydrate), polyethylene glycol (PEG1000), and potassium chloride (KCl) were analytical grade. Lithium chloride, cotton linter (DPW 4580), pyrrole, 5-sulfo-salicylic acid dihydrate (Fluka), and ferric chloride hexahydrate, Di-methylacetamide (DMAC) (Anhydrous 99.8%), 2-propanol were purchased from Sigma Aldrich, USA. Acetone and methanol obtained from Fluka, AR grade.

6.3.2 Synthesis of γ-Ferric oxide nanoparticles

Gamma ferric oxide nanoparticles were prepared as follows [166]. First, 0.006 mol $Fe(NO_3)_3$•$9H_2O$ was dissolved in 100 mL aqueous solution of PEG1000 with a NO_3^- /PEG1000 molar ratio of 1. Then, 0.45 g KCl was added to the above solution. The resulting transparent solution was stirred by a magnetic stirrer and heated at 70 °C until a homogeneous sol-like solution was formed. The sol-like solution was then dried at 110 °C

for 2 h. After that, the obtained gel was kept in a silica crucible and heated in air until the gel was ignited. The resulting as-burned powder was boiled in deionized water to remove the salt. Finally, the products were obtained after filtering, washing with deionized water and ethanol and followed by drying at 80 °C for 2 h.

6.3.3 Preparation of γ-Ferric oxide nanoparticles dispersed RC matrices

0.60 g gamma ferric oxide nanoparticles were added in 10 mL regenerated cellulose solution [25] and then sonicated for 4 h. From the prepared mixture, 3 mL was poured on a glass petri dish to cast each film. The films thus obtained were allowed to stand in air overnight to remove the solvent. Afterwards, the films were cured in a mixture of isopropanol and deionized water (60:40). Finally, the films were dried in air.

Other processes were conducted by the similar procedure described in previous chapter as follows:

- Coating of polypyrrole on RC/ γ-Fe_2O_3 matrix

RC/γ-ferric oxide films were coated with polypyrrole according to the method described in subheading 5.3.3 (second method) to avoid repetition.

- Drug release experiments

Buffer solution was prepared as described in subheading 5.4.1.

- Actual drug content

The actual amount of drug in the drug-loaded film with the dimension of 2.4 cm X 0.6 cm X 70 μm was determined according to the method described in subheading 5.4.3.

- Diffusion studies under electric field

Diffusion studies in in vitro were carried out using a set-up drawn in Figure 5.2 [16]. 0, and 1.0 V electric field were applied across the film, and the buffer solution.

- Spectrophotometric analysis of model drug

The maximum absorption spectra of the model drug and the amount of drug released were calculated according to the method described in subheading 5.4.5.

- Diffusion studies under alternating current magnetic field

To study drug release behaviour under an alternating current (AC) magnetic field an electromagnetic field was produced using the same method described in subheading 5.4.6.

6.4 Matrices characterization

Physical, electrical, chemical, and morphological properties of the matrices were analysed in terms of degree of swelling, conductivity, infrared absorption spectra, and scanning electron microscope (SEM) images.

6.4.1 Physical, morphological, and electrical properties of the matrices

The degree of swelling was measured according to the method described in ref. [157].
The degree of swelling was defined as the water content of the matrices. Percentage degree of swelling was calculated by the following equation:

$$\frac{M - M_d}{M_d} \times 100 \qquad (6\text{-}1)$$

Where, M = weight of the RC/γ-Fe_2O_3/PPySSA sample after submersion in the acetate buffer solution, and M_d = weight of the sample after removing the solvent. RC/γ-Fe2O3/PPySSA matrices showed degree of swelling of 50 %. The result indicates the porous structure of the matrices. Drug release from the matrices involves the following processes: (i) entry of water into the matrices (ii) swelling of the matrices (iii) dissolution and diffusion of the drug towards the outside of the matrices. Therefore, the degree of swelling can play an important role to release the drug from the matrices.

The distribution of gamma ferric oxide (γ-Fe_2O_3) nanoparticles in the RC/γ-Fe_2O_3 matrix was examined by the image of SEM. SEM image (Figure 6.1) shows that gamma ferric oxide nanoparticles can be dispersed into the cellulose matrix.

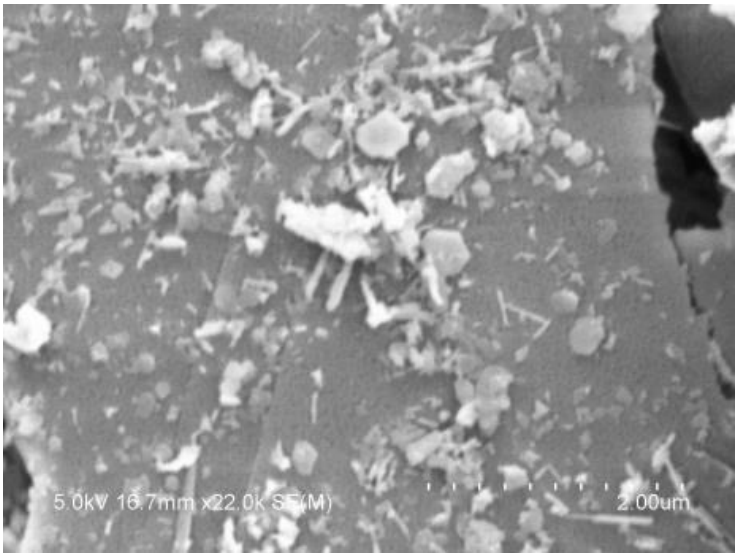

Figure 6.1: SEM image of gamma ferric oxide dispersed RC matrix

Electrical conductivity (σ_s) of the matrices was calculated using the equation (4-1).

Where, l = length, w = width, d = thickness, and $\frac{\Delta I}{\Delta V}$ = the slope of the current versus voltage curve

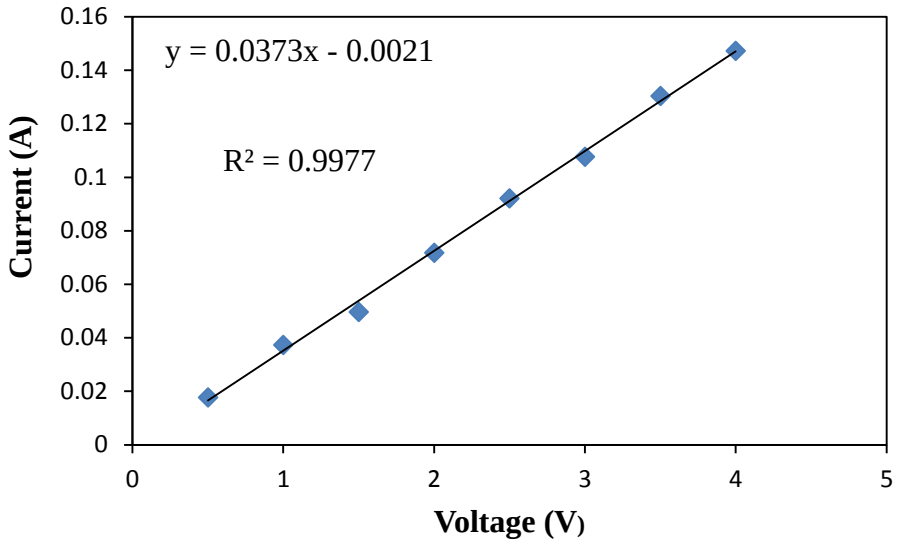

Figure 6.2: Current *vs*. Voltage Curve for RC/γ-Fe_2O_3/PPySSA matrix film, y = Current, x = Voltage, R^2 = Correlation coefficients

The electrical conductivity of the RC/γ-Fe_2O_3/PPySSA film is $1.7 \times 10^0 S/cm$, which is eight orders of magnitude higher compared to the conductivity of RC ($10^{-8}\ S/cm$). Figure 6.2 shows the typical current-voltage sweep curve. The conductivity of the matrix follows the Ohm‘s law.

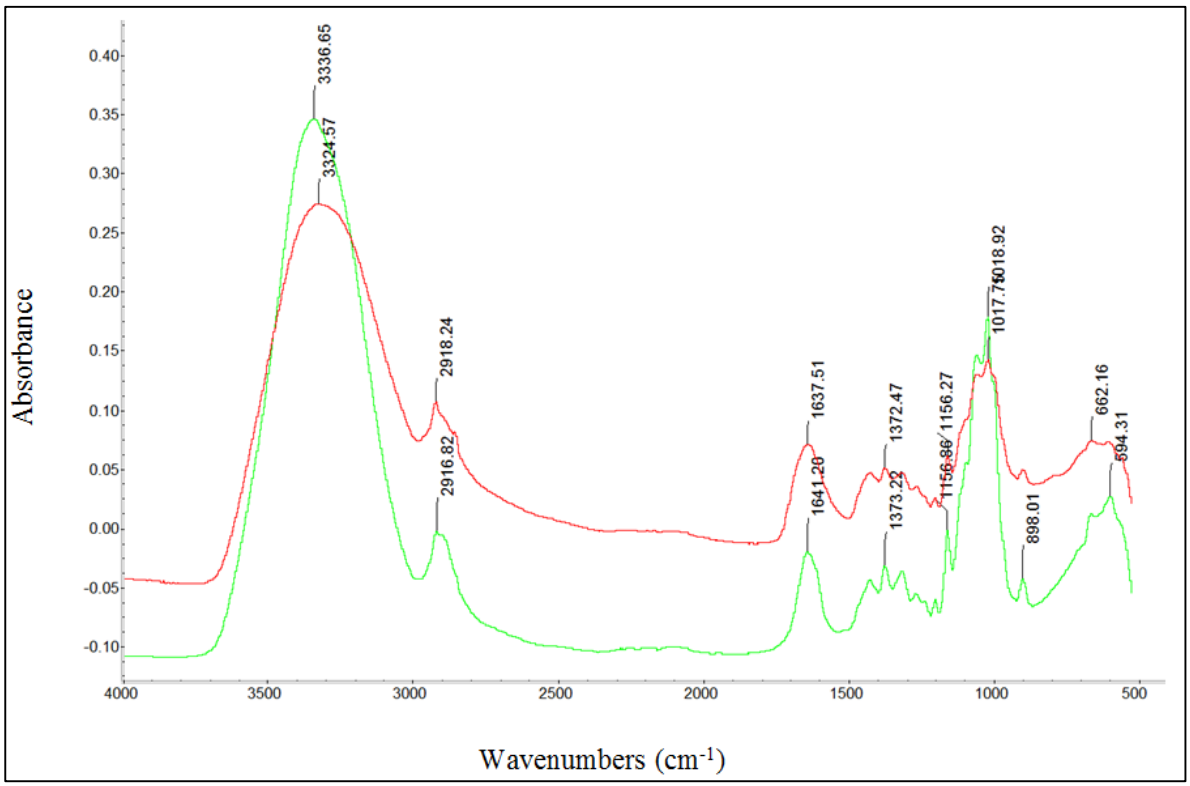

Figure 6.3: FTIR spectra of RC/ γ-Fe_2O_3 (red line) matrices film and γ-Fe_2O_3 (green line) powder

The infrared absorption studies are performed aiming to ascertain the metal-oxygen bond and the vibrational peaks of γ-Fe_2O_3. In Figure 6.3 , RC/γ-Fe_2O_3 film shows absorption peak at 3324 cm^{-1}. This is due to the –OH group of RC. The peak at 594 cm^{-1} of γ-Fe_2O_3 corresponds to the metal-oxygen vibrational modes of the spinel compound [167]. In addition, γ-Fe_2O_3 shows absorption band in the region of 3600–3100 cm^{-1} relating to antisymmetric and symmetric –OH stretching, may be assigned for water of hydration. Hydrates also absorb in the region 1670–1600 cm^{-1} relating to –OH bending [168].

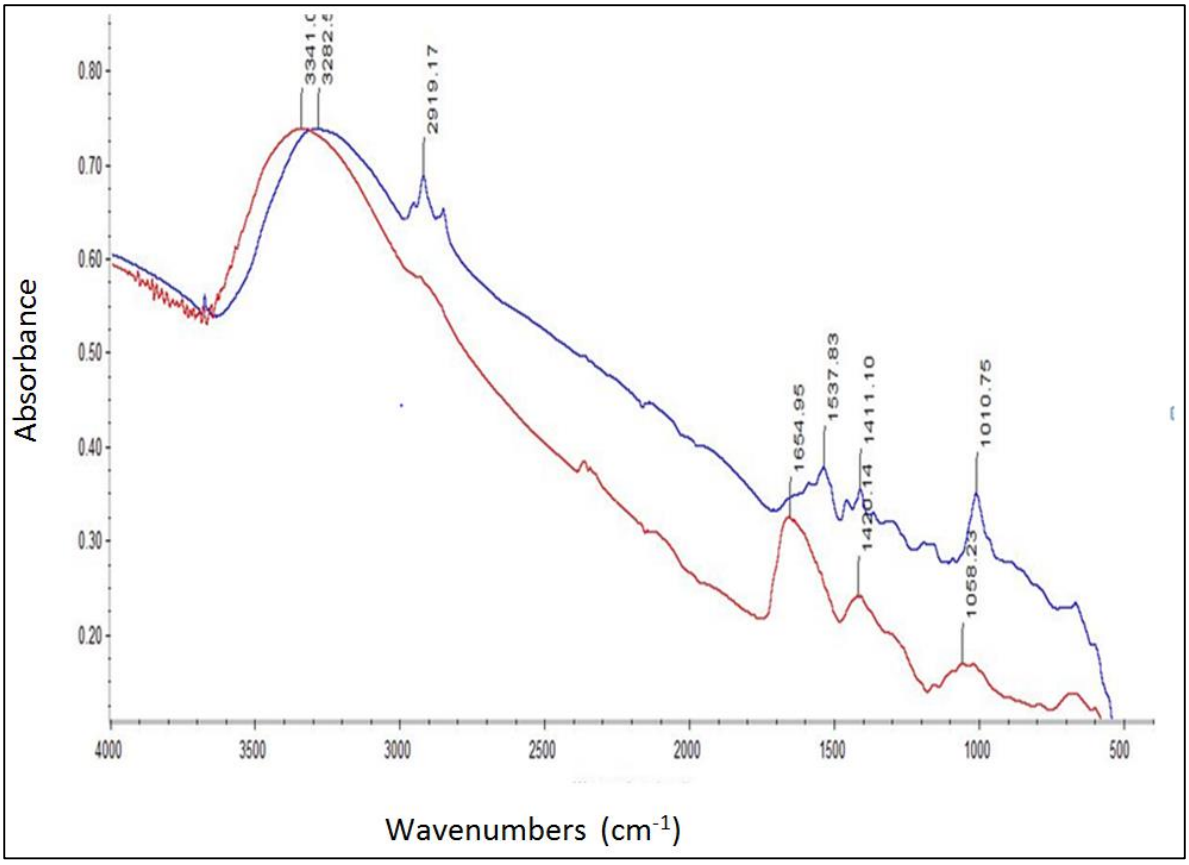

Figure 6.4: Comparison of FTIR spectra of RC/γ-Fe_2O_3 (red line) and RC/γ-Fe_2O_3/PPySSA (blue line)

FTIR spectra in Figure 6.4 exhibit five-membered PPy ring stretching and conjugated C–N stretching vibration bands at 1537 and 1411 cm^{-1}, respectively. In addition, the peak at 2919 cm^{-1} is associated with five membered C–H ring stretching. These observations confirm that the PPy layer is successfully introduced onto the surface of the RC/γ-Fe_2O_3 matrices. For the RC/γ-Fe_2O_3/PPySSA film, the sulfonate groups (SO_3^-) stretching is intensified (1010 cm^{-1}) and the –OH stretching peak has a slight shift between 3000 and 3600 cm^{-1}. These results suggest the H-bonding between the sulfonate groups of sulfosalicylic acid and with the amine group of pyrrole unit of PPy [169].

6.4.2 Kinetics of the drug release profile

Initially, the amount of drug present in the matrices was measured. The amount of drug present in the matrices is about 85.4 ± 0.78 %. In vitro release data were fitted to various kinetic models such as zero order, first order, Higuchi release, Korsmeyer-Peppas to evaluate the mechanism of drug release. The rate constants were calculated from the slope of the respective plots and high correlation was observed for the Higuchi model (Table 6-1). The values of exponent n were obtained with the help of Korsmeyer-Peppas model. The value of the exponent n determines the type of drug release mechanism. Each data point in the plots (figure 6.5-figure 6.9) is an average value from two samples.

Table 6-1: Fitting parameters of the in vitro release data to various release kinetic models for RC/γ-Fe_2O_3/PPySSA matrices

Samples	Order	Electric field strength (V)	Slope	K	R^2
RC/γ-ferric oxide/PPySSA	First order	0 1	0.048 0.096	0.048 0.096	0.761 0.9543
	Zero order	0 1	3.81 7.80	3.81 7.80	0.7584 0.977
	Higuchi	0 1	12.87 25.57	12.87 25.57	0.8192 0.9959
	Korsmeyer Peppas	0 1	0.1135 0.246		0.831 0.9971

The diffusion coefficients of sulfosalicylic acid from the matrices at 0 & 1 volts were calculated from the slope of plots of drug accumulation vs. square-root-of-time (Figure 6.5) according to the Higuchi equation [170]:

$$Q = 2M_0\sqrt{\left(\frac{Dt}{\pi}\right)} \qquad (6\text{-}2)$$

Where Q is the amount of material flowing through a unit cross-section of barrier in unit time, t; M_0 is the initial drug concentration in the matrices; and D is the apparent diffusion coefficient of the drug. Each data point is an average value from two samples.

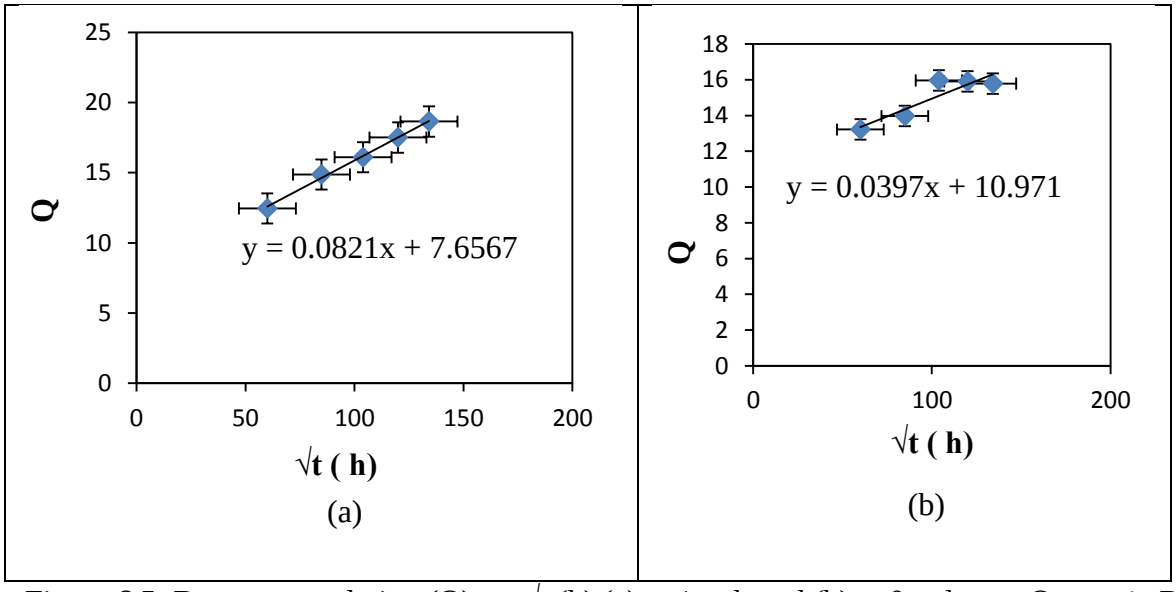

Figure 6.5: Drug accumulation (Q) *vs.* √t (h) (a) at 1 volt and (b) at 0 volt, y = Q, x = √t, R^2 = Correlation coefficients

The diffusion coefficients of sulfosalicylic acid from RC/γ-Fe_2O_3/PPySSA matrices are 1.38×10^{-7} cm^2 s^{-1} in the absence of electric field and 6.66×10^{-7} cm^2 s^{-1} under electric field strength of 1V. This result shows that the diffusion coefficients of the drug depend on the strength of the applied electric field.

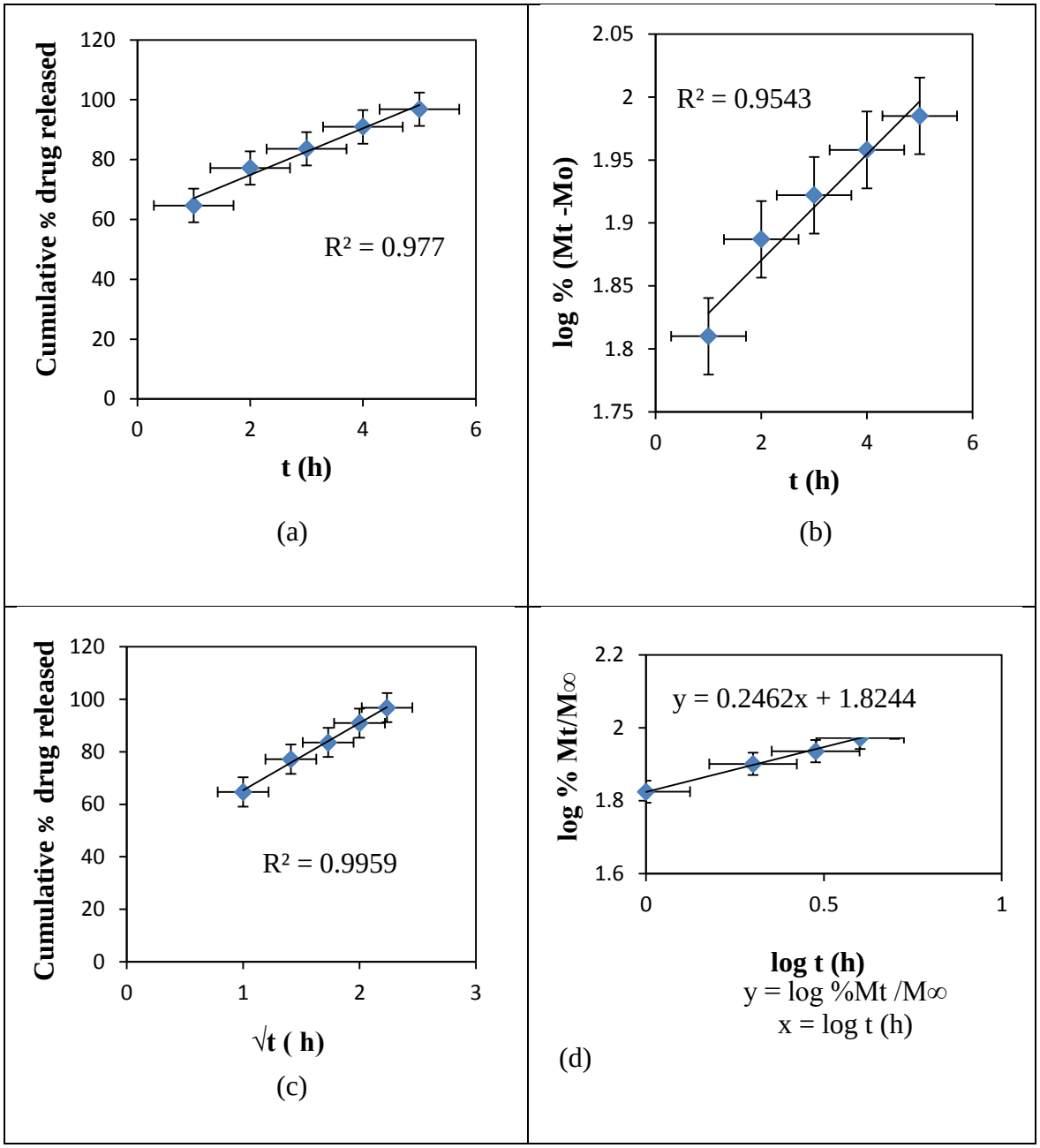

Figure 6.6: Plots of (a) Zero, (b) First, (c) Higuchi, and (d) Koresmeyer- Peppas Release Kinetics of SSA from RC/γ-Fe_2O_3 /PPySSA matrices at E = 1 V, pH 5.5, 37 °C, R^2 = Correlation coefficients

The plots in Figure 6.6 show that the RC/γ-Fe_2O_3/PPySSA matrices (2.4 cm X 0.6 cm with a thickness of 70 - 75 µm) under electric field follow a square-root-of-time dependent drug release kinetics as it has the highest R^2 value. The rate and extent of drug release increase with square-root-of-time. The presence of polypyrrole helps transporting SSA through the matrices. Here polypyrrole release drug in response to electrical signal. Polypyrrole chains

are expanded when the matrices are under electric field, and free space in the PPy chains is generated, thus electric field pushing the ionic drug out by the electrostatic force.

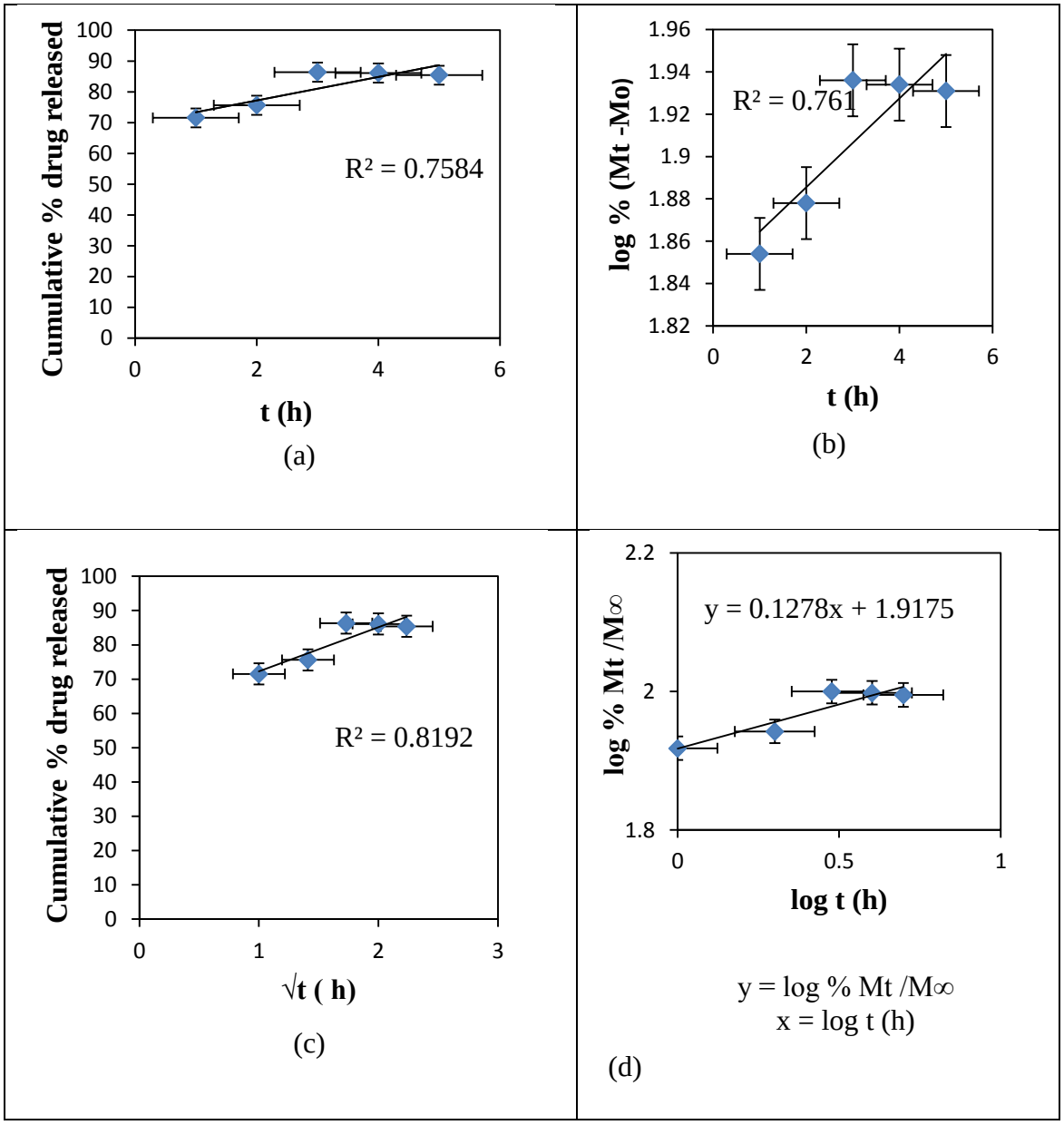

Figure 6.7: Plots of (a) Zero, (b) First, (c) Higuchi, and (d) Koresmeyer- Peppas Release Kinetics of SSA from RC/γ-Fe_2O_3/PPySSA matrices at E = 0 V, pH 5.5, 37 °C, R^2 = Correlation coefficients

The plots given in Figure 6.7 show that RC/γ-Fe_2O_3/PPySSA matrices (2.4 cm X 0.6 cm with a thickness of 70 - 75 µm) at E = 0 V follow a square-root-of-time dependent drug release kinetics in the absence of electric field. The drug release rate gradually increases

with the square-root-of-time and after 3 h reaches equilibrium values. The drug molecules diffuse out of the matrices through the concentration gradient effect in the absence of electric field.

Figure 6.8 shows a comparison of square-root-of-time dependent release kinetics observed by sample-1 & 2. Sample-1 under electric field shows linear increase of drug release with square-root-of-time, whereas sample-2 shows gradual increase of drug release initially and after 3 hours reaches equilibrium values. This is due to the interaction of drug with polypyrrole.

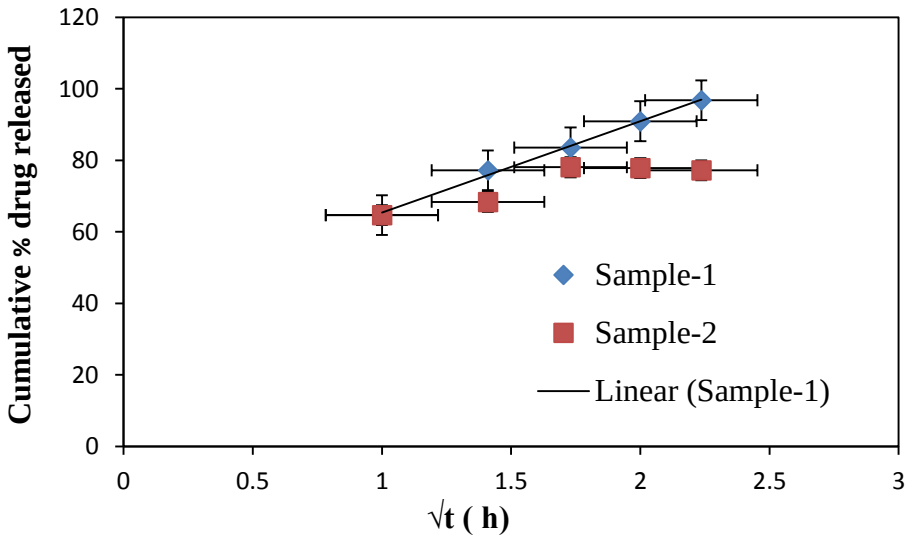

Figure 6.8: Square root of time release kinetics observed by the Sample-1 (1 volt) and Sample-2 (0 Volt)

Drug release kinetics was determined from RC/γ-Fe_2O_3/PPySSA matrices (2.45 cm X 0.6 cm with a thickness of 67-70 µm) under AC magnetic field using zero-order, first order, Higuchi, while the mechanism of drug release was determined using Korsmeyer-Peppas model. For zero-order, first order, and Higuchi model, the correlation coefficient (R^2) was

graphically determined and used to predict the kinetics of drug release from the matrices (Figure 6.9).

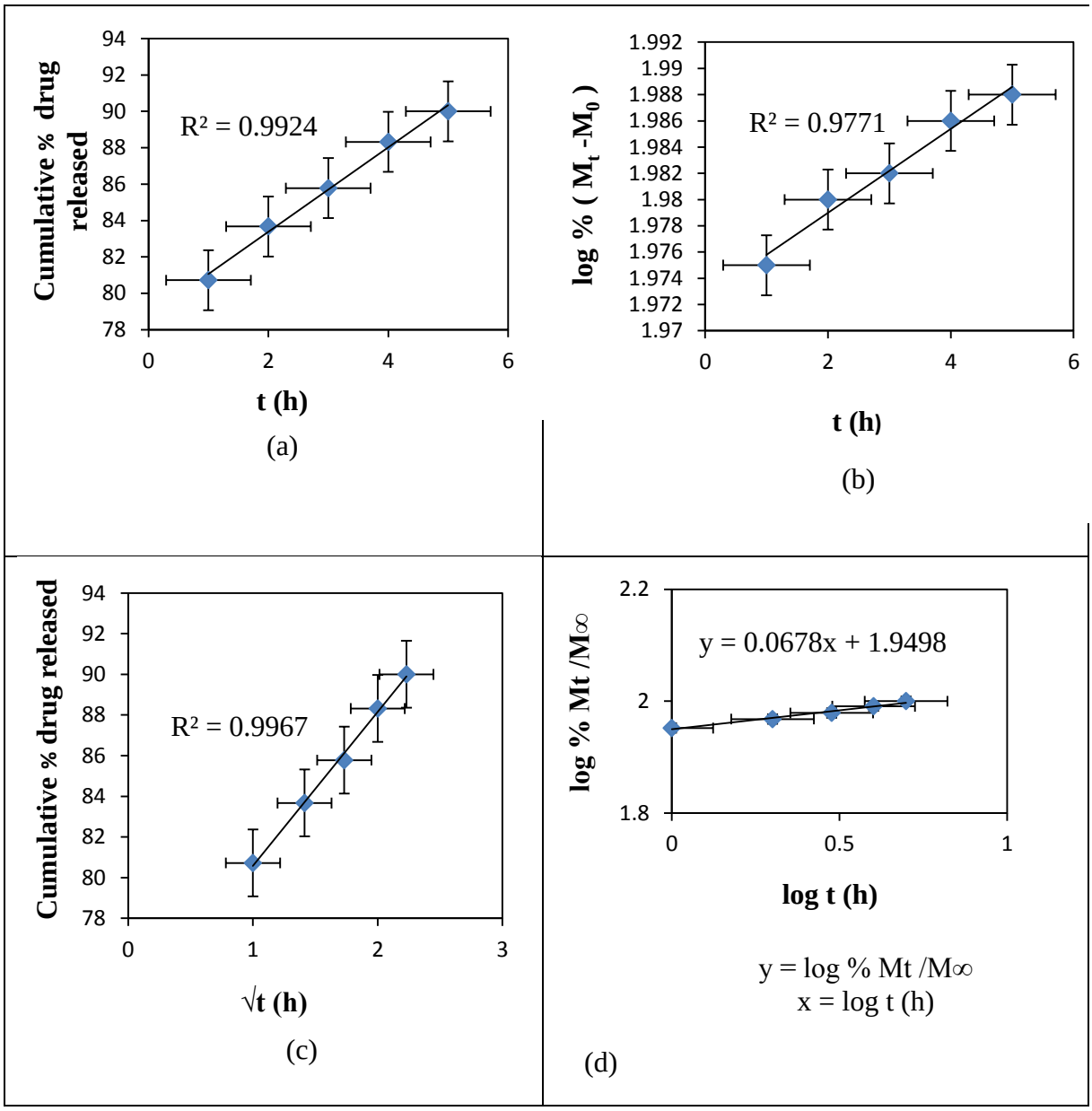

Figure 6.9: Plots of (a) Zero, (b) First, (c) Higuchi, and (d) Koresmeyer- Peppas Release Kinetics of SSA from RC/γ-Fe_2O_3/PPySSA matrices at ACMF 1.15 KHz, 0.1 A, R^2 = Correlation coefficients

According to the plots given in Figure 6.9, the material shows a square-root-of-time dependent release kinetics as the plot of cumulative % drug release Vs √t has the highest value of R^2. The heat produced locally by magnetic particles under alternating current (AC)

magnetic field loosens the polymer (polypyrrole) surrounding the particles. As a result, the drugs attached with the polypyrrole chain come out to the release medium.

6.5 Summary

The release mechanism of sulfosalicylic acid from the RC/γ-ferric oxide/PPySSA matrices with and in the absence of electric field was investigated in this study. RC/γ-ferric oxide /PPySSA matrices showed initial gradual increase of drug release rate with time at E = 0 volt. The release of drug then reached equilibrium values. In the passive drug diffusion (0 V), the diffusion of drug molecules through matrices is caused by the concentration gradient effect. The rate of drug release was linearly increased with square-root-of-time under the electric field strength of 1V. This result indicates that the drug release mechanism is diffusion controlled. In addition, the presence of polypyrrole (expansion of polypyrrole chain) helps transporting SSA through the matrices.

Chapter 7 Discussion, Conclusion and future directions

7.1 Discussion

This chapter gives some highlights on the findings of the work, although the main discussion has been presented in previous chapters. The bending or deswelling behaviour of regenerated cellulose-based electro-active matrices depends on the matrices position relative to the electrodes under electric field is investigated in this study. In addition, the drug release kinetics from the matrices under electric and magnetic field are also investigated with a view to find out better biomedical applications of the developed matrices. Although, the material can be used to develop biomimetic actuators, this work may be easily adapted to developing drug delivery devices.

In this study, a comparative study is performed on the performance of the actuators developed by different preparation processes. The effects of dopant ion and preparation process are compared for the three types of the actuators. Polypyrrole coated actuators give better performance than the actuators with polypyrrole (blends) in terms of electrical conductivity and actuation performance. The layer-by-layer casting actuators are superior to the other types of the actuators in terms of bending displacement, actuation force, and stability. Magnetically induced actuators show better performance at higher frequencies (4Hz) compared to the actuators working under electric field.

7.1.1 Mechanisms and physics behind the results

In layer-by-layer casting actuators, electrode and electrolyte layers are seamlessly connected with one another, which accounts for rapid response in actuation. In addition, ionic liquids are non-volatile, have high ionic conductivities and wide potential windows, which are favourable for rapid response in actuation and stable performance. When an electric potential is applied to the actuators, electric double layers are developed with negatively and positively charged carbon nanofibers as the cations and anions of the built-in ionic liquid may be transported to the cathode and anode sides. These movements of ions cause swelling of the cathode layer and shrinkage of the anode layer, as the former ions are larger than the latter. Consequently, this generates a large bending motion toward the anode side compared to the other actuators developed in this research. The actuators can be actuated magnetically because of the presence of functionalized carbon nanofibers. Functionalized carbon nanofibers possess paramagnetic properties because of the presence of large amount of defects in the graphene layers of the nanofragments. In addition, magnetic moment and ferromagnetic interaction was enhanced by including H-atoms to the zigzag edge in the nanographite system after functionalization.

Table 7-1: A comparative studies of the actuators developed in different preparation processes

Properties	RC/FCNF/PPy (blend) actuators	RC/FCNF/PPy (coated) actuators	Layer-by-layer casting actuators
Conductivity	2.7 X 10^{-3} S/cm Difficult to form conductive paths by the randomly distributed ball-like particles in the mix composite (see Figure 3.14)	5.4 X 10^{-1} S/cm Regularity of polypyrrole chains and inter-chain packing give improved conductivity	1.34 X 10^{-1} S/cm Good dispersion of FCNFs in the polymer matrix makes it more conductive
Actuation force	0.9917 mN	1.49 mN	2.49 mN
Stability	Stable performance at highly humid condition	Stable performance at highly humid condition	Stable performance at ambient humidity because of the built in non-volatile ionic liquid electrolyte layer
Power consumption	0.10 mW cm^{-2}	0.19 mW cm^{-2}	0.32 mW cm^{-2}

Chapter 3 and 4 established the following facts:

- A good dispersion of FCNFs in the cellulose matrix caused an interaction between cellulose and FCNFs and that gave reinforced mechanical behaviour related to output force improvement of the actuators (see Figure 3.11)
- The durability of the actuator was due to the AQSA-Na containing anthraquinone ring, which seemed to inhibit the reaction of PPy with oxygen (see Figure 3.18)
- The net electrical power consumption of RC/FCNF/PPy (coated) and RC/FCNF/PPy (blends) actuators are 0.19 mW cm^{-2}, and 0.10 mW cm^{-2}, which is below the microwave power limit for damaging living organs
- The layer-by-layer casting actuators showed stable performance at ambient humidity due to the built-in ionic liquid electrolyte layer
- The layer-by-layer casting actuators moved in response to the magnetic force direction because of their magnetic properties and responded well at higher frequencies (4Hz) compared to the actuators working under electric field

The advantages of the layer-by-layer casting actuators are easy process of fabrication and their durability. They can be actuated by external stimuli (electrically and magnetically) because of the presence of FCNF in the composites. Consequently, one can also be beneficial from a contactless actuation that is not available in other actuation mechanisms like the electrostatic one.

In this research, a comparative study is performed on the rate of drug release from matrices induced by electric and magnetic field separately. The mechanism of drug release from drug-doped polypyrrole coated matrices includes expansion of conductive polymer chain and the electrostatic force between electron and drug. The combined effect of polypyrrole coating, electrode polarity, and electric potential are compared with the drug release behaviour of the matrices developed in this study. The supply of actuating energy requires either implantation of a battery or electrical leads that cause discomfort to the patient's skin. These problems can be overcome if the drug-doped matrices are actuated magnetically. The magnetically induced drug delivery is superior to the electrically induced drug delivery as magnetic field does not damage healthy tissue. In addition, the matrices containing γ-ferric oxide show square- root-of-time drug release kinetics under magnetic field as well. The matrices responded much better compared to the functionalized carbon nanofibers containing matrices under alternating current (AC) magnetic field. This is due to the matrices improved characteristics in terms of electrical conductivity and paramagnetism.

Chapter 5 investigated in vitro release kinetics of an anti-inflammatory model drug (SSA) from conductive regenerated cellulose-based matrices under an electric and an alternating current (AC) magnetic field.

Chapter 5 investigated the following facts:

- Under electric field, drug ions bound in one redox state of the polypyrrole are released from the other.

- Drug release was effectively increased with increasing applied electric voltages due to the excellent conductivity of the functionalized carbon nanofibers
- RC/FCNF matrices were coated with polypyrrole, which is biocompatible and has antimicrobial property. This property may help minimizing biofouling on the implant matrices [171]
- The matrices were actuated magnetically

However, since the implant situated deep within the body, may not be magnetically induced perfectly [125].

Chapter 6 investigated the following facts regarding the release mechanism of sulfosalicylic acid from the RC/γ-ferric oxide/PPySSA matrices with and in the absence of electric field.

- RC/γ-ferric oxide /PPySSA matrices at E = 0 volt showed gradual increase of drug release initially with square-root-of-time. Drug release then reached equilibrium values. The drug molecules diffused out of the matrices through the concentration gradient effect in the absence of electric field
- Drug release was linearly increased with square-root-of-time under the electric field strength of 1V. The presence of conductive polymer (polypyrrole) helps transporting SSA through the matrices
- The matrices were used as transdermal implants; however, they have potential application as transdermal patches.
- Further, the matrices showed fast release of drug i.e. more than 60% of the loaded drug was released within 1h, which is required for the treatment of illness in an emergency care.

The material also responded well under alternating current (AC) magnetic field. The drug release from the matrices was linearly increased with square- root-of-time under alternating current magnetic field. Chapter 6 investigated the usefulness of the combination of magnetic particles and magnetism in drug delivery systems. Since developing this type of matrix system for drug delivery is a cost-effective measure, further investigation into this type of system should be pursued.

7.2 Future directions

The present research has focused on the synthesis and characterization of simple and inexpensive transdermal implants for drug delivery applications. However, the practical applications require significant improvements in the properties of the matrices. For RC/FCNF/SSA matrices, the non-linear relationship between drug release and voltage / current may be more difficult to solve. The application of electricity to enhance drug release from the matrices was conducted in vitro. To understand the potential of electro-responsive drug release, a large number of in vivo studies will have to be conducted. Thin films work well under external stimuli compared to the thick film. Therefore, optimum time for polymerization will have to be investigated. In addition, synthesis of new matrices with optimum ratio of RC and γ–Fe_2O_3 nanoparticles is essential. Biofilms cause extensive damage to biomimetic devices. Biofilms are densely packed communities of microbial cells that grow on living or inert surfaces and surround themselves with secreted polymers. When biomimetic devices are inserted into our body, it becomes difficult for the body to clear anti-biotic-resistant biofilm infections [172]. The use of nanoparticles such as gold nanoparticles, carbon nanotubes, and iron oxide nanoparticles is a growing new approach against biofilm-mediated infections. Nanoparticles cause bacterial cell walls disruption

through direct interactions or through free radical production [173]. Our future work will be concentrated on how nanoporous polypyrrole coating and nanoparticles can significantly reduce biofilm formation on the implants used for long term.

Chapter 8 **References**

1. Baughman, R.H., *Conducting polymer artificial muscles.* Synthetic Metals, 1996. **78**(3): p. 339-353.
2. Hutchison, A.S., et al., *Development of polypyrrole-based electromechanical actuators.* Synthetic Metals 2000. **113**: p. 121–127.
3. Toribio, F.O. and J.M. SansinÄena, *Soft and Wet Conducting Polymers for Artificial Muscles.* Advanced Materials 1998. **10**(6): p. 491–494.
4. Jaehwan, K., et al., *A comparative study of conductive polypyrrole and polyaniline coatings on electro-active papers.* Polymer Journal, 2006. **38**(7): p. 659-668.
5. Fukushima, T., et al., *Fully plastic actuator through layer-by-layer casting with ionic-liquid-based bucky Gel.* Angew. Chem. Int. Ed, 2005. **44**: p. 2410 –2413.
6. Jaehwan, K. and B.S. Yung, *Electro-active paper actuators.* Smart Mater. Struct., 2002. **11**.
7. Ansari, R., *Polypyrrole conducting electroactive polymers: Synthesis and stability studies.* E-Journal of Chemistry, 2006. **13**(3): p. 186–201.
8. Ferrero, C., D. Massuelle, and E. Doelker, *Towards elucidation of the drug release mechanism from compressed hydrophilic matrices made of cellulose ethers. II. Evaluation of a possible swelling-controlled drug release mechanism using dimensionless analysis.* J Control Release. , 2010. **141**(2): p. 223-33.
9. Colombo, P., R. Bettini, and N.A. Peppas, *Observation of swelling process and diffusion front position during swelling in hydroxypropyl methyl cellulose (HPMC) matrices containing a soluble drug,.* J. Control. Release, 1999. **61**(1-2): p. 83–91.
10. Xie, Y., B. Xu, and Y. Gao, *Controlled transdermal delivery of model drug compounds by MEMS microneedle array.* Nanomedicine, 2005. **1**: p. 184–190.
11. Kanokporn, J., et al., *Electrically controlled release of sulfosalicylic acid from crosslinked poly(vinyl alcohol) hydrogel.* International Journal of Pharmaceutics 2008. **356**: p. 1-11.
12. Cristina, M., Z. Aránzazu, and M.L. José, *Critical factors in the release of drugs from sustained release hydrophilic matrices. Journal of Controlled Release.* 2011. **154**: p. 2-19.
13. Steve, I., B.R.J. Shen, and L. Xiaoling, *Design of controlledrelease drug delivery systems*2004: The McGraw-Hill Companies.
14. Smith, A. and I.M. Hunneyball, *Evaluation of poly(lactic acid) as a biodegradable drug delivery system for parenteral administration.* Int. J. Pharm, 1986. **30**(2-3): p. 215-220.
15. Sungryul, Y. and K. Jaehwan, *A bending electro-active paper actuator made by mixing multi-walled carbon nanotubes and cellulose.* Smart Mater. Struct., 2007. **16**: p. 1471-1476.
16. Murdan, S., *Electro-responsive drug delivery from hydrogels.* Journal of controlled release, 2003. **92**: p. 1-17.

17. Bar-Cohen, Y., *(EAP) Actuators as Artificial Muscles - Reality, Potential and Challenges*. Vol. PM136. 2004: SPIE Press.
18. Shahinpoor, M., Bar-Cohen ,Y., Simpson, J. O., & Smith, J. , *Ionic polymer-metal composites (IPMCs) as biomimetic sensors, actuators and artificial muscles - a review.* Smart mater. and struct,, 1998. **7**(6): p. 2343-2353.
19. Kim, K.J. and M. Shahinpoor, *Ionic polymer–metal composites: II. Manufacturing techniques.* Smart Mater. Struct., 2003. **12**: p. 65-79.
20. Sung-Ryul, Y. and K. Jaehwan, *Discovery of Cellulose as a Smart Material.* Macromolecules, 2006. **39**(12): p. 4202–4206.
21. Sungryul, Y., et al., *Electro-active paper for a durable biomimetic actuator.* Smart Mater. Struct., 2009. **18**(02).
22. Suresha, K.M., Y. Chen, and K. Jaehwan, *Effect of Room Temperature Ionic Liquids Adsorption on Electromechanical Behavior of Cellulose Electro-Active Paper.* Macromolecular Research, 2009. **17**(2): p. 116-120.
23. Matsui, T., et al., *Structure and Morphology of Cellulose Films Coagulated from Novel Cellulose/Aqueous Sodium Hydroxide Solutions by Using Aqueous Sulfuric Acid with Various Concentrations.* Polym J, 1995. **27**.
24. Dawsey, T.R. and C.L. McCormick, *The Lithium Chloride/Dimethylacetamide Solvent for Cellulose: A Literature Review.* Journal of Macromolecular Science, Part C: Polymer Reviews, 1990. **30**(3-4): p. 405-440.
25. McCormick, C.L., A.C. Peter, and H.H.J. Brewer, *Solution studies of cellulose in lithium chloride and N,N-dimethylacetamide.* Macromolecules, 1985. **18**(12): p. 2394–2401.
26. McCormick, C.L. and T.S. Shen, eds. *Macromolecular Solutions*. 1982, (R. B. Seymour and G. S. Stahl, eds.), Pergamon: New York. 101-107.
27. Jaehwan, K., et al., *Electroactive-paper actuator made with cellulose/NaOH/urea and sodium alginate.* Cellulose 2007. **14**(3): p. 217-223.
28. Brendler, E., S. Fischer, and H. Leipner, *7Li NMR as probe for solvent–cellulose interactions in cellulose dissolution. .* Cellulose, 2002. **8**: p. 283-288.
29. Sungryul, Y., et al., *Effect of solvent mixture on properties and performance of electro-active paper made with regenerated cellulose.* Sensors and Actuators B: Chemical, 2008. **129**(2): p. 652-658.
30. Greenwood, N.N. and A. Earnshaw, *Chemistry of the Elements, 2nd edn., 1997*, Butterworthâ€“Heinemann, Oxford, UK.
31. Jaehwan, K., Y. Sungryul, and L. Sun-Kon, *Cellulose Smart Material: Possibility and Challenges.* Intelligent Material Systems and Structures, 2008. **19**.
32. Jaehwan, K., et al., *Paper Actuators Made with Cellulose and Hybrid Materials.* Sensors 2010. **10**: p. 1473-1485.
33. Sungryul, Y., K. Jaehwan, and C. S., *Performance of Electro-active paper actuators with thickness variation.* Sensors and Actuators A., 2007. **133**: p. 225-230.
34. Sungryul, Y. and K. Jaehwan, *Characteristics and performance of functionalized MWNT blended cellulose electro-active paper actuator.* Synthetic Metals, 2008. **158**: p. 521-526.

35. Huang, J., et al., *Polyaniline Nanofibers: Facile Synthesis and Chemical Sensors.* J Am Chem Soc, 2003. **25**: p. 314-315.
36. Wei, C. and D. Srivastava, *Nanomechanics of carbon nanofibers: structural and elastic properties.* Appl Phys Lett., 2004. **85**(12): p. 2208-2010.
37. Machids, S. and S. Miyata, *Chemical synthesis of highly electrically conductive polymer.* Synth. Met., 1989. **31**.
38. Nakata, M., et al., *Synthesis of electrically conductive polypyrrole films by interphase oxidative polymerization.* Macromol. Chem., 1992. **193**.
39. Bjorklund, R.B. and I. Lundstrom, *Conducting polymers with micro or nanometer structure.* J. Electron. Mater, 1984. **13**.
40. Diaz, A. and J. Bargon, *Electrochemical synthesis of conducting polymers.* Handbook of conducting polymers, 1986. **1**: p. 81-115.
41. Malinauskas, A., *Chemical deposition of conducting polymers.* Polymer, 2001. **42**: p. 3957-3972.
42. Saurin, M. and S.P. Armes, *Study of the Chemical Polymerization of Pyrrole onto Printed Circuit Boards for Electroplating Applications.* Journal of Applied Polymer Science, 1995. **56**(1): p. 41-50.
43. Ichinose, I., K. Kurashima, and T. Kunitake, *Spontaneous Formation of Cadmium Oxide Nanostrands in Water.* J. Am. Chem. Soc., 2004. **126**(23): p. 7162-7163.
44. Bocchi, V. and G.P. Gardini, *Chemical synthesis of conducting polypyrrole and some composites.* J. Chem. Soc. Chem. commun., 1986(2).
45. Armes, S.P., *Optimum reaction conditions for the polymerization of pyrrole by iron(iii) chloride in aqueous solution.* Synthetic Metals, 1987. **20**: p. 365 - 371.
46. Rapi, S., V. Bocchi, and G.P. Gardini, *Conducting polypyrrole by chemical synthesis in water.* Synthetic Metals, 1988. **24**: p. 217-221.
47. Dhawan, S.K. and D.C. Trivedi, *Thin conducting polypyrrole film on insulating surface and its applications.* J. Bull. Mater. Sci., 1993. **16**(5): p. 371-380.
48. Alici, G. and N.N. Huynh, *Predicting force output of trilayer polymer actuators.* Sensors and Actuators A: Physical, 2006. **132**(2): p. 616-625.
49. Pei, Q. and O. Inganas, *Electrochemical applications of the bending beam method; a novel way to study ion transport in electroactive polymers.* Solid State Ionics, 1993. **60**(1-3): p. 161–166.
50. Otero, T.F. and S. J.M., *Soft and wet conducting polymers for artificial muscles.* Adv. Mater., 1998. **10**: p. 491–494.
51. Hiroaki, S., A. Masuo, and S.I. Hideki, *On-sieving of electrosynthesized polypyrrole films.* J. Chem. Soc., Chem. Commun., 1986: p. 87-88.
52. Otero, T.F., H.-J. Grande, and J. Rodríguez, *Reinterpretation of Polypyrrole Electrochemistry after Consideration of Conformational Relaxation Processes.* J. Phys. Chem.B., 1997. **101**(19): p. 3688–3697.
53. Skaarup, S., et al., *Simultaneous anion and cation mobility in polypyrrole.* Solid State Ionics, 2002. **159**(1-2): p. 143-147.
54. Bay, L., T. Jacobsen, and S. Skaarup, *Mechanism of Actuation in Conducting Polymers: Osmotic Expansion.* J. Phys. Chem. B, 2001. **105**(36): p. 8492–8497.

55. Wen, L., et al., *Development of Solid-in-Hollow Electrochemical Linear Actuators Using Highly Conductive Polyaniline.* Chem. Mater. 2004, 16, , 2004. **16**(9): p. 1615-1621.
56. Bay, L., et al., *A conducting polymer artificial muscle with 12% linear strain.* Advanced Materials, 2003. **15**(4): p. 310-313.
57. Wusheng, Y., et al., *Conducting composite film based on polypyrrole and crossliked cellulose.* J.Applied Polymer Sci, 2001. **80**(9): p. 1368-1373.
58. Mahadeva, S.K. and J. K., *Enhanced electrical properties of regenerated cellulose by polypyrrole and ionic liquid nanocoating.* Journal of Nanoengineering and Nanosystems, 2011. **225**(1): p. 33-39.
59. Chen, J. and X. Qian, *Effect of manufacture conditions on the conductivity of polypyrrole/pulp fibers conductive paper.* China Pulp and Paper, 2007. **26**(7): p. 4-7.
60. Song, H., X. Qian, and L. Wang, *The conductive paper manufactured with the composite of PAn/pulp fiber (II)–Effects of doping conditions on the performances of conductive paper.* Transactions of China Pulp and Pape, 2006. **21**(3): p. 64–67.
61. Wu, J., et al., *Conducting polymer coated lycra.* Synthetic Metals, 2005. **155**(3): p. 698–701.
62. Ding, C., et al., *Preparation and characterization of conductive paper via in situ polymerization of pyrrole.* BioResources, 2010. **5**(1): p. 303–315.
63. Pulickel, M.A., et al., *Single-walled carbon nanotube-polymer composites: strength and weakness.* Adv Mater, 2000. **12**(10).
64. Brandl, W., et al., *Production and characterisation of vapour grown carbon fiber/polypropylene composites.* Carbon, 2004. **42**(1): p. 5-9.
65. Smrutisikha, B., *Experimental study of mechanical and electrical properties of carbon nanofiber/epoxy composites.* Materials and Design 2010. **31**: p. 2406–2413.
66. Sui, G., et al., *Crystalline Structure and Properties of Carbon Nanofiber Composites Prepared by Melt Extrusion.* Macromol. Chem. Phys. , 2007. **208**: p. 1928-1936.
67. Takahashi, T., et al., *Polycarbonate crystallization by vapor-grown carbon fiber with and without magnetic field.* Macromolecular Rapid Communications, 2003. **24**: p. 763-767.
68. Bernadette, A.H. and J.B. William, *Polycarbonate carbon nanofiber composites.* European Polymer Journal., 2005. **41**: p. 889-893.
69. Weijie, H., et al. , *Sonication-assisted functionalization and solubilization of Carbon nanotubes.* Nano Letters, 2002. **2**(3): p. 231-234.
70. Asif, R., et al., *The efficiency of the oxidation of carbon nanofibers with various oxidizing agents.* Carbon 2007. **45**: p. 1072-1080.
71. Toebes, M.L., et al., *The influence of oxidation on the texture and the number of oxygen-containing surface groups of carbon nanofibers.* Carbon, 2004. **42**(2): p. 307–315.
72. Park, J.-M., et al., *Actuation of electrochemical, electro-magnetic, and electro-active actuators for carbon nanofiber and Ni nanowire reinforced polymer composites.* Composites: Part B 2008. **39**: p. 1161–1169.
73. Yeo-Heung, Y., et al., *Carbon Nanofiber Hybrid Actuators: Part II - Solid Electrolyte-based.* Journal of Intelligent Material Systems and Structures, 2006. **17**.

74. Yeo-Heung, Y., et al., *Carbon Nanofiber Hybrid Actuators: Part I - Liquid Electrolyte-based.* Journal of Intelligent Material Systems and Structures, 2006. **17**.
75. Morinobu, E., S.S. Michael, and M.A. Pulickel, eds. *Potential Applications of Carbon Nanotubes*. Vol. 111. 2008, Springer-Verlag Berlin Heidelberg 2008. 13-62.
76. Magrez, A., et al., *Cellular toxicity of carbon-based nanomaterials.* Nano Lett, 2006. **6**: p. 1121–1125.
77. Kang, I.e.a., *Introduction to carbon nanotube and nanofiber smart materials.* Composites: Part B, 2006. **37**: p. 382–394.
78. Andre´, P., Kenneth, N. M., Shusheng, P., & Mark, P. S., *Ionic Liquids and Their Interaction with Cellulose.* Chem. Rev., 2009 **109**: p. 6712–6728.
79. Audic, N., et al., *An Ionic Liquid-Supported Ruthenium Carbene Complex: A Robust and Recyclable Catalyst for Ring-Closing Olefin Metathesis in Ionic Liquids.* J. Am.Chem. Soc, 2003. **125**(31): p. 9248–9249.
80. Marisa, C.B., R.G. E, and G.C. Richard, *Non-Haloaluminate Room-Temperature Ionic Liquids in Electrochemistry—A Review.* ChemphysChem, 2005. **5**(8): p. 1106-1120.
81. Kimizuka, N. and T. Nakashima, 17, 6759 (2001). *Spontaneous Self-Assembly of Glycolipid Bilayer Membranes in Sugar-philic Ionic Liquids and Formation of Ionogels.* Langmuir, 2001. **17**(22): p. 6759–6761.
82. Ding, J., et al., *Use of Ionic Liquids as Electrolytes in Electromechanical Actuator Systems Based on Inherently Conducting Polymers.* Chem. Mater., 2003. **15**(12): p. 2392–2398.
83. Suresha, K.M. and K. Jaehwan, *Electromechanical Behavior of Room Temperature Ionic Liquid Dispersed Cellulose.* J. Phys. Chem. C, 2009 **113**: p. 12523–12529.
84. Latala, A., et al., *Marine toxicity assessment of imidazolium ionic liquids: Acute effects on the Baltic algae Oocystis submarina and Cyclotella meneghiniana.* Aquatic Toxicology, 2005. **73**(1): p. 91-98.
85. Gil, M.H., M. Mariz, and M.G. Durate, *Polymeric biomaterials as drug delivery systems.* Biomaterials,, 1996: p. 13–19.
86. Chen, L.-L.H. and Y.W. Chen, *Transdermal iontophoretic permeation of luteinizing hormone releasing hormone: characterization of electric parameter.* J. Control. Release, 1996. **40**: p. 187–198.
87. Singh , P. and H.I. Maibach, *Iontophoresis in drug delivery: basic principles and applications.* Crit Rev Ther Drug Carrier Syst, 1994. **11**(2-3): p. 161-213.
88. Andersson, J., J. Rosenholm, and M. Lindén, *Mesoporous Silica: An Alternative Diffusion Controlled Drug Delivery System*, in *Multifunctional Biomaterials and Devices*, N. Ashammakhi, Editor 2008: Turku, Finland.
89. Gul, M.K., *Controlled release oral dosage forms: some recent advances in matrix type drug delivery systems.* The Sciences, 2001. **1**(5): p. 350-354.
90. Ramchandani, M. and D.J. Robinson, *In vitro & invivo release of ciprofloacin from PLGA 50:50 implants.* Control. Release, 1998. **54**.
91. Maasen, S., E. Fattal, and R.H. Muller, *Cell cultures for the assessment of toxicity and uptake of polymeric particulate drug carriers.* STP Pharma Sci, 1993. **3**.

92. Bajpai, A.K., et al., *Responsive polymers in controlled drug delivery.* Progress in Polymer Science, 2008. **33**: p. 1088-1118.
93. Hillery, A.M., W.L. Andrew, and S. James, eds. *Drug Delivery and Targeting for Pharmacists and Pharmaceutical Scientists*. 2001, Taylor & Francis: 11 New Fetter Lane, London EC4P 4EE.
94. Siepmann, J. and N.A. Peppas, *Modeling of drug release from delivery systems based on hydroxypropyl methylcellulose (HPMC),.* Adv. Drug Deliv.Rev., 2001. **48**(2-3): p. 139–157.
95. Siepmann, J. and N.A. Peppas, *Modeling of drug release from delivery systems based on hydroxypropyl methylcellulose (HPMC).* Advanced Drug Delivery Reviews, 2012. **64**: p. 163-174.
96. Korsmeyer, R.W. and N.A. Peppas, *Effect of the morphology of hydrophilic polymeric matrices on the diffusion and release of water soluble drugs.* J. Membr. Sci, 1981. **9**(3): p. 211–227.
97. Higuchi, T., *Mechanism of sustainedsction medication.* J. Pharm. Sci, 1963. **52**: p. 1145-l 149.
98. Langer, R.S. and N.a. Peppas, *Present and future applications of biomaterialsi n controlledd rug delivery systems.* Biomaterials, 1981. **2**.
99. Dahlberg, C., et al., *Polymer mobilization and drug release during tablet swelling, A 1H NMR and NMR microimaging study.* J. Control. Release, 2007. **122**(2): p. 199–205.
100. D'Souza, A.J.M., R.L. Schowen, and M.T. Elizabeth, *Polyvinylpyrrolidone–drug conjugate: synthesis and release mechanism.* Journal of Controlled Release, 2004. **94**(1): p. 91-100.
101. Poste, G., R. Kirsh, and T. Koestler, eds. *Liposom Technology*. G. Gregoriadis ed. 1984, CRC Press, Florida. 1: Florida. .
102. Hans, M.L. and A.M. Lowman, *Biodegradable nanoparticles for drug delivery and targeting.* Current Opinion in Solid State and Materials Science, 2002. **6**: p. 319-327.
103. Torchilin, V.P., *Drug Taegeting.* Eur. J. Pharm. Sci, 2000. **11**: p. 81.
104. Sakhnini, L. and R. Khuzaie, *Magnetic behavior of human erythrocytes at different hemoglobin states.* Eur. Biophys. J, 2001. **30**: p. 467–470.
105. Ellisin, J., in *Handbook of Conducting Polymers*, T. Skotheim, Editor 1986, Marcel Dekker: New York. p. 501.
106. Guihua, Q., Q. Wang, and N. Min, *Polypyrrole-Fe3O4 Magnetic Nanocomposite Prepared by Ultrasonic Irradiation.* Macromol. Mater. Eng, 2006. **291**: p. .68–74.
107. Berry, C.C. and A.S.G. Curtis, *Functionalisation of magnetic nanoparticles for applications in biomedicine.* J Phys D: Appl Phys, 2003. **36** p. 198-206.
108. Altman, R.D. and C.J. Lozada, *Practice guidelines in the management of osteoarthritis.*, 1998.
109. Tobias, N., et al., *Superparamagnetic nanoparticles for biomedical applications: Possibilities and limitations of a new drug delivery system.* Journal of Magnetism and Magnetic Materials 2005. **293**: p. 483–496.
110. Thorek, D.I.J., et al., *Superparamagnetic Iron Oxide Nanoparticle Probes for Molecular Imaging.* Annals of Biomedical Engineering, 2006. **34**(1): p. 23-38.
111. Miller, L.L., et al., *Electrochemically controlled release.* .J.Control. Release, 1987. **6**(1): p. 293-296.

112. Azad, K., et al., *Iontophoretic drug delivery: History and applications.* Journal of Applied Pharmaceutical Science, 2011. **01**(03): p. 11-24.
113. Keller, M.B., R.M. Hirschfeld, and K. Demyttenaere, *Optimizing outcomes in depression: focus on antidepressant compliance.* Int. Clin. Psychopharmacol, 2002. **17**: p. 265–271.
114. Sage, B.H., in *Encyclopedia of pharmaceutical Technology*, J. Swarbrick and J.C. Boylan, Editors. 1993, Marcel Dekker Inc.:: New York. p. 217-247.
115. Lin, R.Y., Y.C. Ou, and W.Y. Chen, *The role of electroosmotic flow on in vitro transdermal iontophoresis.* J. Control. Release., 1997. **43**: p. 23-33.
116. Chien, Y.W., et al., *Facilitated transdermal delivery of therapeutic peptides and proteins by iontophoretic delivery device.* J. Control. Release, 1990. **13**: p. 263–278.
117. Miller, L.L. and G.A. Smith, *Iontophoretic transport of acetate and carboxylate ions through hairless mouse skin. A cation exchange membrane model.* Int.J.Pharm, 1989. **49**(1): p. 15-22.
118. Lo, R., et al., *A passive MEMS drug delivery pump for treatment of ocular diseases.* Biomed. Microdevices, 2009. **11**: p. 959–970.
119. Jackson, N. and J. Muthuswamy, *Flexible chip-scale package and interconnect for implantable MEMS movable microelectrodes for the brain.* J. Microelectromechanical. Syst., 2009. **18**: p. 396–404.
120. Abel, P.U. and T. von Woedtke, *Biosensors for in vivo glucose measurement: Can we cross the experimental stage.* Biosens. Bioelectron., 2002. **17**: p. 1059-1070.
121. Li, P.-Y., et al., *An electrochemical intraocular drug delivery device.* Sens. Actuator., A., 2008. **143**: p. 41–48.
122. Po-Ying, L., et al., *A parylene bellows electrochemical actuator.* J. Microelectromechanical. Syst., 2010. **19**: p. 215–228.
123. Tsai, N.-C. and C.-Y. Sue, *Review of MEMS-based drug delivery and dosing systems.* Sens. Actuator. A., 2007. **134**: p. 555–564.
124. Najafi, N. and A. Ludomirsky, *Initial animal studies of a wireless, batteryless, MEMS implant for cardiovascular applications.* Biomed. Microdevices, 2004. **6**: p. 61–65.
125. Danny, J.H.T., et al., *Approaches and Challenges of Engineering Implantable Microelectromechanical Systems (MEMS) Drug Delivery Systems for in Vitro and in Vivo Applications.* Micromachines 2012. **3**: p. 615-631.
126. Kim, K.J. and M. Shahinpoor, *Ionic polymer–metal composites: II. Manufacturing techniques.* Smart Mater. Struct., 2003. **12**(1): p. 65–79.
127. Clausen, I., et al. *Biofouling on Protective Coatings for Implantable MEMS*. in *IEEE Sensors, Kona, HI, USA, 1–4 November 2010*. 2010.
128. Mercanzini, A., et al., *Demonstration of cortical recording using novel flexible polymer neural probes.* Sens. Actuator. A., 2008. **143**: p. 90–96.
129. Jaehwan, K., S. Chun-Seok, and Y. Sung-Ryul, *Cellulose based electro-active papers: performance and environmental effects.* Smart Mater. Struct., 2006. **15**(3).
130. Suresha, K.M. and K. Jaehwan, *Nanocoating of ionic liquid and polypyrrole for durable electro-active paper actuators working under ambient conditions.* J. Phys. D: Appl. Phys, 2010. **43**(20).

131. Sung-Ryul, Y. and K. Jaehwan, *Multiwalle- carbon nanotubes and polyaniline coating on electro-active paper for bending actuator.* Journal of Physics D: Applied Physics, 2006. **39**: p. 2580-2586.
132. Su, J., et al., *Preparation and characterization of electrostrictive polyurethane films with conductive polymer electrodes.* Polym. Adv. Technol. , 1998. **9**: p. 317-321.
133. Ros, T.G., et al., *Surface oxidation of carbon nanofibres.* Chem.-Eur. J. , 2002. **8**.
134. Rosner, R.B. and M.F. Rubner, *Solid-state polymerization polypyrrole within a Langmuir-Blodgett film of ferric stearate.* Chem. Mater, 1994. **6**: p. 581–586.
135. Balasubramanian, K. and M. Burghard, *Chemically Functionalized Carbon Nanotubes.* Small, 2005. **1**: p. 180-192.
136. Li, C. and Z. Song, *Diffusion-oxidative polymerization of transparent and conducting polypyrrole-poly(ethylene terephthalate) composites.* Synth. Met., 1991. **40**(1): p. 23–28.
137. Suresha, K.M., K. Jaehwan, and J. Chulhee, *Effect of Hydrophobic Ionic Liquid Loading on Characteristics and Electromechanical Performance of Cellulose.* International journal of precision engineering and manufacturing, 2011. **12**(1): p. 47-52.
138. Omastova, M., et al., *Synthesis and structural study of polypyrroles prepared in the presence of surfactants.* Synth Met, 2003. **138**: p. 447–455.
139. Yi, W.Q., et al., *Improved Capacitive Performance of Polypyrrole Doped with 9,10 Anthraquinone sulfonic Acid SodiumSalt.* Acta Phys. Chim. Sin, 2010. **26**(11): p. 2951-2956.
140. Winzer, S.R.e.a., *Designing cofired multilayer electrostrictive actuators for reliability.* J. Am. Ceramic. Soc., 1989. **72**(12): p. 2246-2257.
141. Baughman, R., et al., *Carbon nanotube actuators.* Science, 1999. **284**: p. 1340-1344.
142. Ding, J., et al., *Use of ionic liquid as electrolytes in electro-chemical actuator systems based on inherently conducting polymers.* Chem. Mater, 2003. **15**: p. 2392 – 2398.
143. Dougherty, D.A. and J.C. Ma, *The Cation-π Interaction.* Chemical Reviews, 1997. **97**(5): p. 1303–1324.
144. Fukushima, T., et al., *Fully Plastic Actuator through Layer-by-Layer Casting with Ionic-Liquid-Based Bucky Gel.* Angewandte Chemie International Edition, 2005. **44**(16): p. 2410–2413.
145. Kusakabe, K. and M. Maruyama, *Magnetic nanographite.* Phys Rev B, 2003. **67**(09).
146. Zhang, Y., et al., *First Principle studies of Defect Induced Magnetism in Carbon.* Phys. Rev. Lett., 2007. **99**.
147. Suresha, K.M., Y.Y. Sang, and K. Jaehwan, *Electrical and Electromechanical properties of Cellulose- Polypyrrole- Ionic Liquid Nanocomposite: Effect of Polymerization time.* Nanotechnology, IEEE Transactions on, 2011. **10**(3): p. 445-450.
148. Ma, S., et al., *Magnetism of amorphous carbon nanofibers.* Applied Physics Letters, 2009. **95**.
149. Whiting, C.J., et al., *Shear modulus of polyelectrolyte gels under electric field.* J.Phys. Condens. Matter., 2001. **13**: p. 1381–1393.

150. Chen, G.L. and W.H. Hao, *In vitro performance of floating sustained release capsule of verapamil.* Drug Dev Ind Pharm., 1998. **24**(11): p. 1067-1072.
151. Shah, M.V., G.M. De, and H. Suryakarma, *An evaluation of albumin microcapsules prepared using a multiple emulsion technique.* J Microencapsul, 1987. **4**: p. 223-238.
152. Higuchi, T., *Rate of release of medicaments from ointment bases containing drugs in suspensions.* J. Pharm. Sci, 1961. **50**: p. 874–875.
153. Korsmeyer, R.W., et al., *Mechanisms of solute release from porous hydrophilic polymers.* Int. J. Pharm., 1983. **15**: p. 25-35.
154. Shashank, C., et al., *Approaches to increase the gastric residence time: floating drug delivery systems- A Review.* Asian J Pharm Clin Res, 2013. **6**(3): p. 1-9.
155. Gibaldi, M. and S. Feldman, *Establishment of sink conditions in dissolution rate determinations.* J Pharm Sci., 1967. **56**(10): p. 1238–1242.
156. Wagner, J.G., *Interpretation of percent dissolved-time plots derived from in-vitro testing of conventional tablets and capsules.* J. Pharm. Sci., 1969. **58**(10): p. 1253-1257.
157. Wu, J. and Q. Yuan, *Gas permeability of a novel cellulose membrane.* Journal of Membrane Science., 2002. **204**(1-2): p. 185-194.
158. Li, Q., et al., *Biodegradable and photocrosslinkable polyphosphoester hydrogel.* Biomaterials, 2006. **27**: p. 1027-34.
159. Chien-Shun, W., et al., *A polyvinyl alcohol/p-sulfonate phenolic resin composite proton conducting membrane.* Journal of power sources, 2006. **160**: p. 1204-1210.
160. Toshima, N. and O. Ihata, *Catalytic synthesis of conductive polypyrrole using iron (III) catalyst and molecular oxygen.* Synth. Met., 1996. **79**: p. 165–172.
161. Wise, D.L., *Handbook of pharmaceutical controlled release technology*2000: CRC Press.
162. Green, P.G., *Iontophoretic delivery of peptide drugs.* J. Control. Release, 1996. **41**: p. 33–48.
163. Kagan, V.E.e.a., *Carbon nanotubes degraded by neutrophil myeloperoxidase induce less pulmonary inflammation.* Nature Nanotechnology, 2010. **5**.
164. Chouly, C., et al., *Development of superparamagnetic nanoparticles for MRI: effect of particle size, charge and surface nature on biodistribution.* J Microencapsul, 1996. **13**.
165. Wei, W., H. Quanguo, and J. Changzhong, *Magnetic Iron Oxide Nanoparticles: Synthesis and Surface Functionalization Strategies.* Nanoscale Res Lett 2008. **3**: p. 397-415.
166. Jun, S., et al., *Synthesis of Ferric Oxide Nanoparticles with Controllable Crystal Phases by Salt-assisted Combustion Method. .* Journal of Inorganic Materials, 2010. **25**(7): p. 780-784.
167. Basavaraja, S., et al., *Characterization of γ-Fe2O3 Nanoparticles Synthesized Through Self-Propagating Combustion Route.* Synthesis and Reactivity in Inorganic, Metal-Organic, and Nano-Metal Chemistry,, 2007. **37**(6): p. 409-412.
168. Miller, F.A. and C.H. Wilkins, *Infrared Spectra and Characteristic Frequencies of Inorganic Ions.* Anal. Chem., 1952. **24** (8): p. 1253-1294.

169. Wu, C.S., et al., *A polyvinyl alcohol/p-sulfonate phenolic resin composite proton conducting membrane.* J. Power Sources, 2006. **160**: p. 1204-1210.
170. A-sasutjarit, R., A. Sirivat, and P. Vayumhasuwan, *Viscoelastic properties of carbopol 940 gels and their relationships to piroxicam diffusion coefficients in gel bases.* Pharm. Res, 2005. **22**(12): p. 2134–2140.
171. Nazarzadeh, Z.E., M.M. Lakouraj, and M. Mohseni, *Biodegradable polypyrrole/dextrin conductive nanocomposite: Synthesis, characterization, antioxidant and antibacterial activity.* Synthetic Metals, 2014. **187**(0): p. 9-16.
172. Taylor, E. and T.J. Webster, *Reducing infections through nanotechnology and nanoparticles.* Int J Nanomedicine, 2011. **6**: p. 1463–1473.
173. Zhang, L., et al., *Investigation into the antibacterial behaviour of suspensions of ZnO nanoparticles (ZnO nanofluids).* J Nanoparticle Res., 2007. **9**(3): p. 479–489.